2016

Analysis of a Long-Term Record of Nearshore Currents and Implications in Littoral Transport Processes

Carolina Burnette
University of North Florida, n00613995@ospreys.unf.edu

Analysis of a Long-Term Record of Nearshore Currents and Implications in Littoral Transport Processes

by

Carolina Burnette

A Thesis submitted to the School of Engineering

in partial fulfillment of the requirements for the degree of

Master of Science in Civil Engineering

UNIVERSITY OF NORTH FLORIDA

COLLEGE OF COMPUTING, ENGINEERING AND CONSTRUCTION

August, 2016

This Thesis titled “Analysis of a Long-Term Record of Nearshore Currents and Implications in Littoral Transport Processes” is approved:

_____ _____
William Dally, Ph.D., P.E.
Thesis Advisor and Committee Chair Person

_____ _____
Donald Resio, Ph.D.
Committee member

_____ _____
Thobias Sando, Ph.D., P.E.
Committee member

Accepted for the School of Engineering:

_____ _____
Murat Tiryakioglu, Ph.D.
Director

Accepted for the College of Computing, Engineering and Construction:

_____ _____
Mark A. Tumeo, Ph.D., P.E.
Dean

Accepted for the University:

_____ _____
Dr. John Kantner
Dean of the Graduate School

DEDICATION

This work is dedicated to my beloved daughters Sophia and Abigail for their unconditional love that has empowered me to live a more purposeful life and motivated me to pursue my dreams.

ACKNOWLEDGMENTS

First, I wish to thank my advisor, Dr. Dally, who has been very supportive since the first day I began working on my thesis; Dr. Dally has helped me not only by providing academic advice, but also by encouraging me during difficult times.

I also want to say thank you to Dr. Resio, who gave me the opportunity to be part of the Coastal Engineering program by funding me through Taylor Engineering Research Institute. He also became an inspiration to follow and has guided me and mentored me through the investigation phase of my thesis. I wish to thank Dr. Sando for being part of my thesis committee, a thesis reader and a very supportive person. Also I want to thank Dr. Bacopoulos with whom I worked with for more than a year in the data processing and analysis of my thesis.

I want to thank my mother: her support has been unconditional all these years and without her help I never could have finished my master's degree.

TABLE OF CONTENTS

Page

LIST OF TABLES

Page

LIST OF FIGURES

Page

ABSTRACT

A seasonal and long-term analysis of the vertical structure of currents in the nearshore is conducted to determine the role of the wind in driving currents and consequently affecting littoral transport processes. Approximately ten years (January, 2002 – October, 2011) of nearshore current profiles are examined using the data collected with an Acoustic Doppler Current Profiler (ADCP) installed off of Spessard Holland North Beach Park located in Melbourne Beach, Florida. Additionally, wind data collected with a directional anemometer from September, 2002, until October, 2008, are used to further characterize the long-term hydrodynamic forcing. With the shoreline oriented nominally 17^{o} west of magnetic north, both the current profiles and the wind vectors have been rendered into longshore and cross-shore components. The water level record from a NOAA tide station located at the Trident Pier at nearby Port Canaveral is utilized in establishing the water depth and conditioning the data for statistical analysis. Monthly mean vertical profiles reveal that during the winter months the surface currents are usually toward the south, and toward the north in the summer. In spring and fall, they are mixed, demonstrating a clear seasonality in both direction and intensity of the longshore current. Subjecting the longshore and cross-shore current data to Empirical Orthogonal Function Analysis reveals that the first spatial Eigenfunction accounts for more than 98% of the variability in the vertical profile of the longshore current, and more than 86% of the variability in the profile of the cross-shore current. However, there is a rotation of the current to the right (clockwise) with the rotation angle increasing and the variance decreasing with depth below the surface. The spiral structure of the water column follows a surface

Ekman veering, but for very shallow water. The upper layer of the current is almost aligned with the direction of the wind. Monthly correlations between 2-hour average time series of longshore current and 2-hour average time series of wind speed reveal the seasonal patterns of the wind and longshore current in which the upper layer of the water column is highly correlated with the longshore component of the wind speed for most of the year and slightly less correlated for the lower layer of the water column. Most importantly, on average, wave height (H_{mo}) is larger when the longshore current is heading to the south (H_{mo}=0.95 m) than when the current is going to the north (H_{mo}=0.73 m). Additionally, there is a stronger correlation between southerly directed currents and incident wave energy flux than northerly directed currents and wave energy flux. These results indicate that the net long-term north-to-south sediment transport known to characterize the region is heavily influenced by wind-driven currents.

CHAPTER 1: INTRODUCTION

Field data collection has proven to be essential in most aspects of coastal science and engineering. According to Absalonsen and Dean (2010), in the State of Florida developing and maintaining long-term nearshore wave and wind information is considered crucial to understanding the causes of shoreline changes over time. Hurricanes and extratropical storms (nor'easters), seasonal behavior, sea level rise, and man-made coastal projects such as beach nourishment, navigation channels, and inlet jetties are considered the leading causes of shoreline evolution in the state.

Acoustic Doppler Current Profiler (ADCP) measurements have been widely used in the study of the vertical structure of the water column in coastal and estuarine systems. The data generated by the ADCP includes the time-dependent fluid speed and direction over most of the water column. During recent years, the data have been used to study the characteristics of nearshore waves, and to test the ability of numerical models to replicate both nearshore waves and storm surge. As a component of the Florida Coastal Forcing Project (FCFP), initially sponsored by the Florida Department of Environmental Protection (FDEP), Surfbreak Engineering Sciences Inc. (SES) collected over 10 years of measurements of nearshore waves, winds, currents and water levels using an ADCP wave gauge and a directional anemometer at Spessard Holland North Beach Park in Melbourne Beach on the central Atlantic coast of Florida (Leadon, Dally, & Osiecki, 2002). In a thesis by Montoya (2014) and a subsequent paper by Montoya and Dally (2016), the high-quality nearshore directional wave data collected at Spessard were examined in detail. The

researchers were particularly interested in determining if the net long-term longshore forcing induced by breaking waves, due to Radiation Stress (S_{xy}) and consequently sand transport, was indeed from north-to-south, as indicated by the shoreline offsets at two nearby jettied inlets. Surprisingly, it was found that the net wave forcing over the ten-year period was only very slightly north-to-south (7.2 N/m of shoreline), whereas the standard deviation was 77.2 N/m. That is, the net was the small difference between large quantities, and consequently not as convincing an explanation as anticipated. The researchers also found that it required the accumulation of 4 to 5 years of data before the net magnitude and direction of S_{xy} conclusively revealed itself, also contrary to expectations.

In the work described herein, the vertical current profiles measured by the same ADCP over the 10-year period are to be examined in hopes that their behavior will shed light on this enigma. Because the ADCP was located approximately 610 m from the shoreline in 8.5 m mean depth, i.e., well seaward of the surf zone except during the most extreme storm events, it is justifiably assumed that the surface currents at this location are in general forced by the direction and intensity of the local winds. The 3D structure below the surface is influenced by bed shear, wave mixing processes, tide-induced flow, and by the cross-shore mass balance imposed by the proximity of the shoreline.

The effect of the wind in the water column was studied by Ekman (1905), who found that for an ocean of infinite depth, the surface-current is directed 45^{o} to the right of the direction of the wind, and this angle further increases with the depth of the water column in the northern hemisphere. Coriolis acceleration (1835) explains this deviation of the surface-current as a clear consequence of the earth's rotation. Ekman’s theory in the case of an ocean of finite depth states

that the angle between the wind and the surface-current is not exactly 45^{o} degrees. Instead, the angle of deflection depends on the ratio between the depth of the sea (h) and the depth of wind current, D (depth at which the wind is able to produce any sensible motion). If h/D is a small fraction, the angle between the wind and the surface-current is small, and the current is nearly aligned in the direction of the wind.

During the summer of 1996, Munchow and Chant (2000) conducted an experiment for three months to study wind-driven currents on a shallow shelf. The site selected for the study was 30 km off the coast of New Jersey where four acoustic Doppler current profilers (ADCP) and eight electromagnetic current meters were deployed in 12 m, 19 m, and 25 m depth. Collecting simultaneous data at inshore and offshore locations allowed for the comparison of the behavior of the currents at different depths in response to local winds. Currents offshore did not show much longshore variation in speed and direction. However, the longshore variability of the depth-averaged currents inshore was significantly higher. Using Complex Empirical Orthogonal Function (cEOF) analysis it was found that the first cEOF mode of the depth-averaged currents accounted for more than 78% of the total variance and the second cEOF mode accounted for 12% of the total variance. The mode-1 was characterized by a 30^{o}–70^{o} counterclockwise current veering with depth in the bottom Ekman layer for the whole record. Although Ekman dynamics in shallow water play a role in the veering, buoyancy from the intermittent Hudson coastal current also contributed forcing that opposed the local wind-driven response. Munchow and Chant (2000) interpreted the first mode as wind- and buoyancy-forced motions that were both strongly affected by bottom friction and only weakly affected by vertical stratification. In contrast, the second mode

was labeled a frictional and baroclinic response to surface wind forcing. It apparently included the effects of both surface and bottom Ekman layers.

Cosoli, Gacic, and Mazzoldi (2008) Utilized Complex Empirical Orthogonal Function Analysis to analyze the response of near-surface currents to highly variable winds. The data were collected with a set of ADCP's deployed in the Adriatic Sea in relatively shallow water (~17 m), approximately 14.6 km from the coast during September 2002 to October 2002. The cEOF analysis determined that only two modes were required to explain more than 90% of the variance in the vertical structure of the current, with EOF mode-1 explaining more than 78% of the total variance. The results of Cosoli, Gacic, and Mazzoldi (2008) demonstrated a fast response of the currents to local wind stress, where currents vectors were directed to the right of the wind stress vectors according to a surface Ekman veering, but with smaller angles than typically encountered in deep-water. In contrast, the current vectors below the 8 m depth show a counterclockwise rotation towards the bottom, according to the dynamics of a frictionally dominated flow in shallow water; thus, in shallow water, this indicates the importance of bottom friction on the motion of the entire water column.

The studies mentioned above were carried out in deeper water than the experiments conducted by Hubertz (1986), who collected measurements of nearshore and surf zone currents between 1982 and 1984 at the USACE Field Research Facility in Duck, North Carolina. The results showed the importance of winds on driving the longshore current in the nearshore and are the most germane to the present shallow water study.

Most of the studies found in the literature described above were based on short-term records; consequently, a complete analysis of the vertical structure of the water column over

seasonal time scales could not be performed. Thus, the availability of an extensive data set collected for almost ten years from the Spessard station allows seasonal and longer-term analysis of the longshore and cross-shore currents and will aid understanding of how they originate. In fact, it is generally assumed that currents in the nearshore are mainly wave–induced. However, outside the surf zone examination of the behavior of currents and winds and evaluating their correlation will permit us to determine the role of the wind in driving currents and consequently their effect on littoral processes in the nearshore.

CHAPTER 2: DATA COLLECTION METHODS

The data collection station utilized in this study was located at Spessard Holland North Beach Park in Melbourne Beach, on the coast of east-central Florida between Port Canaveral, 38 km to the north and Sebastian Inlet, 24 km to the south, both of which are jettied entrances (Figures 2.1 a and b). There are distinct shoreline offsets at the port and the inlet (Figures 2.1 c and d) indicating net N-S longshore transport in the region, as noted by Montoya and Dally (2016).

The ADCP was installed offshore approximately 600 m from the dune at a mean water depth of ~8.5 m. The weather station included a directional anemometer mounted to a 10 m tall tower, installed at the top of the dune (Dally, 2011). The ADCP measured current speed and direction over the water column for nominally ten years (September 2001 to October 2011), whereas the directional anemometer collected wind speed and direction over a six-year period (September 2002 to October 2008). The ADCP was attached to a jetted spud so that the instrument could be located sufficiently above the bed to avoid burial by sediment. As opposed to a bottom-resting frame, the spud always maintained its vertical orientation and did not settle into the bed. Two different spud locations, approximately 180 ft. apart, were used during the data collection through the years. Spud #1 was located at N28° 32.672; W80° 32.672’ at an altitude of approximately 1 meter above the bed, while spud #2 was located at N28° 3.355; W80° 32.701’at an altitude of 1.64 m.

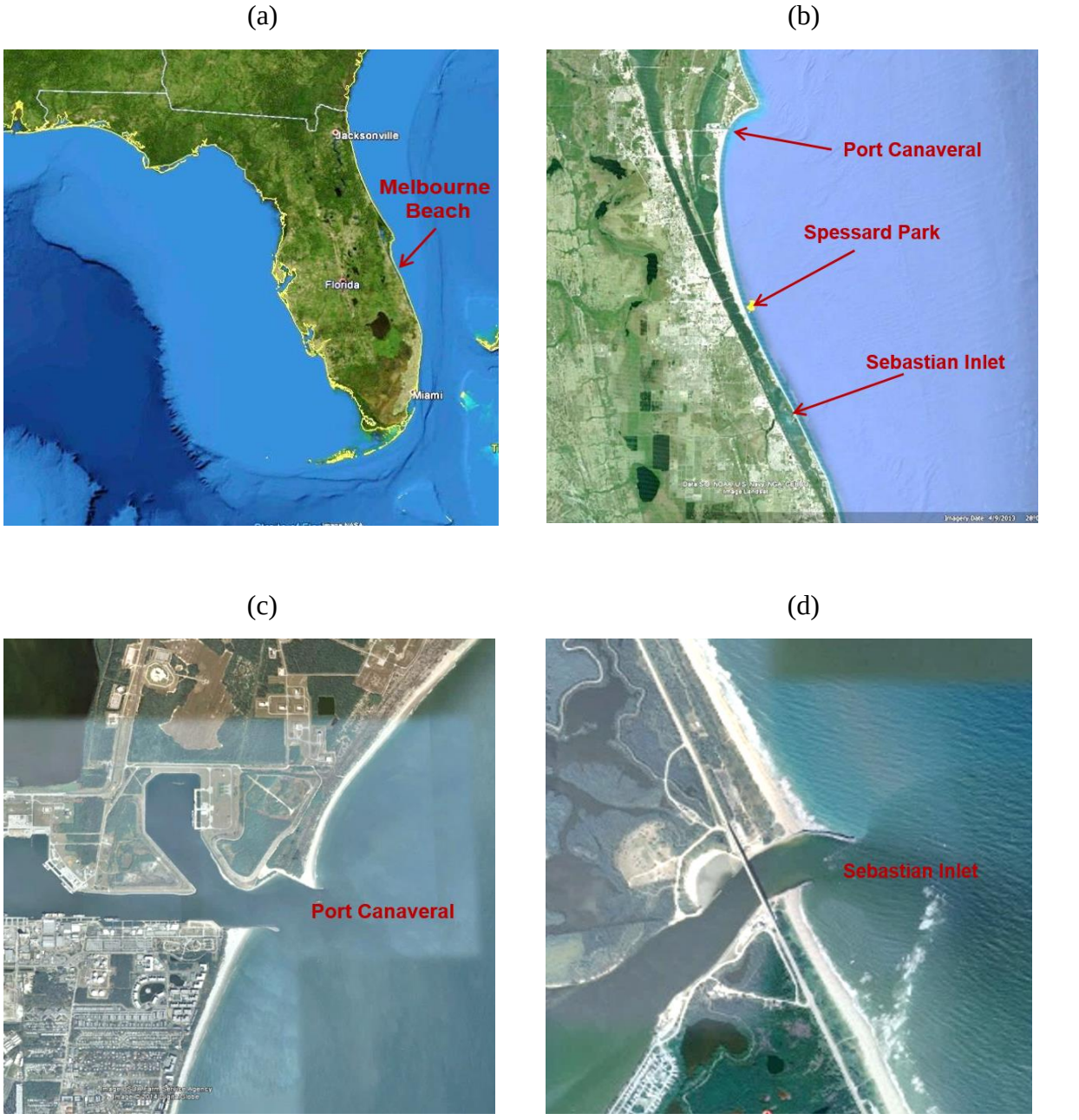

Figure 2.1. (a) Florida Peninsula showing the location of Melbourne Beach. (b) The locations of Port Canaveral, the Spessard ADCP, and Sebastian Inlet. (c) Aerial of Port Canaveral showing its N-S offset. (d) Aerial of Sebastian Inlet showing its N-S offset.

CHAPTER 3: ADCP CURRENT DATA PROCESSING

The raw data files were processed using the ADCP manufacturer's (RD Instruments) proprietary software called WavesMon. The acoustic capabilities of the instrument were used for processing the wave parameters using the Format 8 of the WavesMon software, which generated both a wave parameter file and a directional spectrum file. After analyzing the ten-year record of water depth, it was noticed that the pressure gauge was clogged during several periods of time.

As a substitute, the 6-minute water elevation record from the Trident Pier, FL station (#8721604) was used to obtain the mean water depth for the ten years. Time series were shifted 12 minutes to compensate for the lag in time between the Spessard station and the Trident pier station. Also, the WavesMon software generated speed and direction for the bins above the blanking distance of the instrument. The bin distribution was set initially as 26 bins, 0.30 m width, with a blanking distance of 0.83 m. Later in 2005 it was changed to 16 bins, 0.50 m width, with a blanking distance of 1.05 m. The number of bins, their respective width, and blanking distances were taken into consideration to assemble the currents files each year.

Figure 3.1 presents the distribution of currents processed with the WinADCP software for a short time record from February 23 to March 1, 2002, displaying the mean water surface elevation above the blanking distance of the instrument on the left scale, and the bin distribution on the right side. It is clear that the ADCP often ranged above the water surface, which are considered to be contaminated measurements.

Book, Perkins, Signell, and Wimbush (2007) achieved a significant contribution in describing the contamination of the measurements at the surface of the water, and suggested a truncation from the ADCP datasets as they contain false current signals. The height above the transducer head where contamination starts is the range from the ADCP transducer head to the surface multiplied by the cosine of the beam angle (20 degrees), concluding that bins contaminated by surface echo should be truncated from the ADCP datasets.

The present study intends to analyze the behavior of the currents throughout the total water column, particularly to find the correlation between local winds and the behavior of the upper layers of the water column. Therefore, since it is important for us to have a very accurate near-surface record, the total ten-year of current data were screened by truncating the surface bins based upon the water level records measured every 6 minutes from the Trident pier station. In other words, edited current data follow the sea-surface height, minus 6% of the total water depth above the instrument, as recommended by Book et al. (2007).

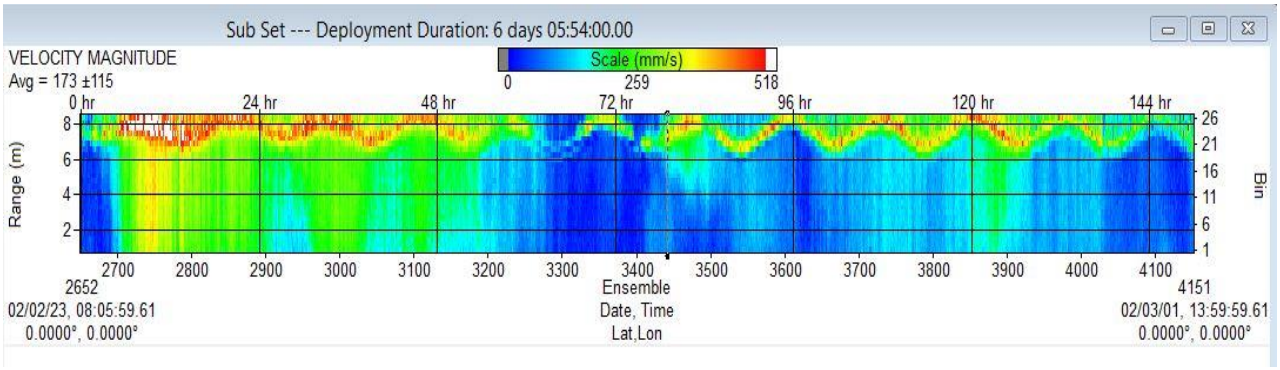

Figure 3.1. Currents distribution processed with WinADCP software.

The currents measured at the Spessard station are “to which” relative to magnetic north; whereas, the winds are “from which” relative to magnetic north. Thus, the wind record was rotated to the “to which” convention ($+180^o$). With the shoreline oriented nominally 17^o west of magnetic north (Kennedy and Dean, 2005), both the current profiles and the wind vectors have been rendered into longshore and cross-shore components (to which in direction). Therefore, a direction of 73^o from magnetic North is regarded as a wind coming perfectly normal to the shoreline in the onshore direction, and a measured current direction of 73^o from magnetic North is considered a current going offshore normal to the shoreline. The data record of wind and currents has been decomposed into a cross-shore component (V_{cross}) being positive going from west to east, and the longshore component (V_{long}) being positive going from south to north. Figure 3.2 and Figure 3.3 show examples of the vertical distribution of longshore and cross-shore currents from 02/23/2002 08:00 until 02/27/2002 00:00, after deleting the contaminated data below the sea-surface.

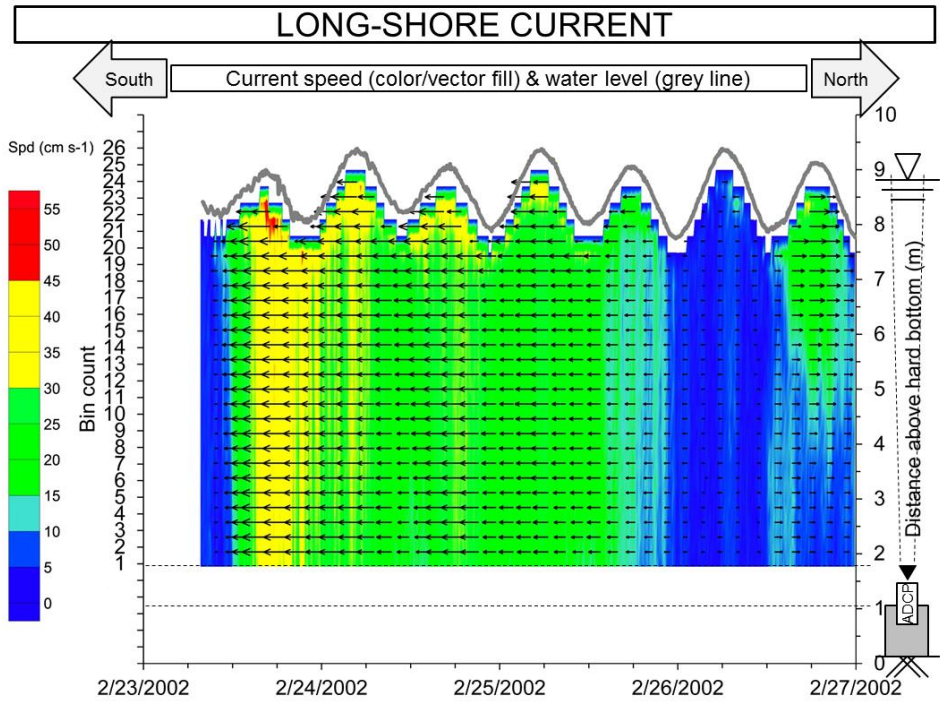

Figure 3.2. Time series of vertical distribution of longshore current.

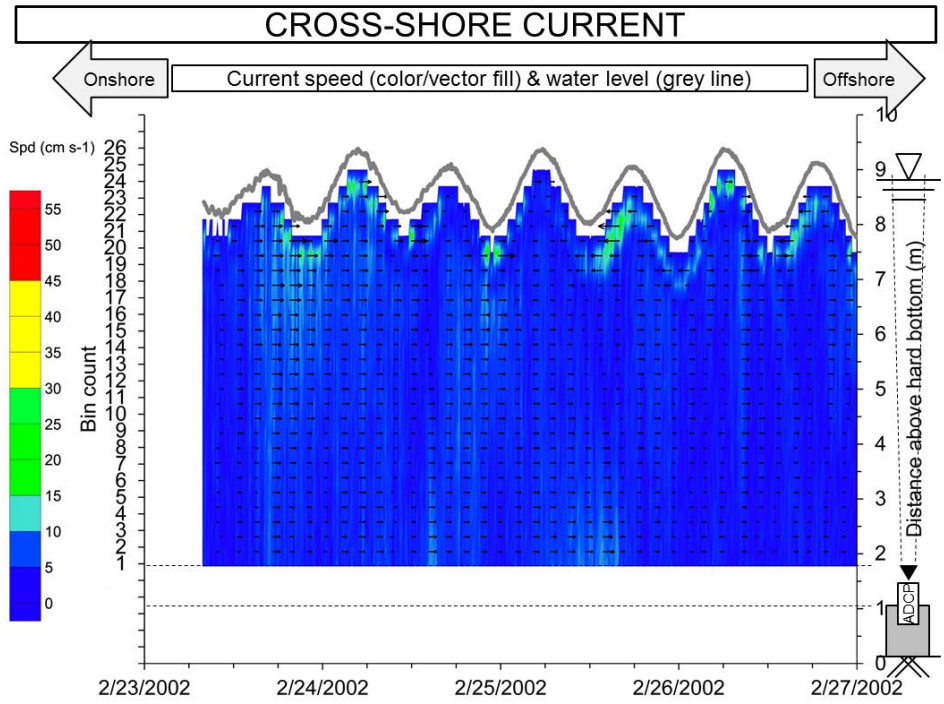

Figure 3.3. Time series of vertical distribution of cross-shore current.

CHAPTER 4: BASIC EXAMINATION OF CURRENT DATA

The processed current data provides speed and direction for every one of the equally distributed bins above the instrument blanking distance, over the water column. To meaningfully render the response of the longshore and cross-shore currents to wind forcing it was necessary to convert the physical elevation of the bins throughout the water column to normalized elevations, thereby suppressing the influence of tides in the statistical analysis. Normalization was accomplished by simply dividing the physical bin elevation by the mean of the water depth during each current burst. After normalizing, the data were fit into a matrix with 21 rows going from 0 to 1 on a non-dimensional scale. Each time series was subjected to two-hour block averages which reduces the number of points in the time series from 52,560 to 4,380 points for each year. Figure 4.1 presents a time series of the upper layer of the normalized water column with the velocity vectors averaged every 2 hours as noted above. The cross-shore current speed component (V_{cross}) is positive going from west to east, and the long-shore currents speed component (V_{long}) is positive going from south to north.

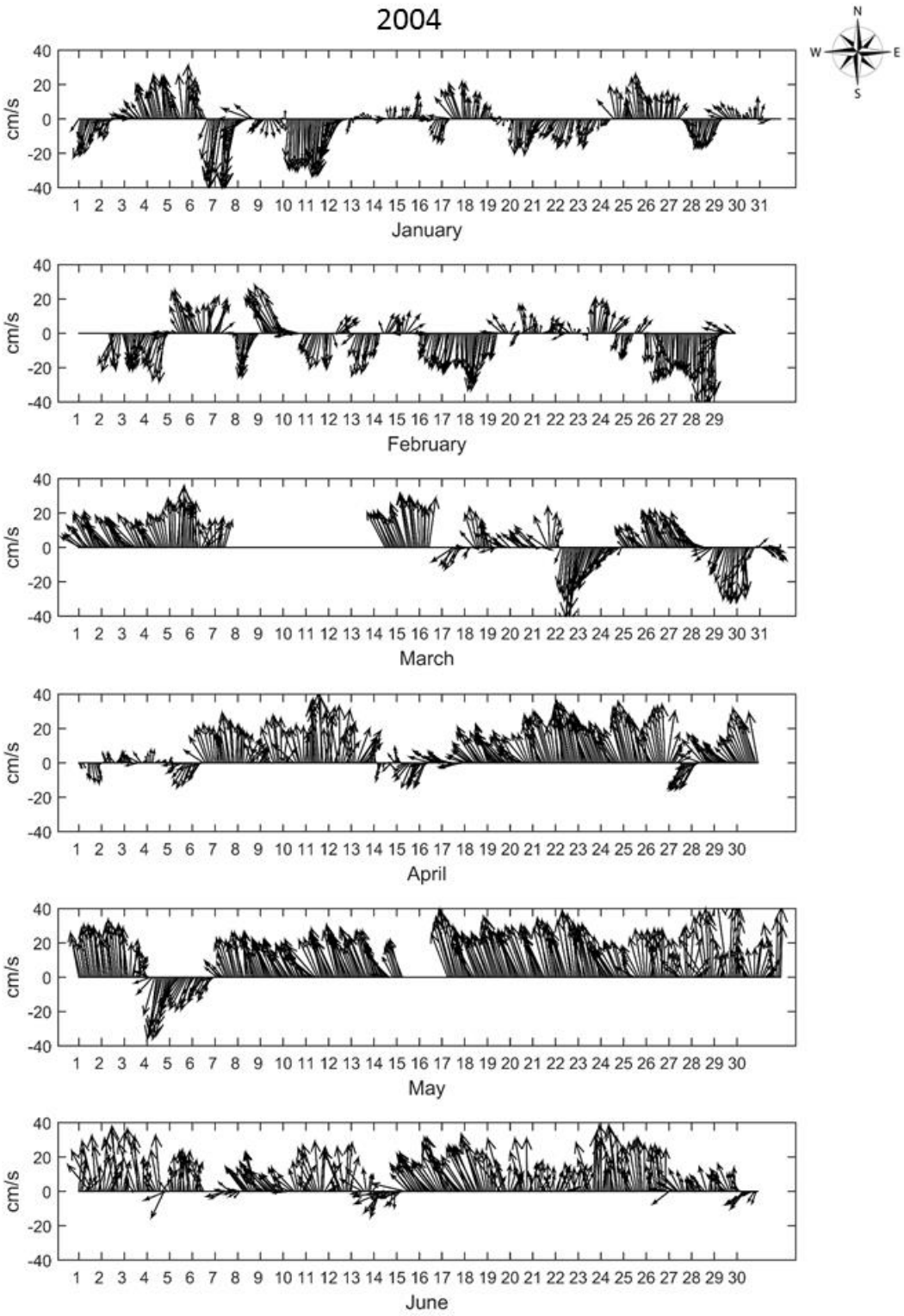

Figure 4.1 a. Time series of the velocity vectors for the upper layer of the depth normalized water column from January to June, 2004.

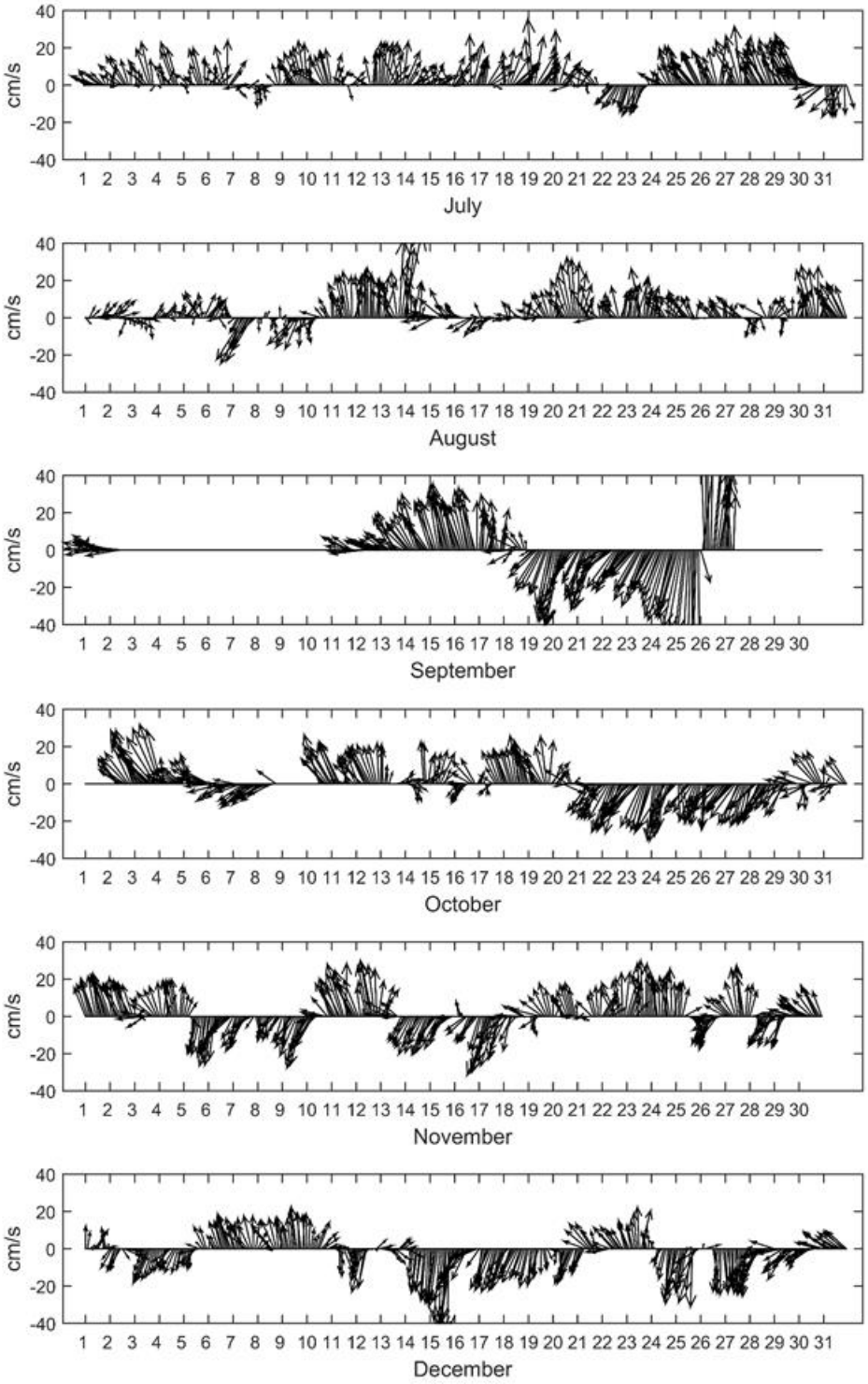

Figure 4.1 b. Time series of the velocity vectors for the upper layer of the depth normalized water column from July to December, 2004.

4.1 Mean vertical profiles and basic statistics

After normalizing the elevation of the longshore current bins for each of the ten years of record, it is found that the vertical profile changes constantly due to the wind forces and the storm presence. Monthly averages of the longshore vertical profile showed that during the winter months the surface currents are usually toward the south, and toward the north in the summer. In spring and fall, they are mixed, demonstrating a clear seasonality in both direction and intensity of the longshore current. Figure 4.2 presents the mean vertical profiles for the months of March, June, September and November for the ten years, where this seasonality is evident.

Yearly averages of the longshore and cross-shore vertical profiles do not reveal significant insight because the annual mean profile is the small result of many large positive (Northeast) and large negative (Southwest) values. Figure 4.3 presents the yearly mean profiles of longshore and cross-shore current for each of the ten years in the record. The net longshore surface current each year is directed towards the north; however, at the bottom of the water column, the net mean longshore currents appear to be to the south, although the elevation of the instrument and its blanking distance prevent measurements in the lower third of the water column. The mean profile of the longshore current usually shows larger absolute values in the upper layers of the water column than at the bottom for most of the years, generally showing one zero-crossing point below mid-depth. Similarly, the net cross-shore surface current over the ten years is directed onshore (west) showing one zero-crossing point, around 0.90 normalized elevation, characteristic of the return flow. For all the years the mean profile of the cross-shore current shows significant larger magnitudes in the upper layers of the water column than at the bottom.

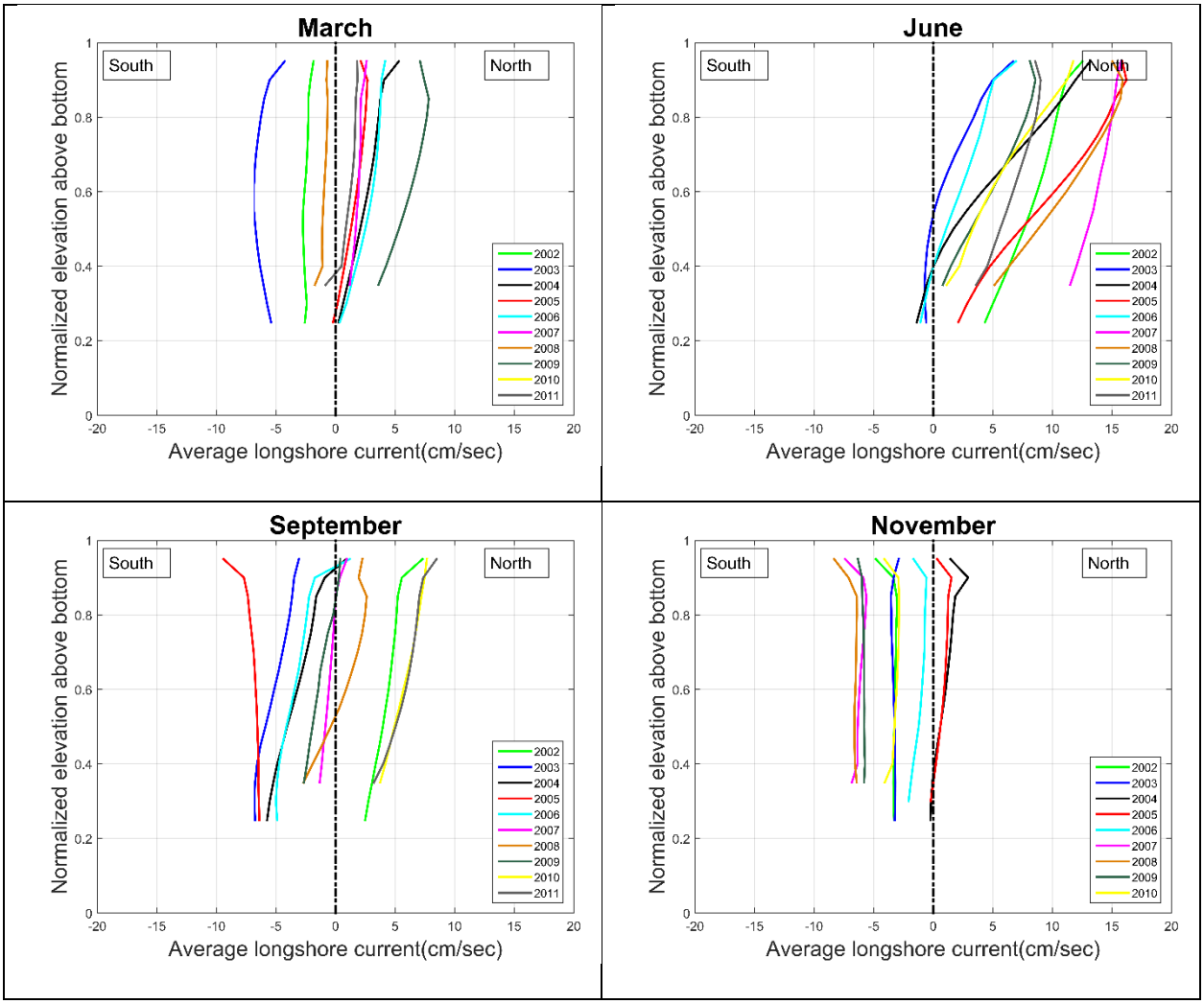

Figure 4.2. Mean depth-normalized profiles of the longshore current for the months of March, June, September and November.

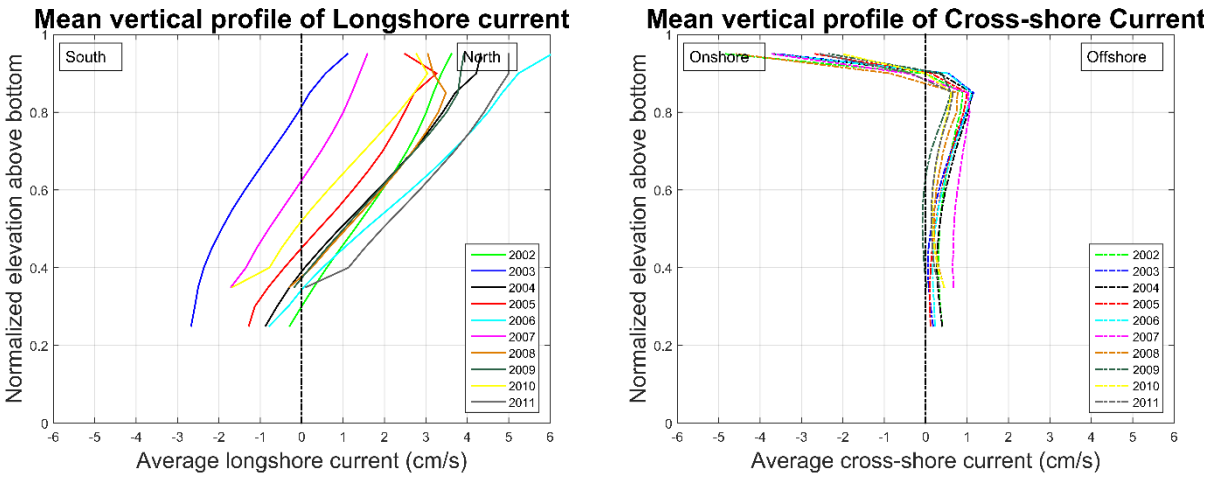

Figure 4.3. Annual mean depth-normalized profiles of the longshore current and cross-shore current.

The ten-year current record available was subjected to a yearly statistical analysis. First of all, five levels from the normalized water column, equally separated, are selected for this analysis. The closest level to the bottom is located at 0.35 normalized elevation, and the closest level to the water surface is located at 0.95. This approach reduces the number of levels through the water column from 20 to 5, facilitating the interpretation of the results while keeping enough information to illustrate the vertical structure of the currents.

Basic statistical properties, i.e. the mean, standard deviation, and maxima, were computed annually for the longshore current (positive going North), and the cross-shore current (positive going East). These results are summarized in Table 4.1. As expected for both the longshore and cross-shore currents, the largest values for the mean and standard deviation were found at the level closest to the surface.

Table 4.1: Annually based statistics for the longshore and cross-shore currents, including mean, standard deviation, and maxima values.

Year	Norm. elevation above the bottom	Longshore Current				Cross-shore Current			
		Mean (cm/s)	Standard Deviat. (cm/s)	Max North (cm/s)	Max South (cm/s)	Mean (cm/s)	Standard Deviat. (cm/s)	Max East (cm/s)	Max West (cm/s)
2002	0.95	3.6	15.6	55.4	-71.0	-4.8	6.2	49.5	-34.1
	0.8	3.0	13.5	64.1	-49.0	0.8	2.4	33.2	-35.9
	0.65	2.3	12.8	48.9	-47.6	0.5	1.8	29.9	-23.6
	0.5	1.3	11.8	48.1	-45.7	0.3	1.8	28.4	-20.2
	0.35	0.3	10.7	47.0	-46.4	0.3	2.0	30.8	-15.9
2003	0.95	1.1	15.5	47.0	-55.0	-3.6	5.7	23.8	-52.8
	0.8	-0.1	13.7	46.0	-50.6	1.0	2.4	33.6	-49.9
	0.65	-1.1	12.6	46.7	-48.9	0.5	2.0	33.3	-36.5
	0.5	-1.9	11.4	39.6	-49.1	0.1	1.9	27.3	-15.7
	0.35	-2.5	10.2	33.3	-49.0	0.1	2.1	17.2	-17.9
2004	0.95	4.3	16.9	124.7	-97.8	-3.7	5.6	22.2	-23.2
	0.8	3.4	14.9	117.1	-93.6	1.0	2.4	28.2	-17.9
	0.65	2.3	14.1	117.8	-95.4	0.6	2.1	28.4	-16.9
	0.5	0.9	13.1	119.8	-95.3	0.3	2.1	31.8	-10.2
	0.35	-0.3	12.0	118.7	-94.8	0.3	2.2	36.1	-8.9
2005	0.95	2.5	17.1	54.7	-54.0	-2.7	5.8	23.9	-27.6
	0.8	2.5	15.4	47.3	-47.0	0.9	2.5	24.2	-15.7
	0.65	1.6	14.5	43.5	-47.8	0.5	2.1	19.3	-21.8
	0.5	0.4	13.3	43.9	-48.9	0.2	2.1	17.4	-27.9
	0.35	-0.8	12.0	41.9	-47.0	0.1	2.3	15.2	-18.4
2006	0.95	6.0	16.1	48.3	-74.0	-3.7	5.8	22.6	-27.7
	0.8	4.5	14.4	52.1	-68.4	1.0	2.7	19.8	-15.9
	0.65	3.2	13.3	51.1	-65.8	0.5	2.1	18.6	-15.0
	0.5	1.5	12.0	47.3	-65.0	0.2	2.0	20.7	-10.6
	0.35	0.0	10.5	34.1	-63.9	0.2	2.3	16.3	-13.8
2007	0.95	1.6	16.9	49.6	-62.1	-3.7	6.8	28.4	-26.5
	0.8	1.0	14.4	48.0	-54.7	1.1	2.7	22.3	-14.1
	0.65	0.2	13.4	46.9	-52.1	0.8	2.1	17.3	-10.6
	0.5	-0.8	12.1	46.1	-48.2	0.7	2.0	16.8	-13.3
	0.35	-1.7	10.8	44.0	-46.0	0.7	2.2	15.1	-11.8
2008	0.95	3.0	17.5	63.1	-67.7	-4.6	6.4	30.6	-38.2
	0.8	3.3	15.9	66.8	-58.1	0.7	4.4	96.5	-103.9
	0.65	2.3	14.8	54.0	-55.9	0.3	3.2	81.2	-92.7
	0.5	1.1	13.3	47.4	-55.1	0.2	2.4	25.7	-23.7
	0.35	-0.3	11.4	36.9	-55.5	0.4	2.7	17.5	-12.9
2009	0.95	3.9	14.8	70.9	-68.0	-2.3	6.7	77.4	-82.8
	0.8	3.5	14.2	77.9	-56.4	0.5	4.7	130.9	-61.1
	0.65	2.3	13.2	54.1	-49.6	0.0	3.5	72.0	-48.6
	0.5	1.0	12.2	35.5	-46.5	-0.1	3.0	20.4	-19.0
	0.35	-0.2	10.7	33.5	-44.9	0.0	3.1	17.3	-14.8
2010	0.95	2.8	16.0	56.7	-67.3	-2.0	6.8	31.8	-37.1
	0.8	2.3	13.5	48.9	-55.0	0.5	4.4	32.1	-23.6
	0.65	1.1	12.2	43.3	-53.0	0.2	3.6	29.4	-20.5
	0.5	-0.2	10.9	37.6	-49.2	0.2	3.2	27.1	-17.5
	0.35	-1.7	9.7	31.0	-46.6	0.4	3.3	25.9	-16.3
2011	0.95	5.0	14.8	53.1	-98.7	-2.5	8.4	56.6	-47.8
	0.8	4.4	12.7	66.9	-87.8	0.6	4.6	50.0	-43.0
	0.65	3.3	11.5	51.3	-83.1	0.2	3.7	51.7	-32.7
	0.5	1.9	10.4	35.7	-81.2	0.1	3.4	46.1	-25.5
	0.35	0.1	9.2	33.2	-77.6	0.3	3.6	41.0	-23.1

For the longshore current, the largest north (positive) value is 124.7 cm/s and the largest south (negative) value is -97.8 cm/s both associated with the landfall of Hurricane Jeanne (September 26, 2004). For the cross-shore current, 2009 contains the largest east (positive) value of 130.9 cm/s and the largest west (negative) value of -103.9 cm/s. For both components, the standard deviation decreases in amplitude from the surface to the bottom, demonstrating that most of the variability occurs in the upper layers of the water column. The findings show that the resulting average flow for 2003 and 2007 is directed southward, and directed northward for the remainder of the years.

4.2 Volume flux

In addition to velocity profiles, it is germane and interesting to examine the total volume flux in the water column. Integrating the mean longshore and cross-shore currents over the water column produces the volume flux in each component,

$$Q_l = \sum_{i=1}^{N} V(z)\,\Delta z \quad ; \quad Q_c = \sum_{i=1}^{N} U(z)\,\Delta z \tag{4.1}$$

Where Q is the Volume flux ($\frac{m^3/s}{m}$), V is the time series of speed at the respective bin for the longshore current, U is that for the cross-shore current (m/sec), and Δz is the bin width (m).

Unfortunately, there are no velocity measurements close to the bottom due to the elevation of the instrument above the bed and its associated blanking distance. Therefore, the volume flux

for this study was computed only with the measured velocities from the first bin (closest to the instrument) to the last bin (closest to the water surface). Table 4.2 presents the longshore and cross-shore volume flux results for each one of the ten years in the record. As was shown in Figure 4.3, the mean vertical profile of the longshore current for most of the years was oriented toward the north, although 2003 and 2007 were southerly directed. Also, 2003 and 2007 were the only years with a total longshore volume flux toward the south. The total Q_l (net) longshore volume flux above the lowest bin for the ten years is 32,775 $\frac{m^3/s}{m}$. Although it is toward the north, an estimate of the volume flux near the bed is unobtainable. The Q_c results are more than an order of magnitude smaller (1,135 $\frac{m^3/s}{m}$) than the longshore volume flux results above the 1st bin, indicating an almost balanced cross-shore volume flux as should be expected given the proximity of the shore.

Figure 4.4 presents a day-long running average of the volume flux for 2003, where it is evident that Q_l is predominantly towards the south. The net cross-shore volume flux is an order-of-magnitude less. If measurements were available both above the uppermost bin (where wave-induced Stokes Drift takes place (Starr, 1947)), and between the blanking elevation and the bottom (expected to be offshore-directed), ideally the cross-shore volume flux would always be zero, unless there is large-scale circulation present (e.g. rip currents). Figure 5.2 shows the cross-shore Spatial Eigenfunctions of the vertical structure for the first EOF mode along the water column, showing a one zero-crossing between 0.60 and 0.70 normalized elevation. Figure 4.5 presents a similar plot for 2004, where Q_l is directed toward the north. The Q_c net appears to be offshore; however, once again this is problematic because of the lack of data in the extreme upper and lower parts of the water column.

Table 4.2: Annual total longshore and cross-shore volume fluxes for the 10-year record.

Year	Longshore Volume Flux $Q_l(net)$ $[\frac{m^3/s}{m}]$	Cross-shore Volume Flux $Q_c\,(net)$ $[\frac{m^3/s}{m}]$
2002	4,914	91
2003	-3,680	291
2004	4,961	610
2005	2,025	371
2006	5,049	271
2007	-175	297
2008	5,259	-448
2009	4,940	-263
2010	2,149	55
2011	7,314	-141
Total	**32,755**	**1,135**

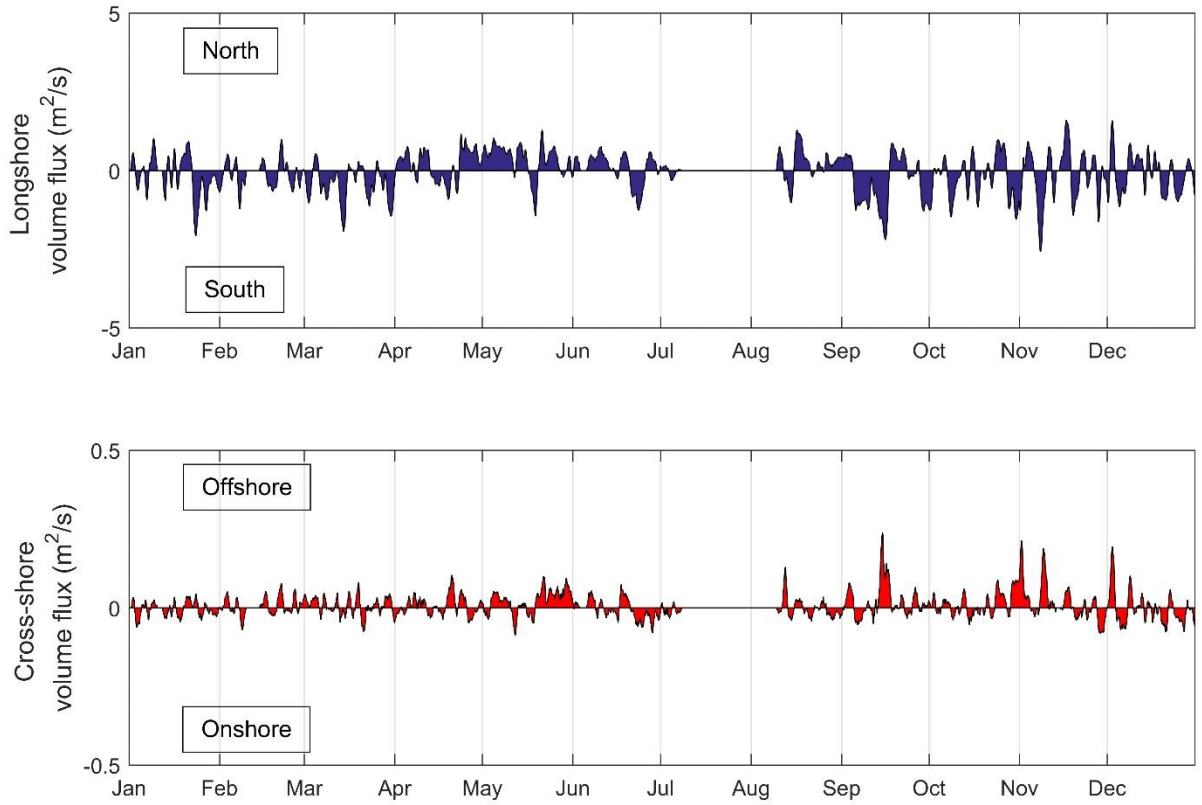

Figure 4.4. Daily running average of longshore volume flux and cross-shore volume flux for 2003, showing that the net longshore volume flux is towards the south and the net cross-shore volume flux is in order of magnitude less and ideally should be zero.

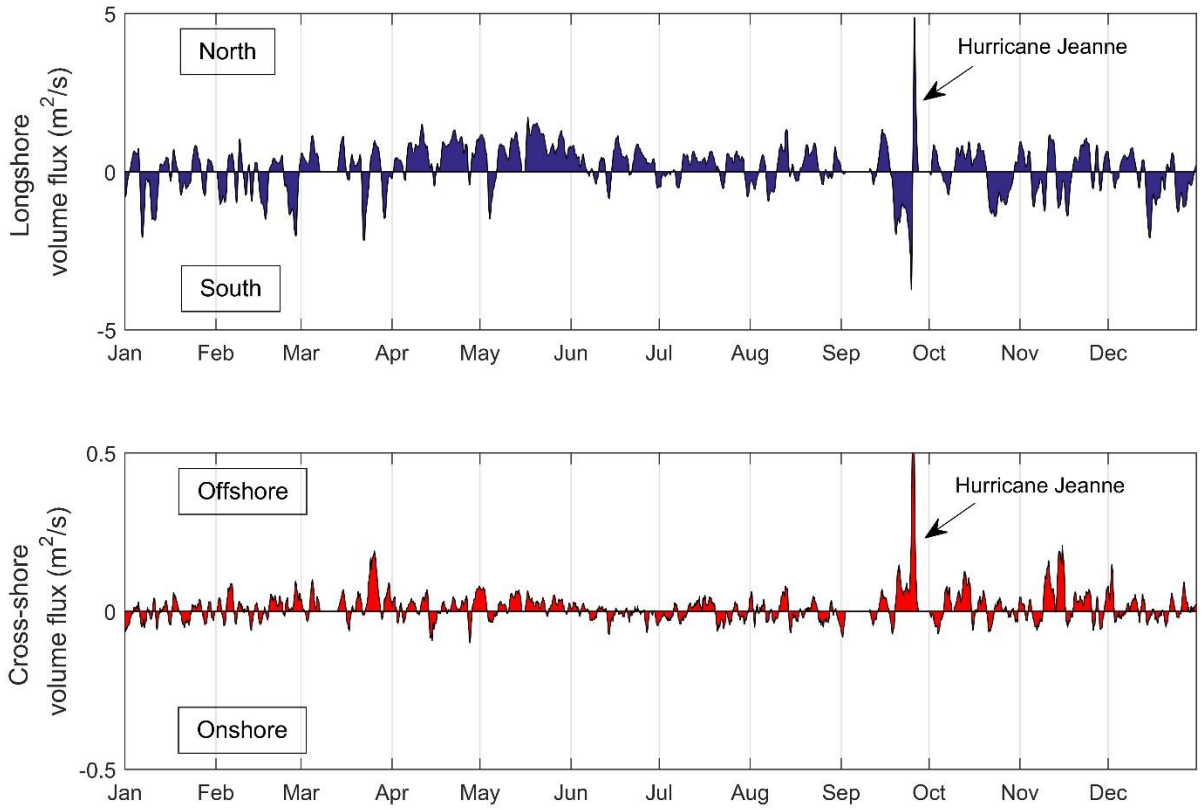

Figure 4.5. Daily running average of longshore volume flux and cross-shore volume flux for 2004, showing that the net longshore volume flux is directed toward the north, and the net cross-shore volume flux appears to be offshore.

Taking into consideration that the ADCP was installed relatively close to the shore, the cross-shore volume flux should always have shown a zero balance, due to the return flow. As mentioned, notable limitations are affecting these results, one being the inability to measure velocities close to the bed due to the instrument structure height and the blanking distance of the ADCP, which leaves out almost 25% of the water column. Another significant limitation encountered is the ADCP surface echo, which does not permit measurements of sufficient quality at the surface. Therefore, as waves pass there is no recorded data to account for the volume flux, Stokes Drift, they generate going onshore (Stokes, 1847). That volume would be returning offshore

in the lowest portion of the water column, which is going to influence the computed cross-shore volume flux toward offshore. The lower panel of Figure 4.5 shows how Hurricane Jeanne (September 21-26) has a large cross-shore volume flux going offshore. Therefore, to achieve a balance of zero, it would be necessary to measure the volume flux generated by the waves which are above the mean water level.

CHAPTER 5: EOF ANALYSIS OF LONGSHORE AND CROSS-SHORE CURRENT

Analysis of data consisting of a number of spatially distributed time series is known as multivariable analysis. With the current measurements rendered into a time series of vertical profiles of longshore and cross-shore components, stacked in a column of fixed normalized bins, the data are now in a form that easily lend themselves to this type of analysis. The method of Empirical Orthogonal Functions (EOF), also known as Principal Component Analysis (PCA) is a powerful statistical tool to study the variability in this type of data set. (Venegas, 2001). This analysis is defined in such a way that the first principal component has the largest possible variance (that is, it accounts for as much of the variability in the data as possible), and each succeeding component has the next lower variance under the constraint that it is orthogonal to the preceding components. The resulting vectors (eigenvectors) are an uncorrelated orthogonal basis set. The principal components are orthogonal because they are the eigenvectors of the covariance matrix, which is symmetric.

The present analysis will perform two separate EOF analyses, one for the cross-shore current component and other for the longshore current component. To prepare the data, we define the two matrices as ($\mathbf{V_{cross}}$) and ($\mathbf{V_{long}}$), with the same length in time, t = 1…N, where each point in time contains measurements of speed in the cross-shore and longshore directions respectively through the entire normalized water depth, m = 1…M; that is, there are M time series each of length N for each current component. First, the respective temporal mean is subtracted from the

$\mathbf{V_{cross}}$ & $\mathbf{V_{long}}$ time series at each normalized depth before performing the EOF analysis (covariance matrix approach). The dimensions of $\mathbf{V_{cross}}$ & $\mathbf{V_{long}}$ data arrays are N x M, where N rows are the times (t) of the data, and M columns are the normalized depths. Thus, the covariance is calculated from the following matrixes:

$$\mathrm{Cov}(V_{cross},V_{cross}) = E[V_{cross} \,.\, V_{cross}] - E[V_{cross}] \,.\, [V_{cross}] \quad (5.1)$$

$$\mathrm{Cov}(V_{cross},V_{long}) = E[V_{cross} \,.\, V_{long}] - E[V_{cross}] \,.\, [V_{long}] \quad (5.2)$$

$$\mathrm{Cov}(V_{long},V_{cross}) = E[V_{long} \,.\, V_{cross}] - E[V_{long}] \,.\, [V_{cross}] \quad (5.3)$$

$$\mathrm{Cov}(V_{long},V_{long}) = E[V_{long} \,.\, V_{long}] - E[V_{long}] \,.\, [V_{long}] \quad (5.4)$$

Where $E[V_{cross}]$ is the expected value of $\mathbf{V_{cross}}$, (i.e. the mean), and $E[V_{long}]$ is the expected value of $\mathbf{V_{long}}$. The present analysis will focus on the inner product $\langle V_{long}, V_{long} \rangle$ or $\mathrm{Cov}\langle V_{long}, V_{long} \rangle$ and the inner product $\langle V_{cross}, V_{cross} \rangle$ or $\mathrm{Cov}\langle V_{cross}, V_{cross} \rangle$. These operations produce two symmetric and square matrices of covariance each one with dimensions M x M, which contain the entire set of linear interrelationships among the cross-shore and longshore speeds over the water column above the instrument's head. Then, to reduce this M-dimensional problem, the EOF analysis is performed per each year of the 10-year record. The square matrix S has dimensions of M x M, where its column vectors S^k are the eigenvectors of the covariance matrix for the cross-shore and longshore component, with K being the modes of the EOF decomposition. Each eigenvector S^k (dimensions of M x 1, where M is the number of normalized bin elevations) represents the spatial EOF pattern of mode k. Table 5.1 displays the EOF analysis results for the first three modes for each of the 10 years of measurements.

$$S = \begin{bmatrix} S_1^1 & S_1^2 & \dots S_1^M \\ S_2^1 & S_2^2 & \dots S_2^M \\ S_M^1 & S_M^2 & \dots S_M^M \end{bmatrix} \quad ; \text{Where } S^k \text{ is the Spatial Eigenfunction} \qquad (5.5)$$

Table 5.1: Eigenfunction analysis of the covariance matrix for the cross-shore and longshore current from 2002 to 2011, providing the first three EOF modes with their respective variances and the cumulative variances.

Year	EOF mode	Cross-shore Current			Longshore Current		
		Eigenvalue	Eigenvalues variance (%)	Eigenvalues cumulative variance (%)	Eigenvalue	Eigenvalues variance (%)	Eigenvalues cumulative variance (%)
2002	EOF-1	153.35	93.50	93.50	5910.70	99.30	99.30
	EOF-2	9.73	5.90	99.40	25.40	0.40	99.70
	EOF-3	0.83	0.50	99.90	14.00	0.20	99.90
2003	EOF-1	145.8	89.90	89.90	8311.90	99.10	99.10
	EOF-2	14.96	9.20	99.10	62.90	0.70	99.80
	EOF-3	1.15	0.70	99.80	9.90	0.10	99.90
2004	EOF-1	131.86	86.30	86.30	8110.30	99.00	99.00
	EOF-2	19.46	12.70	99.00	61.70	0.80	99.80
	EOF-3	1.22	0.80	99.80	18.30	0.19	99.99
2005	EOF-1	152.61	92.80	92.80	8119.10	99.50	99.50
	EOF-2	10.81	6.50	99.30	26.40	0.30	99.80
	EOF-3	0.95	0.60	99.90	15.90	0.19	99.99
2006	EOF-1	183.23	90.00	90.00	7461.10	99.40	99.40
	EOF-2	19.06	9.40	99.40	31.50	0.30	99.70
	EOF-3	1.06	0.50	99.90	14.30	0.20	99.90
2007	EOF-1	127.60	92.70	92.70	4586.70	99.40	99.40
	EOF-2	9.67	7.00	99.70	15.30	0.30	99.70
	EOF-3	0.23	0.20	99.90	7.60	0.20	99.90
2008	EOF-1	168.83	90.40	90.40	9372.70	99.30	99.30
	EOF-2	16.33	8.70	99.10	51.00	0.50	99.80
	EOF-3	1.08	0.60	99.70	9.80	0.10	99.90
2009	EOF-1	103.05	87.90	87.90	3820.00	98.60	98.60
	EOF-2	12.98	11.10	99.00	45.70	1.20	99.80
	EOF-3	0.92	0.80	99.80	1.60	0.10	99.90
2010	EOF-1	88.72	89.30	89.30	6443.60	99.20	99.20
	EOF-2	10.00	10.10	99.40	35.90	0.60	99.80
	EOF-3	0.52	0.50	99.90	8.40	0.10	99.90
2011	EOF-1	257.74	94.60	94.60	4491.50	98.2	98.20
	EOF-2	13.85	5.10	99.70	67.70	1.5	99.70
	EOF-3	0.55	0.20	99.90	10.10	0.2	99.90

After performing the EOF analysis for each year of the 10-year record, it is found that mode-1 of the longshore current accounts for more than 98% of the total variance each year for all ten years, whereas about 2% of the total variance is explained by the higher-order modes. Similarly, mode-1 of the cross-shore current accounts for more than 86% of the total variance each year, mode-2 accounts for more than 5% of the total variance, and 9% of the total variance is explained by the higher-order modes. For the cross-shore current two modes were required to reach the 90% of total variance, a reasonable threshold for truncating an EOF expansion (Venegas, 2001).

Figures 5.1 a, b and c present the vertical structure of the first two spatial EOF modes for each year of the ten-year record of longshore and cross-shore currents. For the longshore current, mode-1 exhibits most of the variability at the upper layers of the normalized water column, with a significant reduction in variability at the bottom. Similarly, mode-2 displays most of the variability at the upper part of the normalized water column and a significant reduction in variability at the bottom. The mode-2 of the longshore current shows one zero-crossing between 0.75 and 0.85 normalized elevation showing phase opposition of the surface and bottom layers. Mode-1 of the cross-shore current also exhibits most of the variability at the upper layers of the normalized water column, and a small reduction in variability at the bottom, but with phase opposition of the surface and bottom layers. Additionally, the cross-shore mode-1 shows one zero-crossing between 0.60 and 0.70 normalized elevation, which is physically consistent with the idealized solution of wind blowing over a bounded domain, as it is shown in Figure 5.2. Mode-2 of the cross-shore current exhibits most of the variability in the upper part of the normalized water column and a small

reduction in variability at the bottom. Mode-2 consistently shows two zero-crossing points, between 0.80 and 0.90 and between 0.40 and 0.50 normalized elevation.

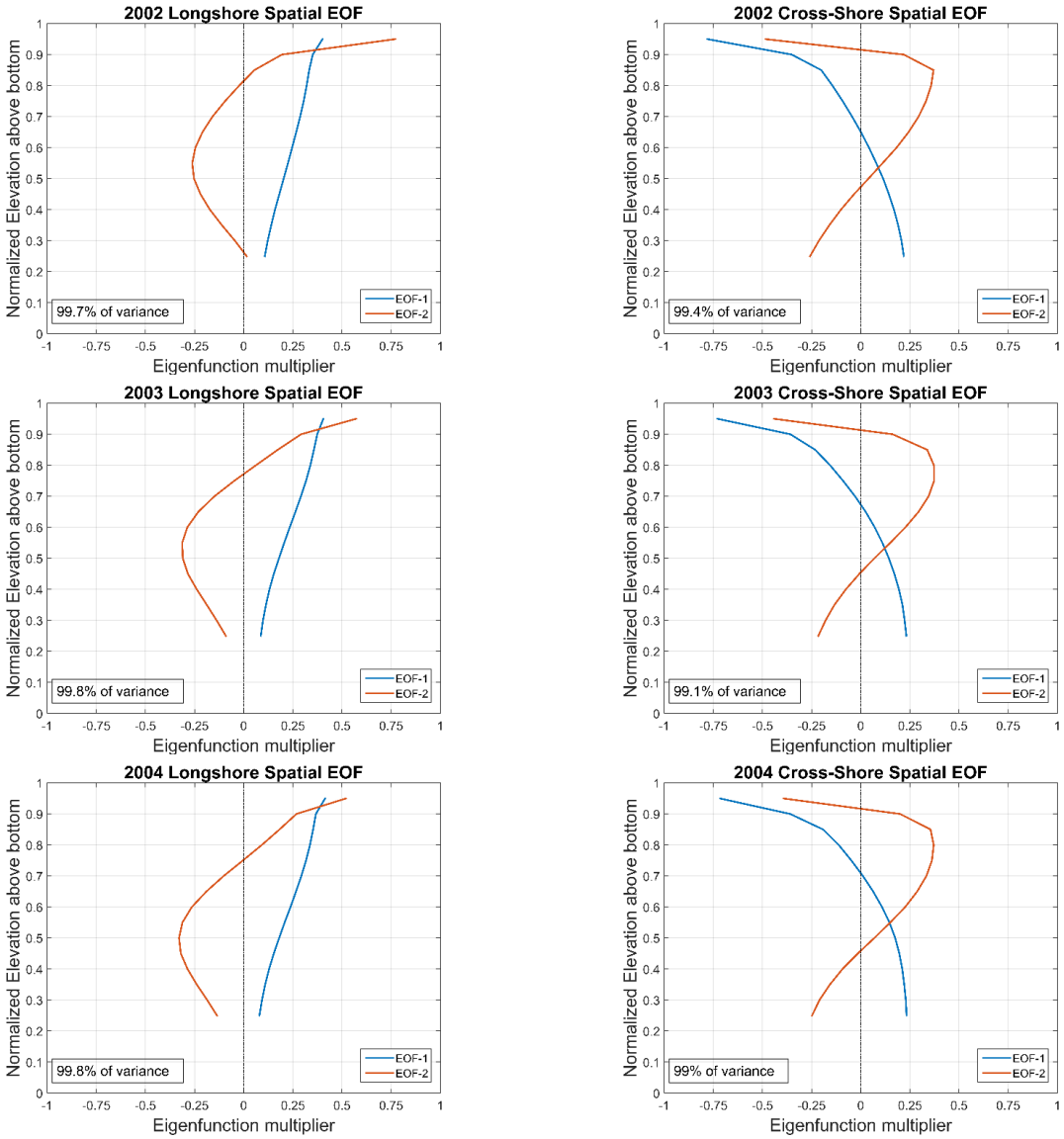

Figure 5.1. Longshore and cross-shore Spatial Eigenfunctions showing the vertical structure for the EOF mode-1 and mode-2 along the water column accounting for more than the 99% cumulative variance (continued).

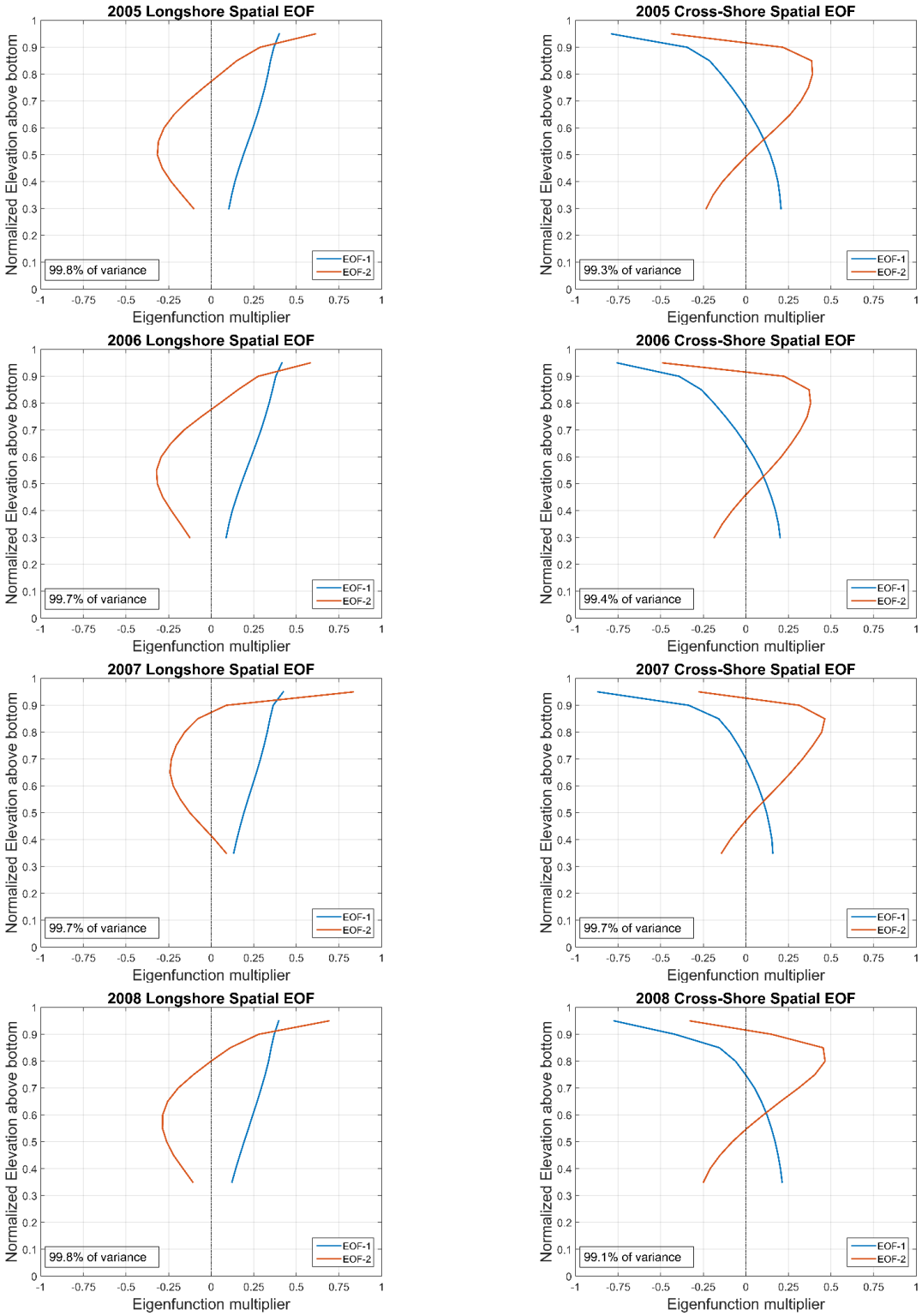

Figure 5.1. Longshore and cross-shore Spatial Eigenfunctions showing the vertical structure for the EOF mode-1 and mode-2 along the water column accounting for more than the 99% cumulative variance (continued).

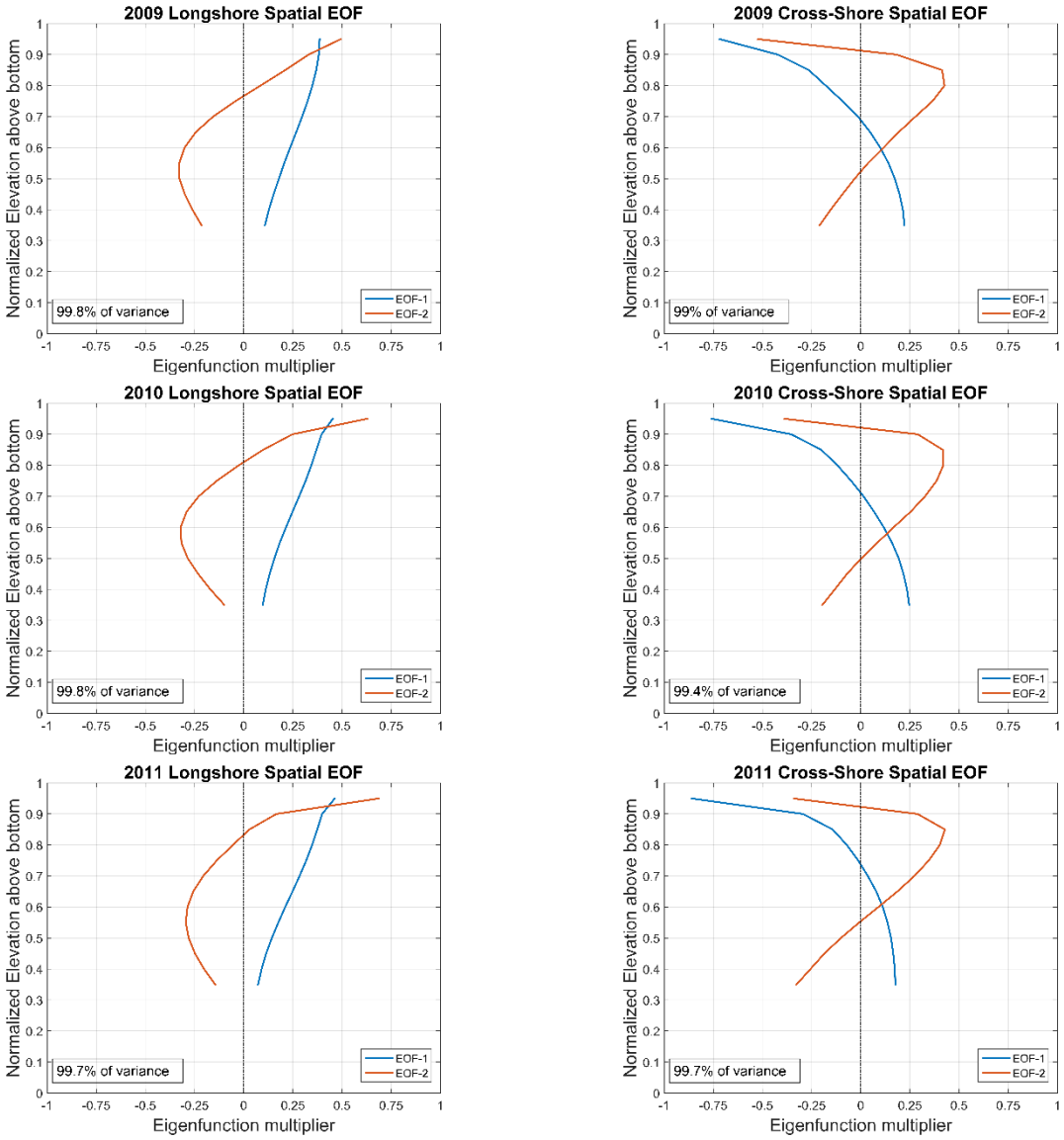

Figure 5.1. Longshore and cross-shore Spatial Eigenfunctions showing the vertical structure for the EOF mode-1 and mode-2 along the water column accounting for more than the 99% cumulative variance (concluded).

Figure 5.2 shows the normalized vertical structure of the 1^{st} spatial eigenfunctions of the longshore and cross-shore current profiles for the entire record, the similitude of the 1^{st} spatial eigenfunctions for the ten years is quite remarkable.

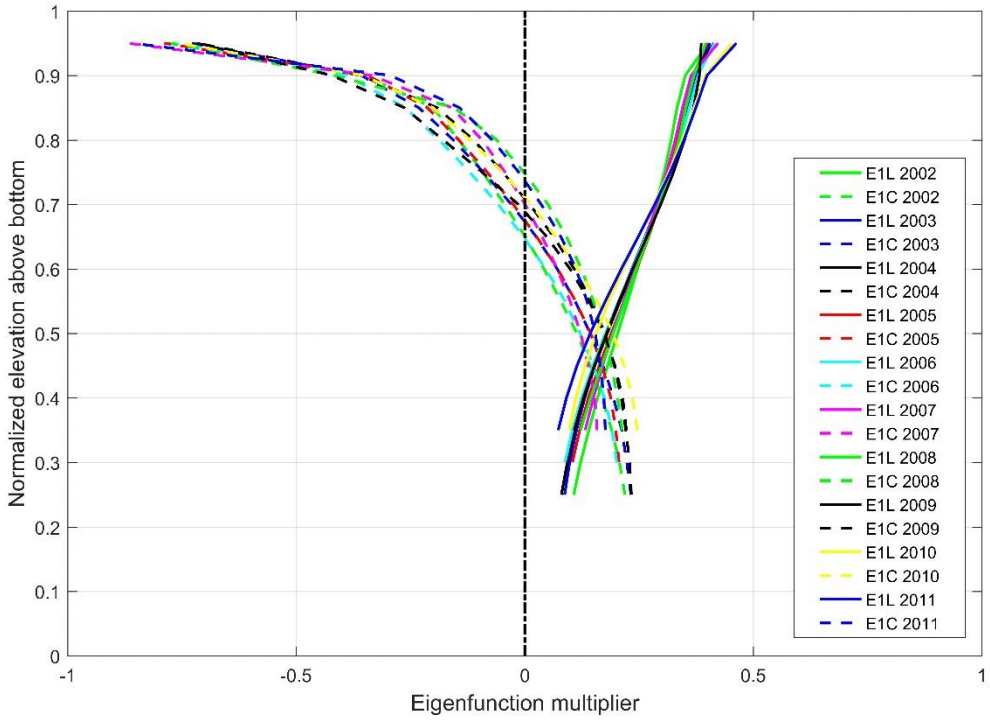

Figure 5.2. Ten years of Spatial Eigenfunctions showing the vertical structure for the first spatial EOF modes through the water column, with more that 98% cumulative variance and Cross-shore Spatial Eigenfunctions showing the vertical structure for the first EOF mode along the water column with more that 86% cumulative variance.

The general 3D structure of the nearshore currents can be reconstituted by combining the longshore and cross-shore modes at each normalized bin elevation. Figure 5.3 presents the 3D vertical structure of the EOF mode-1 and EOF mode-2 for each of the 10 years where it is evident that most of the variability occurs in the upper layers of the water column with a clockwise rotation with depth, and with significant reductions in amplitude at the bottom. This structure is expected due to the effect of a bottom-friction dominated bottom boundary layer (Munchow and Chant, 2000). Figure 5.4 shows overhead views of the representation of the mode-1 for every year. It clearly illustrates that there is a rotation of the current to the right (clockwise) in the surface Ekman layer sense for every one of the ten years. This angle increases with depth and the variance

decreases with depth below the surface. Applying Ekman's theory in the case of an ocean of finite depth, for our case, h is ~ 8.5m, which is considered a shallow water depth, and D is ~ 75 m (a very common mean value of D according to Ekman); the angle between the wind and the surface-current depends on the ratio h/D, which in this case is very small (~ 0.11). As a result, the surface current should follow the wind direction.

The 3D representation of the EOF mode-2 shows most of the variability in the upper part of the normalized water column with a significant reduction in variability at the bottom, also with a clockwise rotation with depth. Similar EOF mode-1 and mode-2 results were found by Cosoli, Gaˇcic, and Mazzoldi (2008) for measurements taken in 17 m of water nominally 14.6 km from the coast. They interpreted the 3D vertical structure of the EOF mode-1 as the barotropic mode of the system, which represents a flow in which the density depends only on the pressure, and the EOF mode-2 as a baroclinic induced structure, where temperature and salinity contribute to the dominantly horizontal stratification.

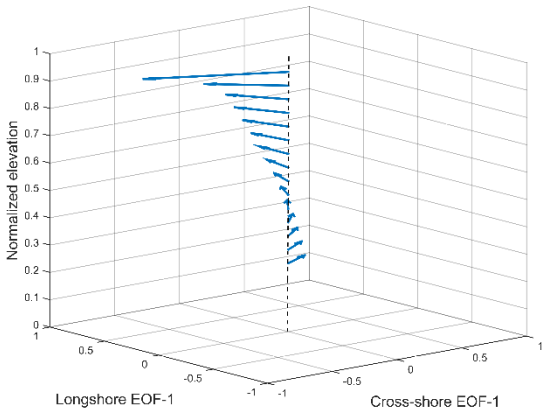

2002 EOF mode-1

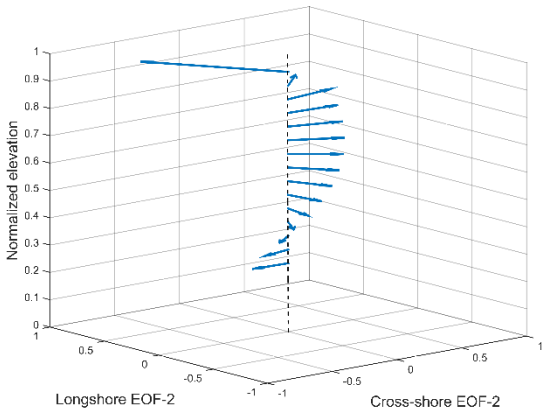

2002 EOF mode-2

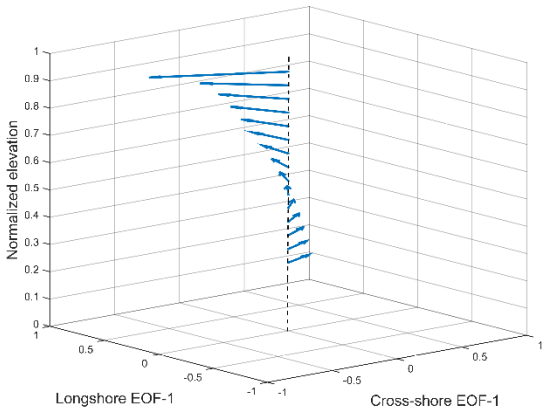

2003 EOF mode-1

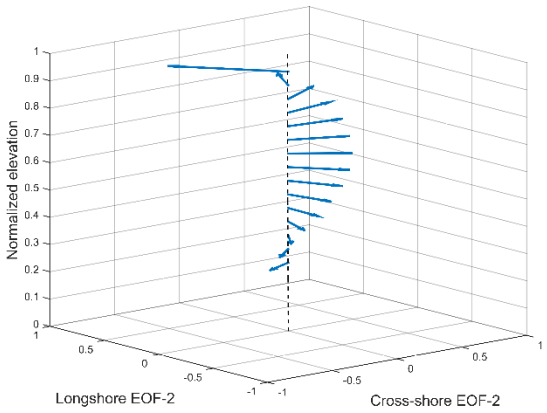

2003 EOF mode-2

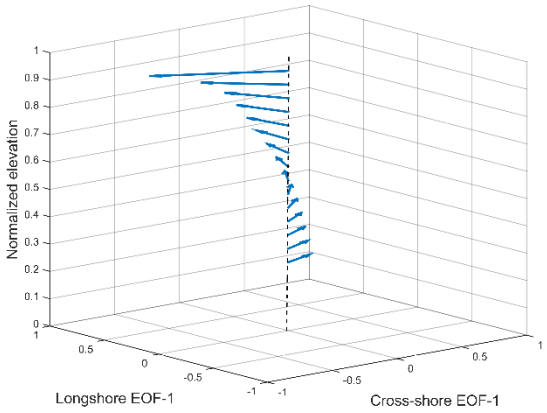

2004 EOF mode-1

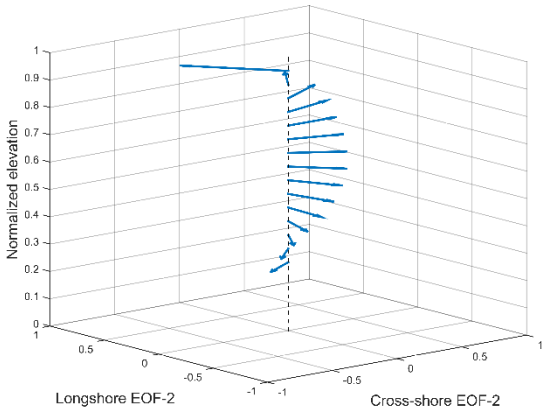

2004 EOF mode-2

Figure 5.3. Annually based 3D vertical structure of the water column for the EOF mode-1 and mode-2, accounting for more than the 99% cumulative variance (continued).

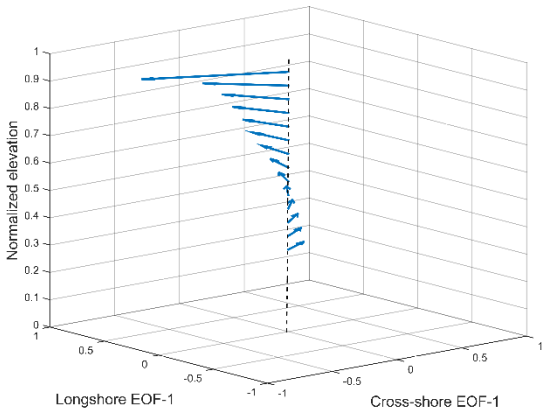

2005 EOF mode-1

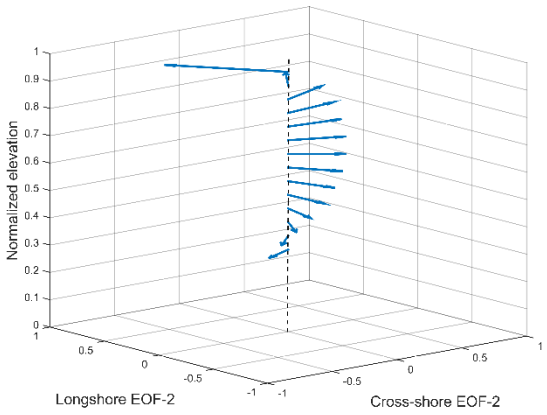

2005 EOF mode-2

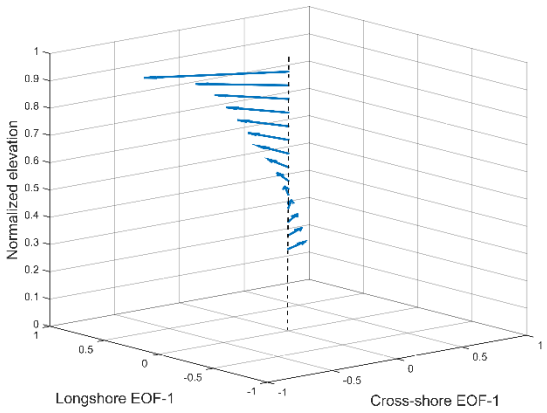

2006 EOF mode-1

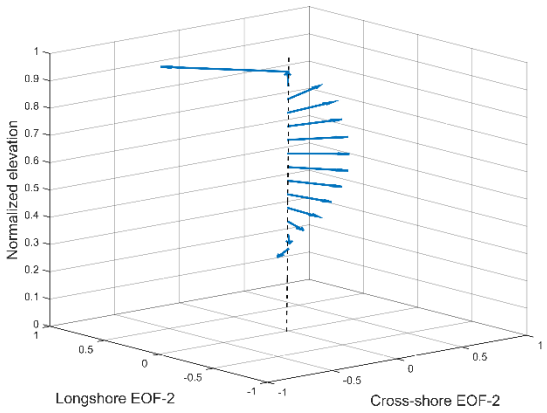

2006 EOF mode-2

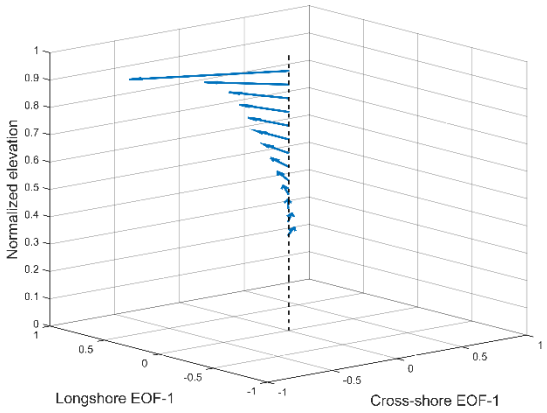

2007 EOF mode-1

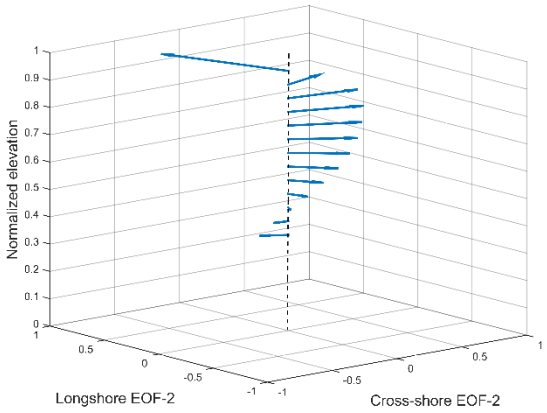

2007 EOF mode-2

Figure 5.3. Annually based 3D vertical structure of the water column for the EOF mode-1 and mode-2, accounting for more than the 99% cumulative variance (continued).

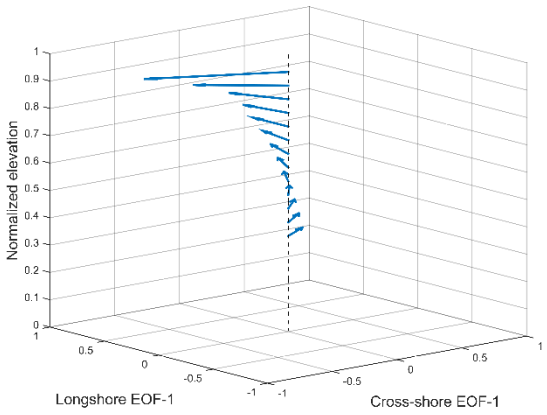

2008 EOF mode-1

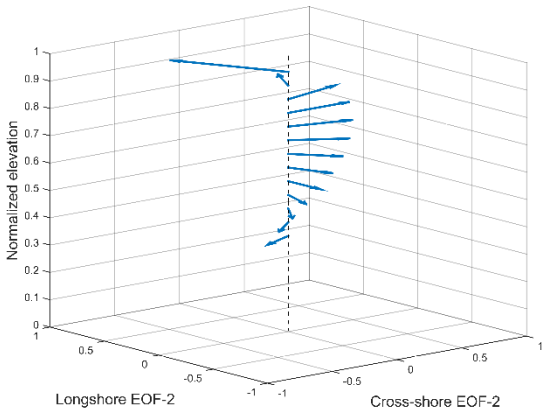

2008 EOF mode-2

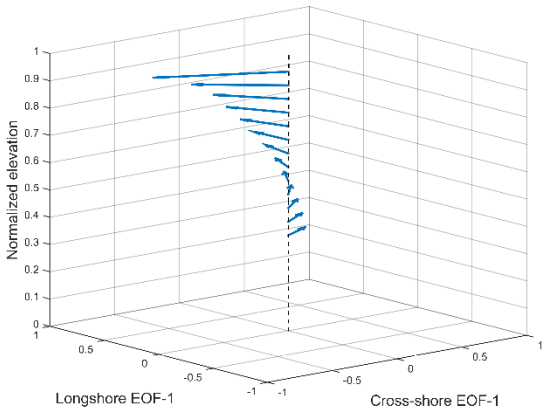

2009 EOF mode-1

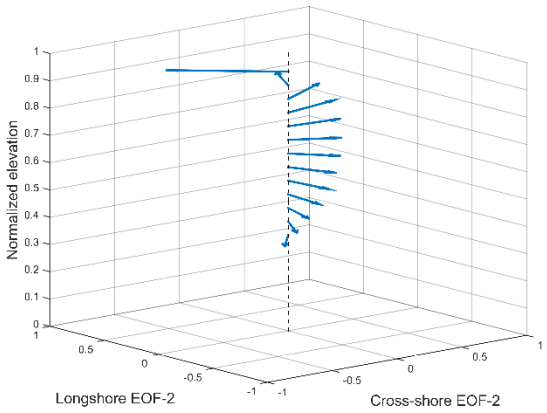

2009 EOF mode-2

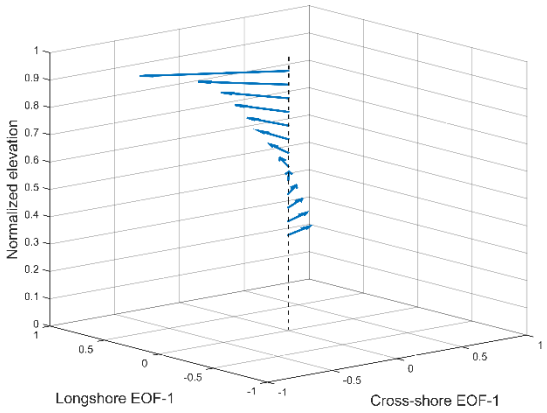

2010 EOF mode-1

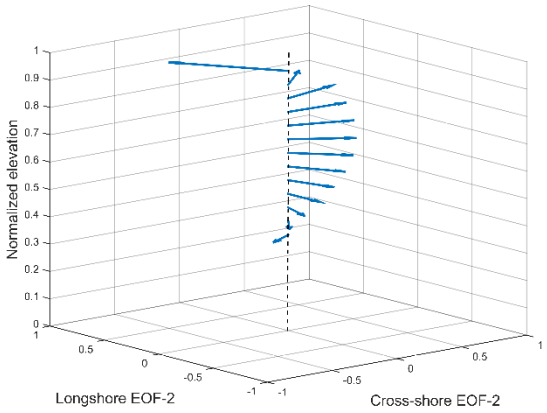

2010 EOF mode-2

Figure 5.3. Annually based 3D vertical structure of the water column for the EOF mode-1 and mode-2, accounting for more than the 99% cumulative variance (continued).

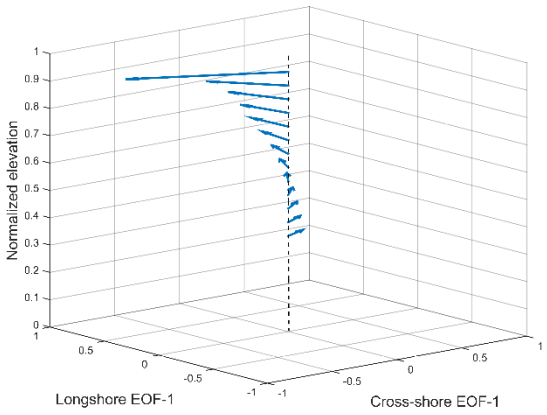

2011 EOF mode-1

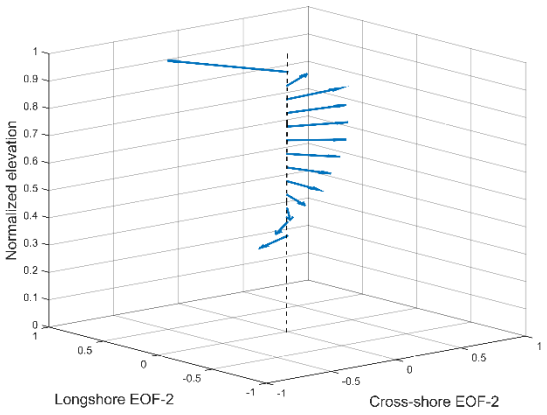

2011 EOF mode-2

Figure 5.3. Annually based 3D vertical structure of the water column for the EOF mode-1 and mode-2, accounting for more than the 99% cumulative variance (concluded).

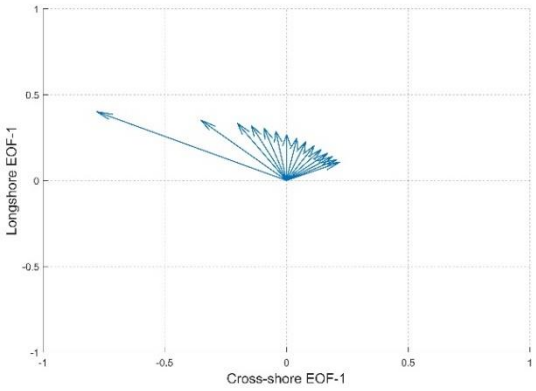

2002 EOF mode-1

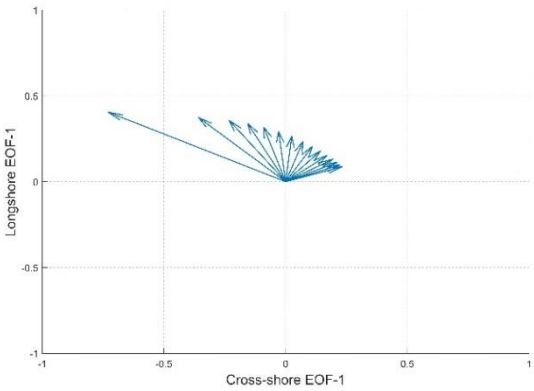

2003 EOF mode-1

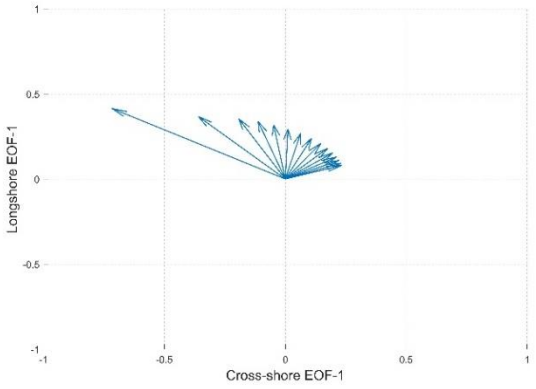

2004 EOF mode-1

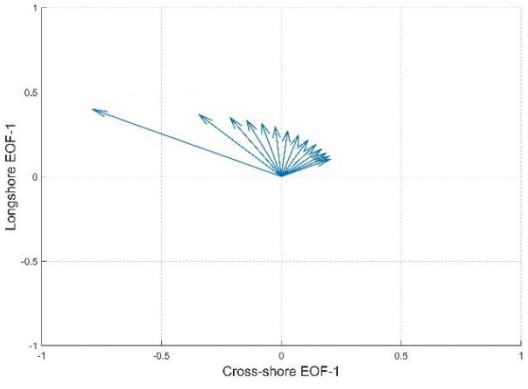

2005 EOF mode-1

Figure 5.4. Annually based overhead view of the vertical structure of the variance in the water column for the EOF mode-1 (continued).

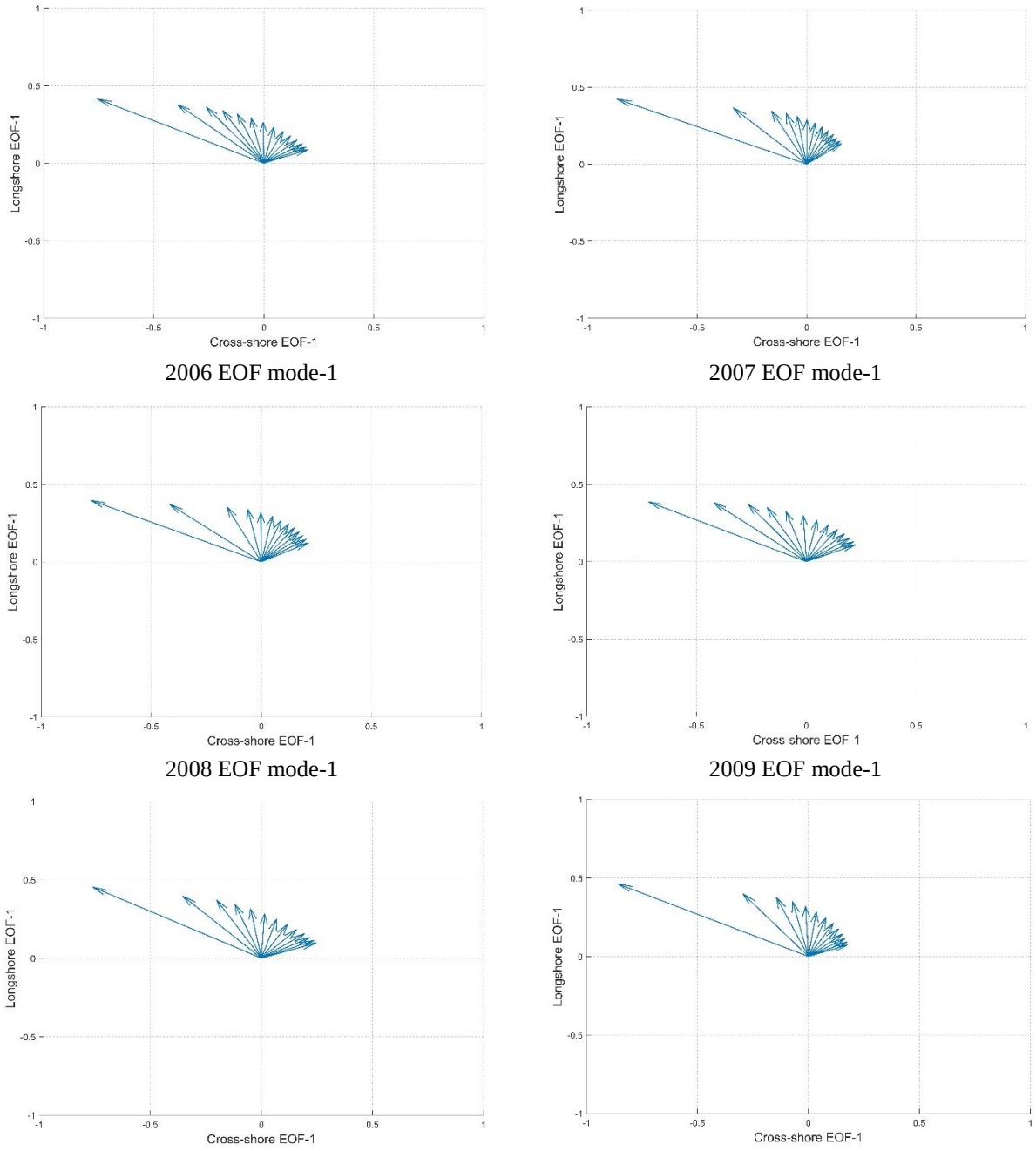

Figure 5.4. Annually based overhead view of the vertical structure of the variance in the water column for the EOF mode-1 (concluded).

Reducing the dimensionality of the system provides a new "optimal" coordinate system with which examine the temporal patterns in the data. Consequently, the data were reconstituted applying an inner product to obtain the Temporal Eigenfunctions.

$$T_{rk} = \sum_{i}^{n} O_{ki}(t) * S_{ri} \tag{5.6}$$

Where, T_{rk} = Temporal Eigenfunction, O_{ki} (t) is the demeaned $\mathbf{V_{cross}}$ and $\mathbf{V_{long}}$ matrices from t=1…N, r is the temporal mode function, k is the time of the observation, *i* is the eigenvector number, n is the total number of temporal eigenvectors.

Principal Component Analysis is used to study complex data sets by keeping enough factors to account for 90% or more of the variation in the data. In the present case, it allows representation of the data using only the first three spatial and temporal eigenvectors to examine the evolution of the data while accounting for nominally 99% of the variance in both components.

Figure 5.5 and 5.6 present annual time series for 2004 of long-shore temporal eigenfunctions and cross-shore temporal eigenfunctions respectively for the first three EOF modes, which encapsulate 99% of the total variance. As expected, the 1^{st} temporal eigenfunctions (TL1 & TC1) represent the largest variability for the total year (99% and 86.30%); the 2^{nd} temporal eigenfunction (TL2 & TC2) less variability (0.80% and 12.70%), and the 3^{rd} temporal eigenfunction (TL3 & TC3) even smaller variability (0.19% and 0.80%).

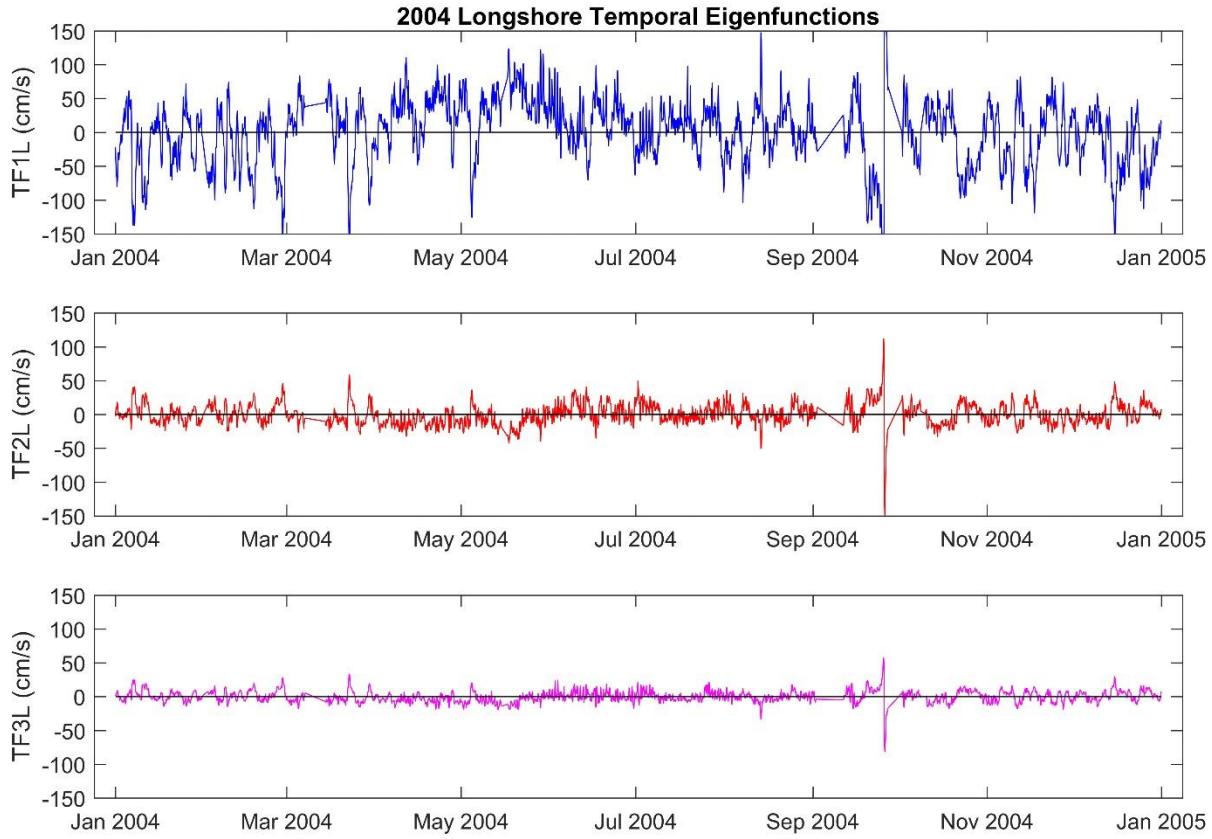

Figure 5.5. Long-shore Temporal Eigenfunctions for the first three EOF modes for 2004.

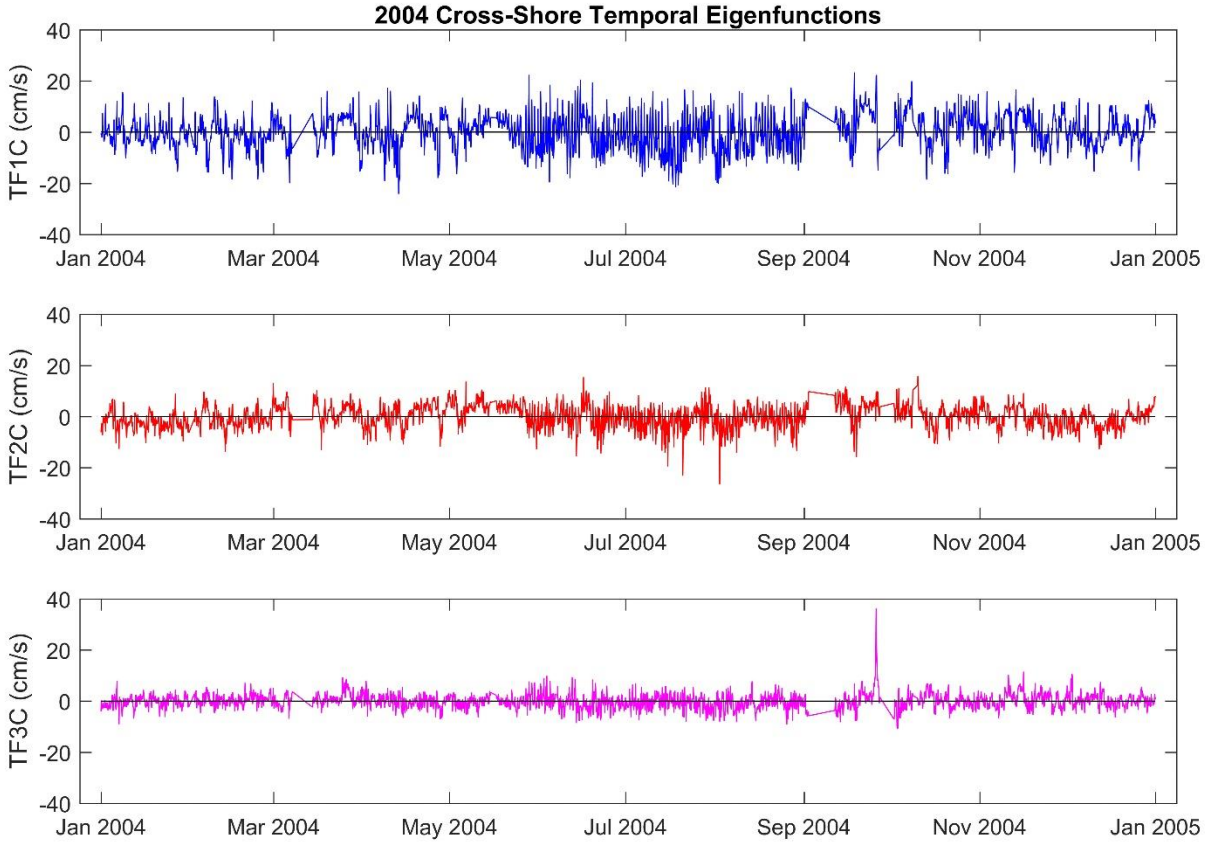

Figure 5.6. Cross-shore Temporal Eigenfunctions for the first three EOF modes for 2004.

Figure 5.7 (a) and (b) present the three Temporal Eigenfunctions for January 2004, whereas Figure 5.8 (a) and (b) show those for June 2004 to illustrate the seasonal behavior of the currents. As one might expect, a typical winter month (January), would have dominant longshore currents to the south (negative values), due to strong northerly winds, and a typical summer month (June), would have a prevailing longshore current to the north (positive values).

(a)

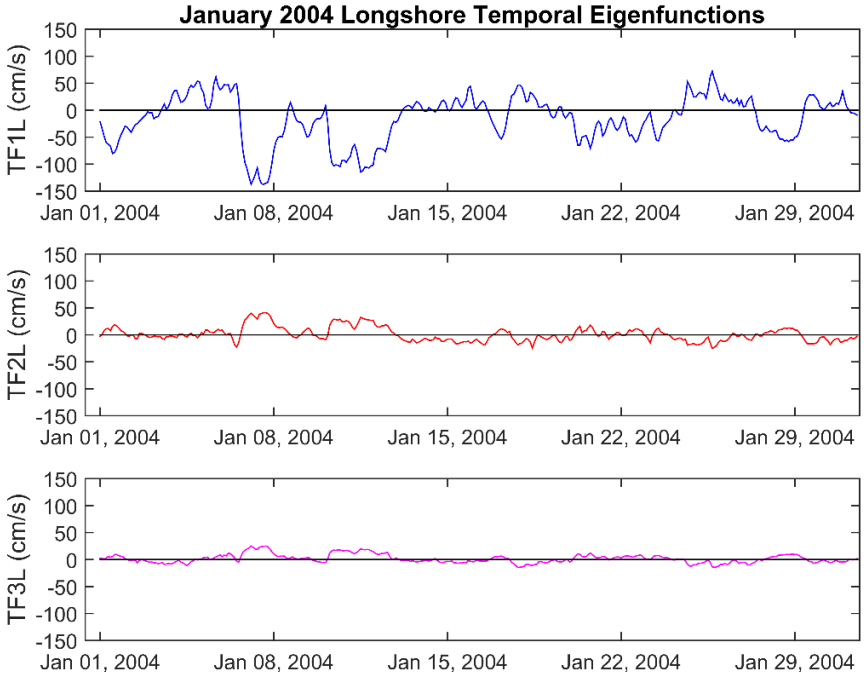

(b)

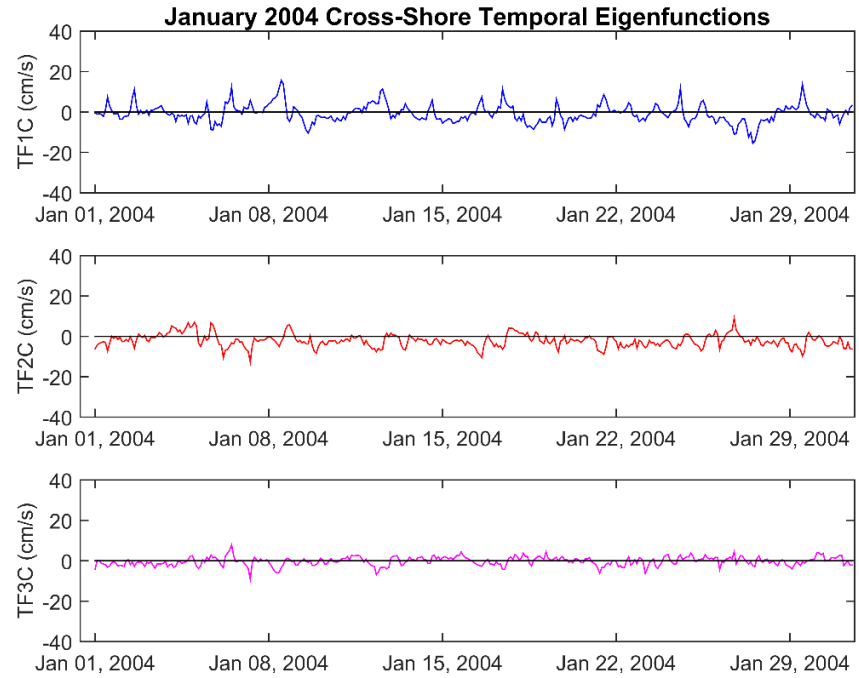

Figure 5.7. Temporal Eigenfunctions for the first three EOF modes of January 2004 a) Longshore, b) cross-shore.

(a)

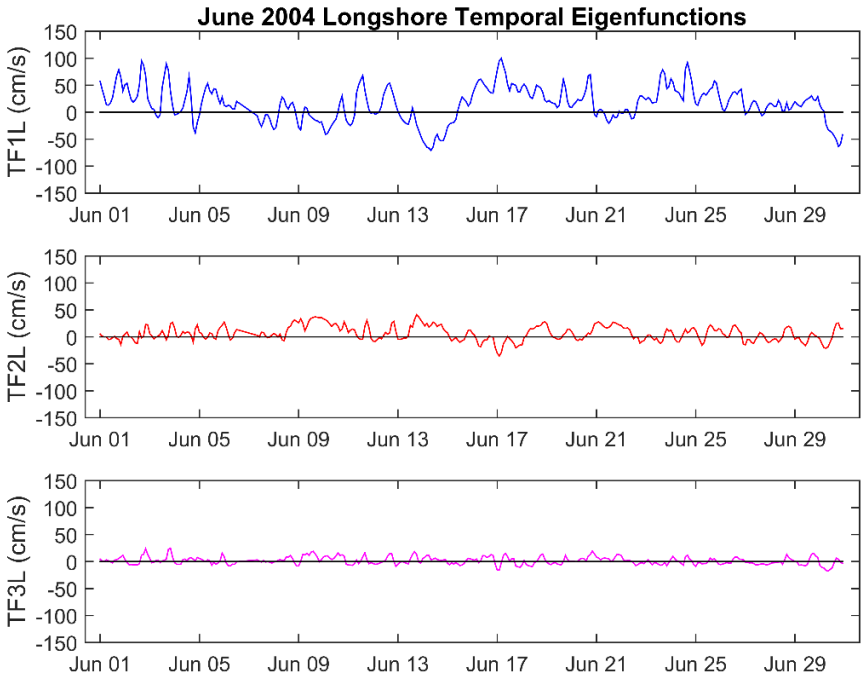

(b)

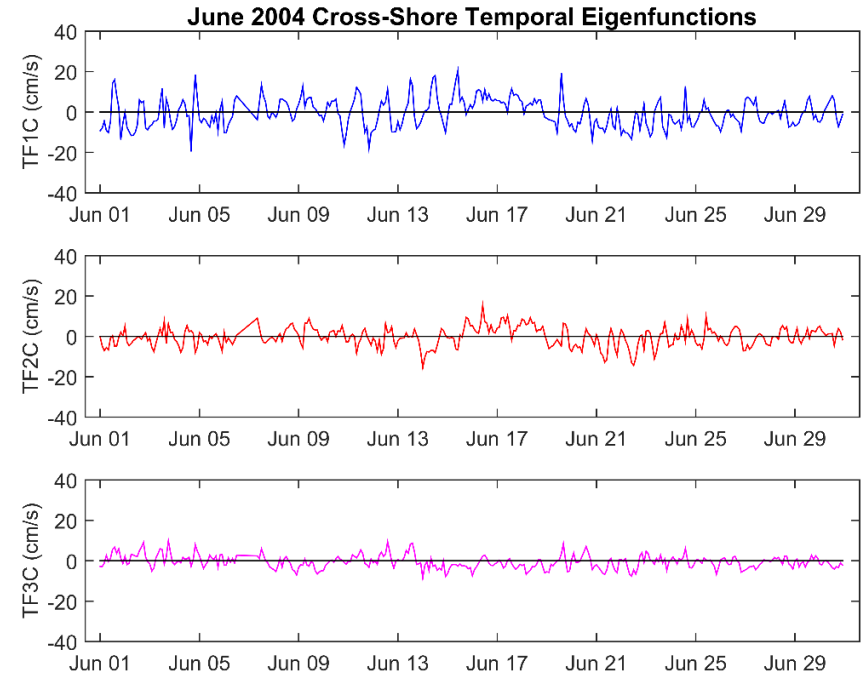

Figure 5.8. Temporal Eigenfunctions for the first three EOF modes of June 2004 a) Longshore, b) cross-shore.

Figure 5.9 presents the time series of the 1^{st} temporal eigenfunction for the longshore current during 2004, showing the behavior over time in the top panel. If each longshore current profile is first vertically averaged it is found that the 1^{st} temporal eigenfunction (upper panel) closely mimics the vertically averaged longshore current (lower panel) with a 0.99 correlation. Figure 5.10 presents the time series of the 1^{st} temporal eigenfunction for the cross-shore current (upper panel) pattern over time, as well as that for the vertically averaged cross-shore current (lower panel). The 1^{st} Temporal Eigenfunction shows little correlation (-0.09) with the vertically averaged cross-shore current. This is expected because the vertically averaged cross-shore current ideally is very small due to the balance between the onshore flow and the return flow characteristic of the nearshore cross-shore current.

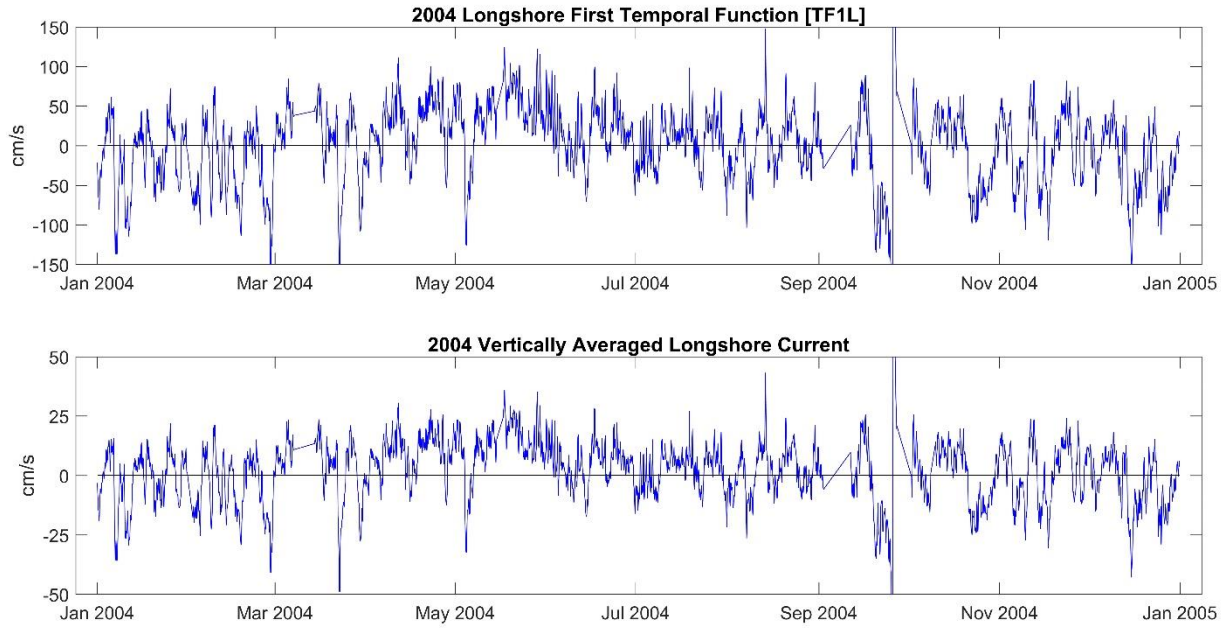

Figure 5.9. Time series of the 1^{st} Temporal Eigenfunction for the longshore current and the vertically averaged longshore current for 2004.

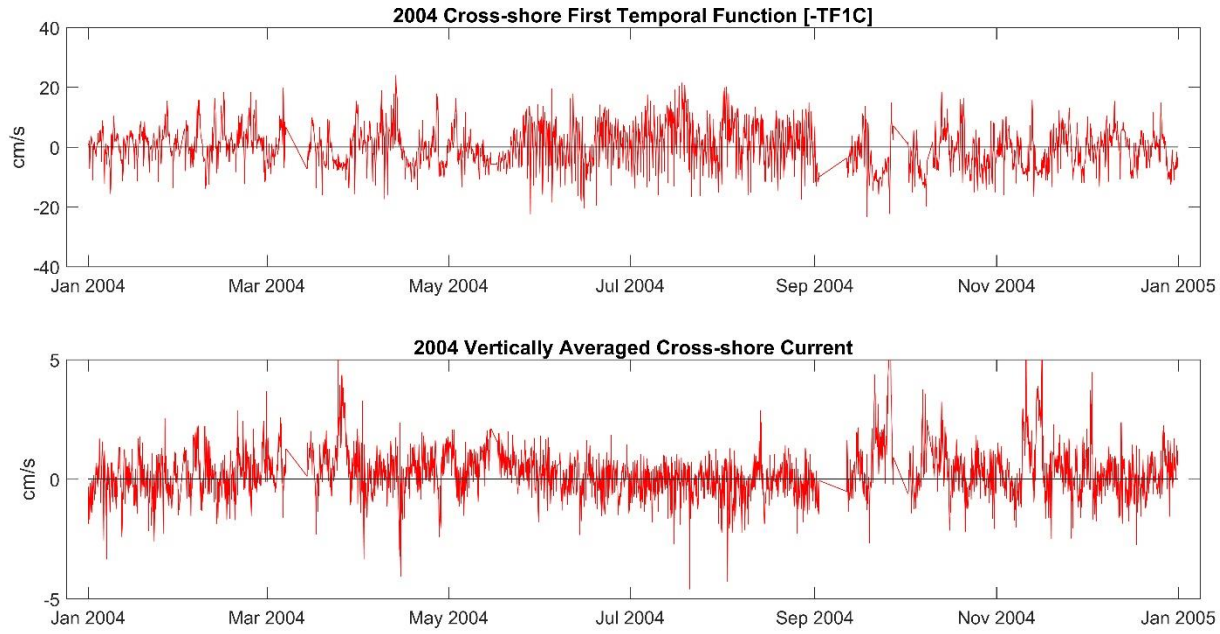

Figure 5.10. Time series of the 1^{st} Temporal Eigenfunction for the cross-shore current and the vertically averaged cross-shore current for 2004.

CHAPTER 6: CORRELATION OF CURRENTS WITH WIND

6.1 Correlation with wind speed and direction analysis

Hubertz (1986) analyzed two data sets collected between 1982 and 1984 of nearshore and surf zone currents at the USACE Field Research Facility in Duck, North Carolina, and found that local winds play an important role in driving the longshore current in the nearshore. In the present study, four years of wind measurements from Spessard station and almost six years of wind measurements from the Trident Pier station are examined.

From the depth-normalized longshore and cross-shore current profiles, 2-hour average time series were derived according to true vector averaging techniques; the resultant 2-h average velocity vectors were plotted at three different levels of the normalized water column together with 2-h average wind velocity vectors to show the wind effect through the water column. Because the normalized water column is non-dimensional, the upper layer represents the level closest to the surface; the lower layer represents the closest level to the ADCP head, and the middle layer is the intermediate level between the upper and lower layer. From the ten-year record two winter months and two summer months were selected with which to examine the correlation of the nearshore current with the wind.

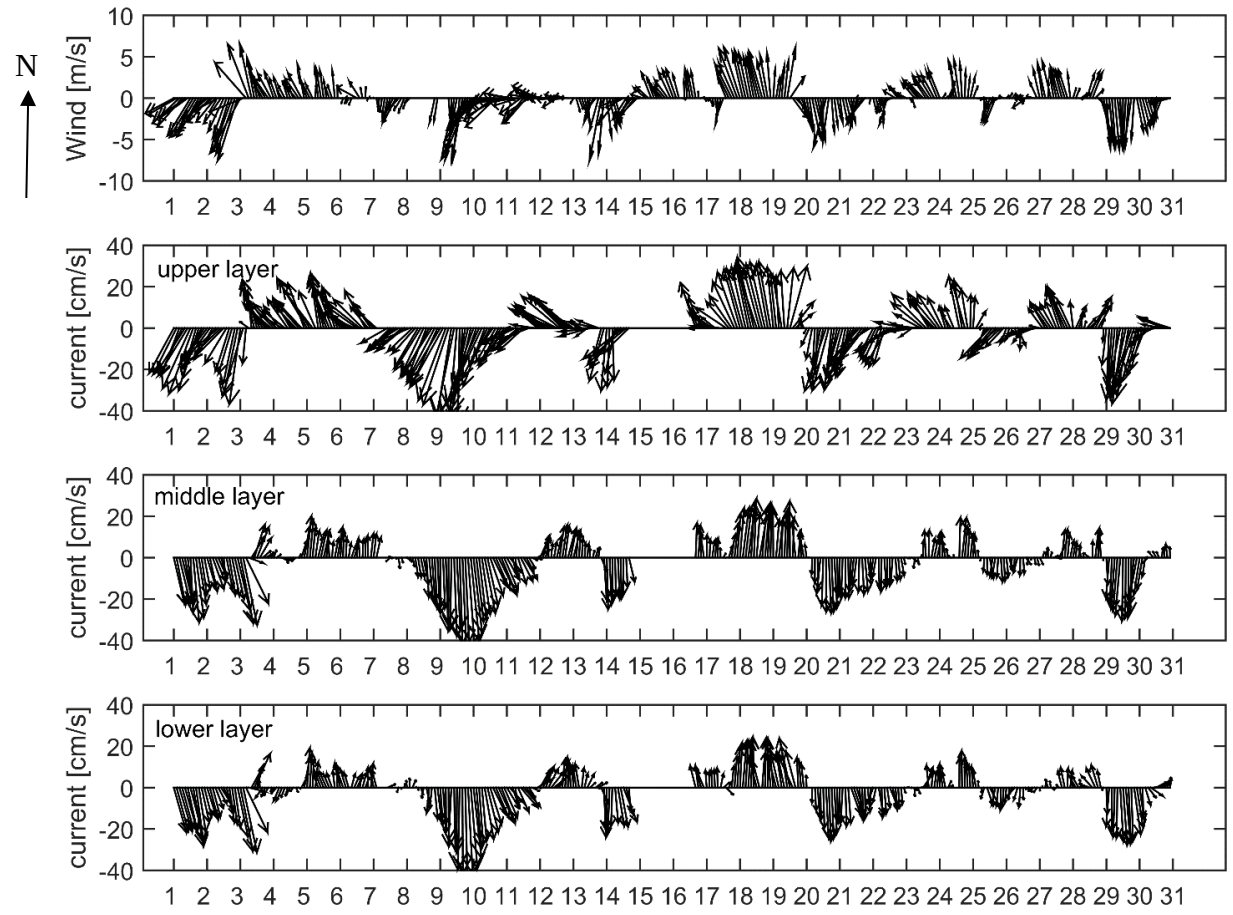

Figure 6.1. Time series of wind vectors (upper panel) and currents at three elevations in the depth-normalized water column for November 2003.

Figure 6.1 presents data for a winter month (November, 2003) where the agreement between the wind speed and direction (upper panel) and the current speed and direction at the upper layer of the water column (lower panel) is clearly evident. When strong winds are blowing from north to south, the currents move in the same direction through the entire water column as is shown for November 8 to 11, November 18 to 19, and November 29 to 30. Alternately, when winds have active onshore component (to the left), the upper layer of the current profile follows suit, whereas the middle and lower layers display compensating offshore flow.

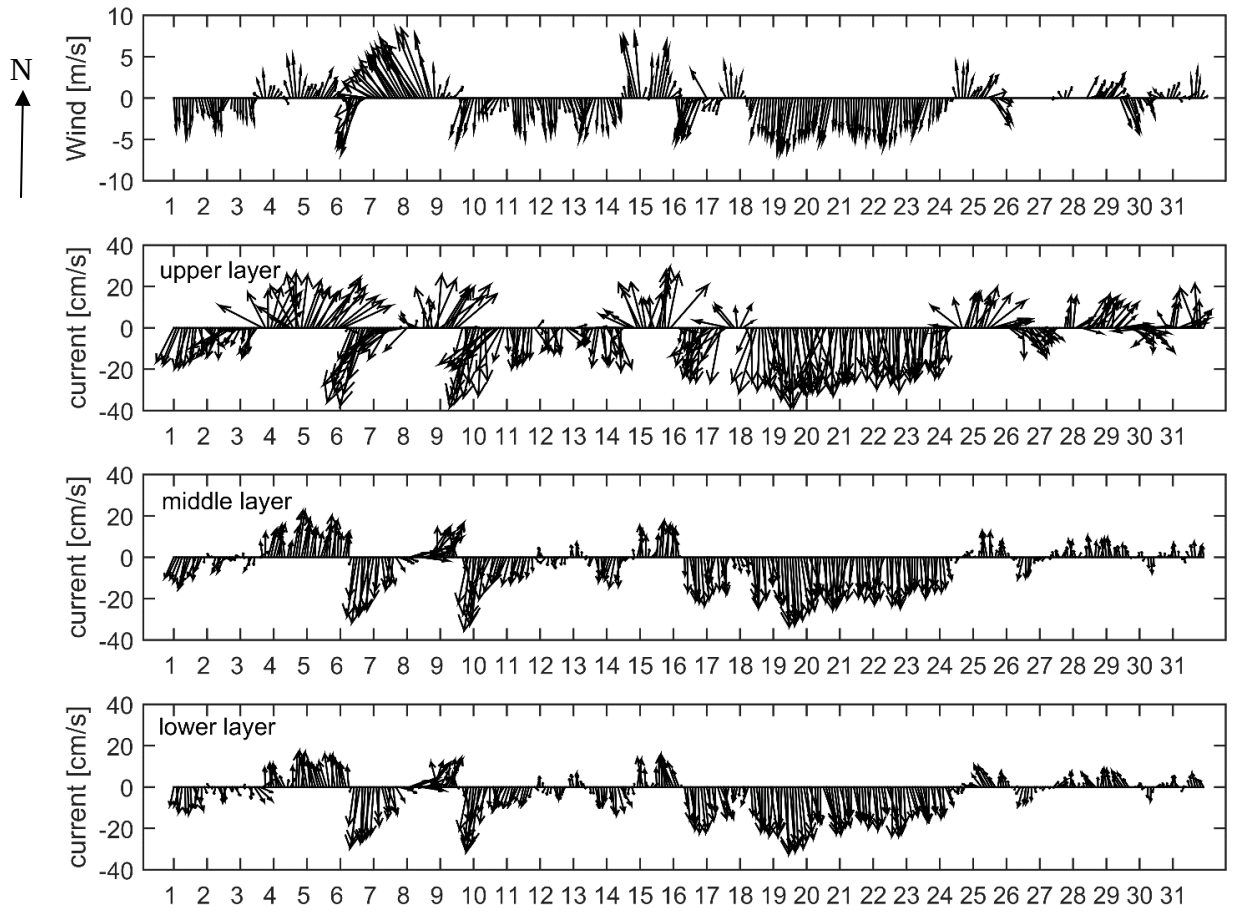

Figure 6.2. Time series of wind vectors (upper panel) and currents at three elevations in the depth-normalized water column for December 2005.

Similarly, Figure 6.2 presents another winter month (December, 2005) showing the agreement between the wind speed and direction (upper panel) and the current speed and direction at the upper layer of the water column (second panel). When strong winds are blowing from north to south, the currents move in the same direction throughout the entire water column, as is evident from December 18 to 24.

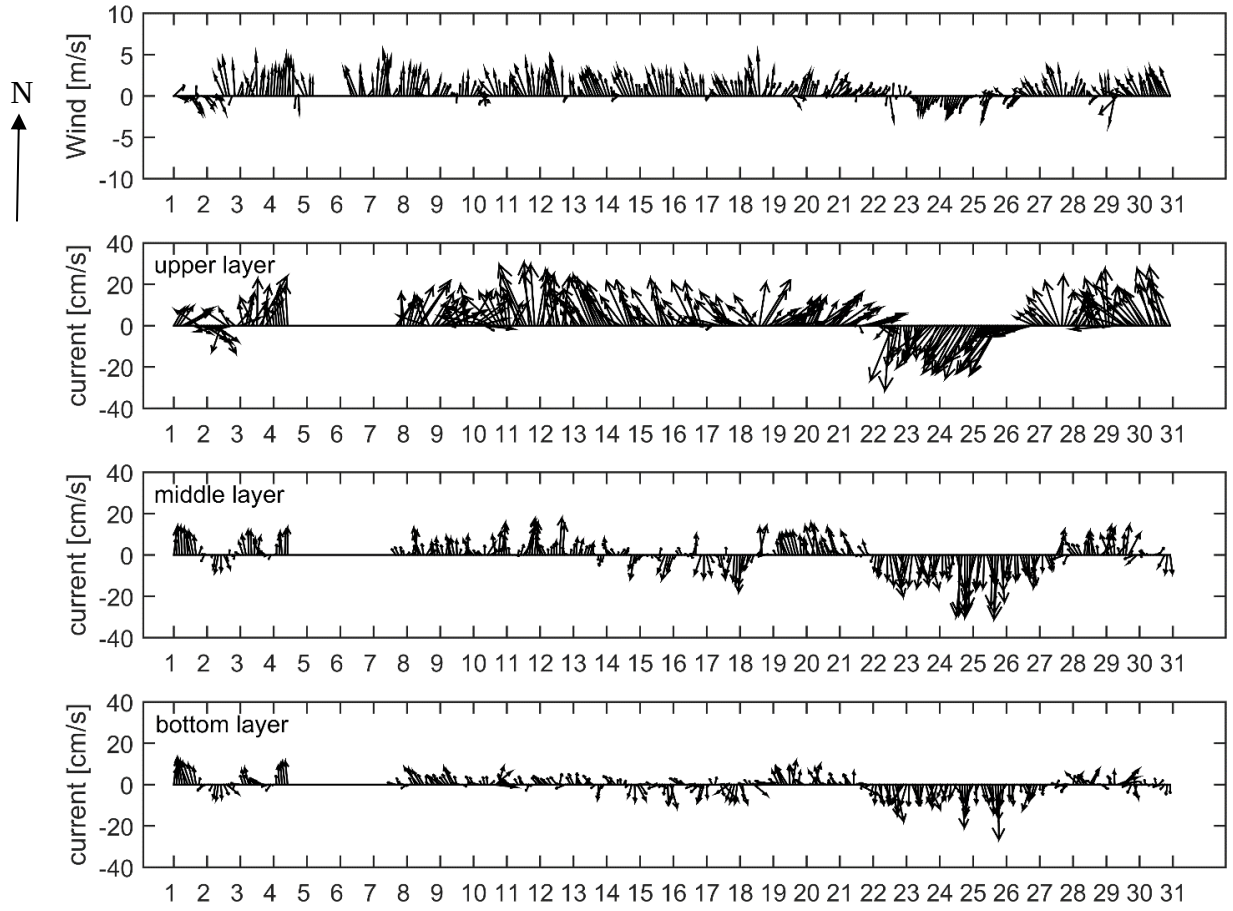

Figure 6.3. Time series of wind vectors (upper panel) and currents at three elevations in the depth-normalized water column for June 2003.

Figure 6.3 presents a summer month (June, 2003) where winds are mainly directed toward the north. The wind speed and direction (upper panel) and the current speed and direction at the upper layer of the water column (second panel) are highly correlated. However, at the lower layer, the wind does not force the current with the same intensity. In summer, winds typically blow from south to north, and their magnitudes are smaller than the north to south winter winds; consequently, during weak wind conditions, it is common to find current reversals between the upper and the lower layer of the water column as, e.g., from June 14 to 18.

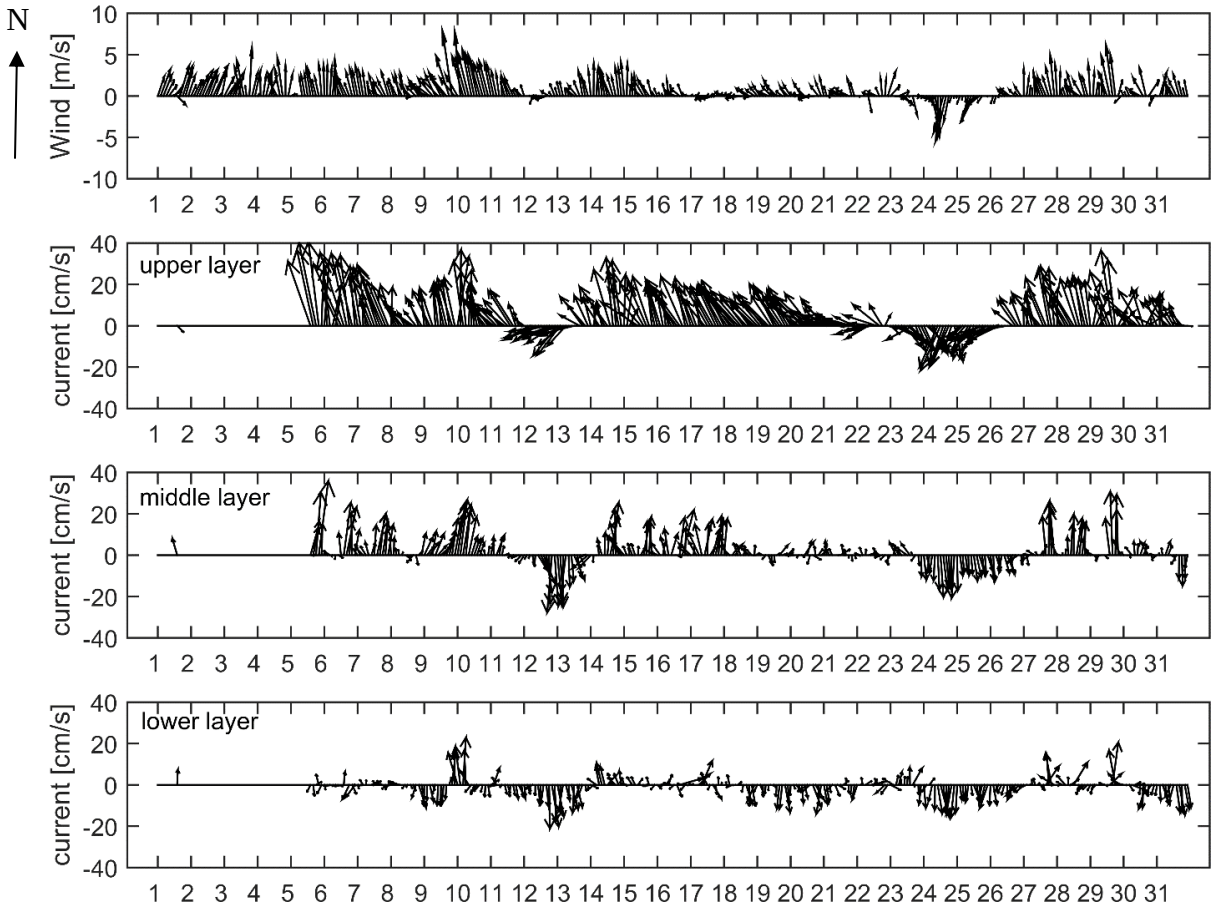

Figure 6.4. Time series of wind vectors (upper panel) and currents at three elevations in the depth-normalized water column for July 2005.

Figure 6.4 presents the wind and current vectors from July (2005) where winds are mainly directed toward the north. The wind vectors (upper panel) and the current vectors in the upper layer of the water column (lower panel) are highly correlated, but the lower layer of the current does not follow the same pattern as, e.g., from July 6 to 10 and from July 15 to 24.

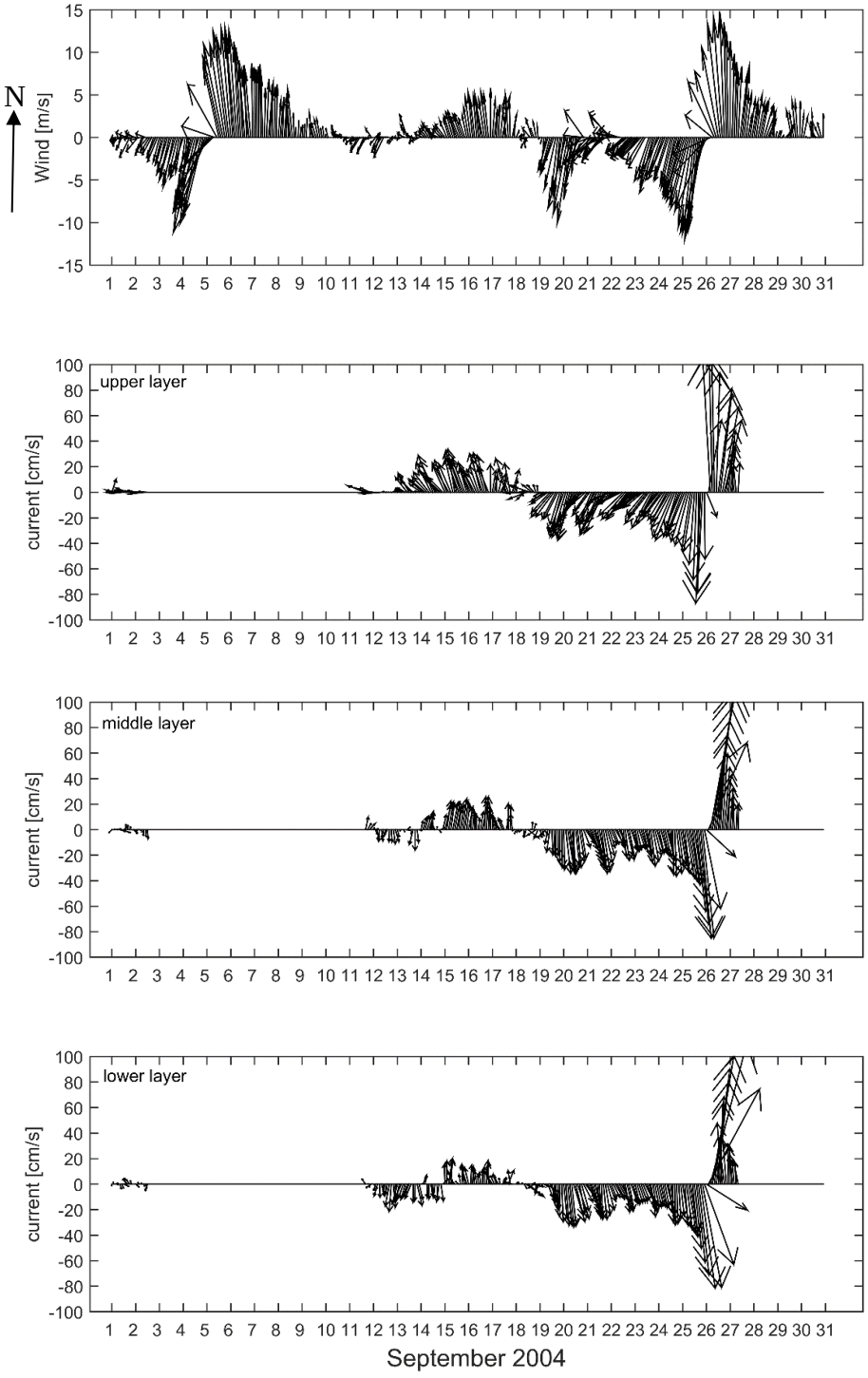

Figure 6.5. Time series of wind vectors (upper panel) and currents at three elevations in the depth-normalized water column showing Hurricane Frances (September 6, 2004) and Hurricane Jeanne (September 26, 2004).

Figure 6.5 presents a unique set of wind and currents measurements due to the occurrence of two hurricanes in the same month. The first one was Hurricane Frances in early September 2004, where winds were recorded, but currents measurements were missed because the ADCP shut down as a result of a premature power outage at the park. The second one was Hurricane Jeanne, which made landfall on September 26, 2004. From the wind record the similarity in magnitude and direction of the two hurricane events can be appreciated, where strong winds start blowing from north to south and suddenly their direction changs by almost 180 degrees at landfall. An identical behavior is observed in the currents record, which is nearly uniform with depth. The magnitude of the current speed during Hurricane Jeanne was twice that of other storms recorded during the 10-year study. With the penetration of strong longshore currents all the way to the lower layer of the water column one would expect significant longshore transport of sediment as well.

Figure 6.6 presents a composite year for the ten years of monthly correlation between 2-hour average time series of longshore current and 2-hour average time series of wind speed (upper panel) and for the cross-shore current and cross-shore wind speed (lower panel). The respective correlations were computed at the layer closest to the surface of the water column (upper layer), and at the layer closest to the ADCP's head (lower layer). The present long-term analysis allows seasonal patterns to be identified, where the longshore current at the upper layer of the water column is highly correlated with the longshore component of the wind speed for the most of the winter months, but for the most of the summer months, their correlation is lower than the winter months. The correlation coefficients at the lower layer of the water column are smaller than at the upper layer of the water column, but they follow the same pattern where winter months are more highly correlated than summer months. Similarly, the cross-shore current at the upper layer of the

water column is highly correlated with the cross-shore component of the wind speed for most of the winter months; but, for most of the summer months, their correlation is lower than the winter months. The correlation coefficients at the lower layer of the water column are showing a negative correlation which can be attributed to the return flow of the water going offshore at the bottom part of the water column.

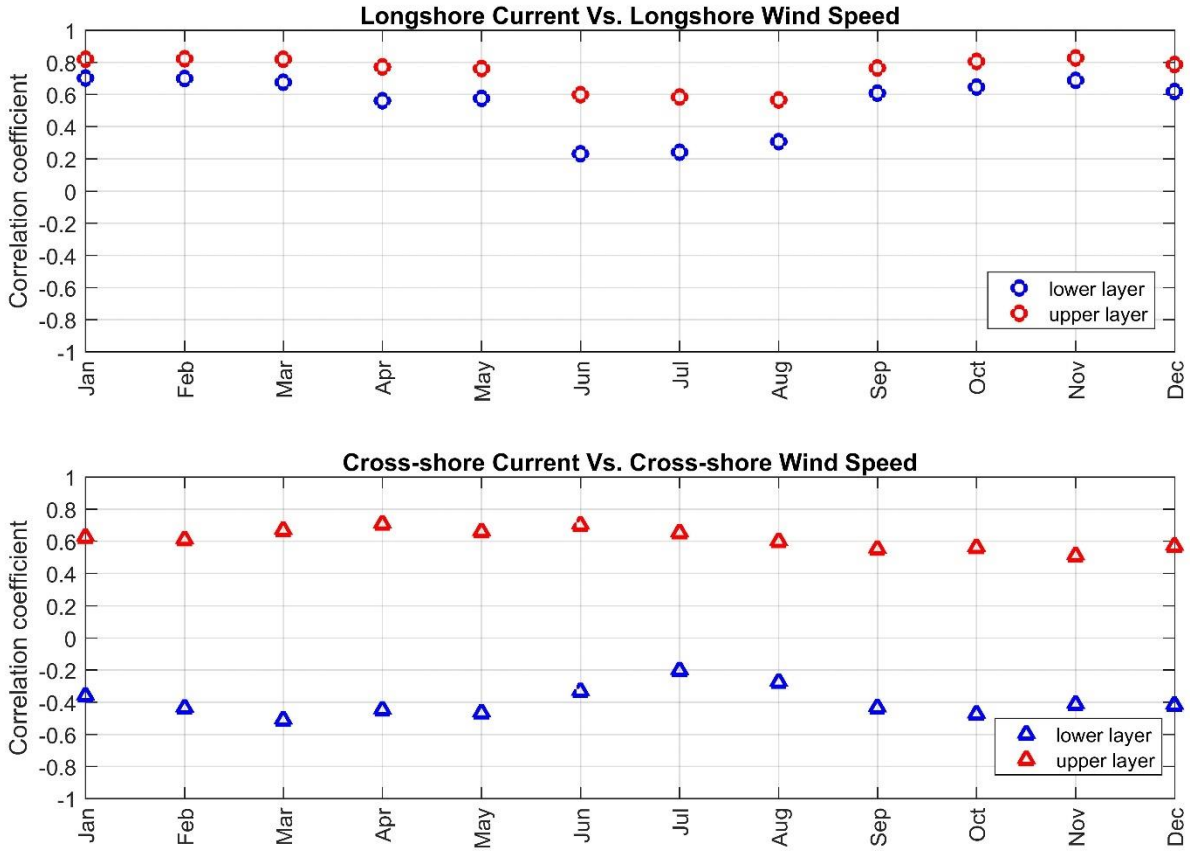

Figure 6.6. Composite year of monthly correlations between 2-hour average time series of currents and 2-hour average time series of wind speed for the longshore and cross-shore component at the upper and lower layers of the water column.

6.2 Correlation with wind stress

The wind stress vector, $\vec{\tau}$, for each 10-minute average provided by each anemometer is estimated using

$$\vec{\tau} = \rho\, C_d\, \overrightarrow{U_{10}}\, \left|\overrightarrow{U_{10}}\right| \tag{6.1}$$

Where ρ is the air density ($\sim 1.2\ kg/m^3$), $\overrightarrow{U_{10}}$ is the wind velocity at 10 m elevation (m/s) above the ground, and C_d is a drag coefficient calculated from the following equation proposed by Garratt (1977)

$$C_d = 0.001(0.8 + 0.065\ \left|\overrightarrow{U_{10}}\right|) \tag{6.2}$$

Decomposition of the wind stress into longshore and cross-shore components is performed, from which yearly averages of wind stress are computed. Table 6.1 shows that during the entire record, although four out of the ten years had a positive (south to north) average longshore wind stress, the net average for the ten years is distinctly negative (-0.0030N/m^2), confirming that there is a dominant north-to-south longshore wind forcing for the 10-year record. For the cross-shore wind stress, Table 6.1 shows that eight of the ten years have negative (onshore) wind stress. Furthermore, the net cross-shore is negative (-0.0560N/m^2), and an order-of-magnitude greater than the longshore net wind stress, showing that winds coming from the east and going onshore are dominant during the ten-year record.

Table 6.1 Longshore and Cross-shore average wind stress for the ten-year record.

Average Wind stress $[N/m^2]$		
Year	Longshore Wind stress	Cross-shore Wind stress
2002	-0.0008	-0.0101
2003	-0.0018	-0.0100
2004	0.0009	-0.0144
2005	-0.0007	-0.0150
2006	0.0016	-0.0008
2007	-0.0019	-0.0053
2008	0.0012	-0.0006
2009	0.0011	0.0009
2010	-0.0022	0.0014
2011	-0.0002	-0.0021
Net	**-0.0030**	**-0.0560**

A two-hour block-averaged time series is constructed for the longshore wind stress component for each one of the ten years of record. These ten time series are then used to create a composite year of wind stress by averaging the available wind data at each 2-hour time step. Figure 6.8 presents a weekly running-average for the longshore wind stress of this composite year, where the seasonality of the winds is clearly evident, with a dominant longshore wind stress directed to the north during the summer months, and a dominant longshore wind stress directed toward the south during the winter months. Similarly, a composite year is constructed from the 2-hour averaged time series of the vertically averaged longshore current. Figure 6.9 presents a weekly running-average for the composite year of the vertically averaged longshore current, where once

again the seasonality of the longshore current is clearly evident, with a dominant northerly directed longshore current during the summer months, and a prevailing southerly longshore current during the winter months. Although the net longshore wind stress is slightly to the south, as found in the results of the volume-flux analysis in Table 4.2, the net volume flux for a composite year appears to be to the north.

The plots of composite years show a high correlation (R=0.91) between the longshore wind stress and the vertically averaged longshore current.

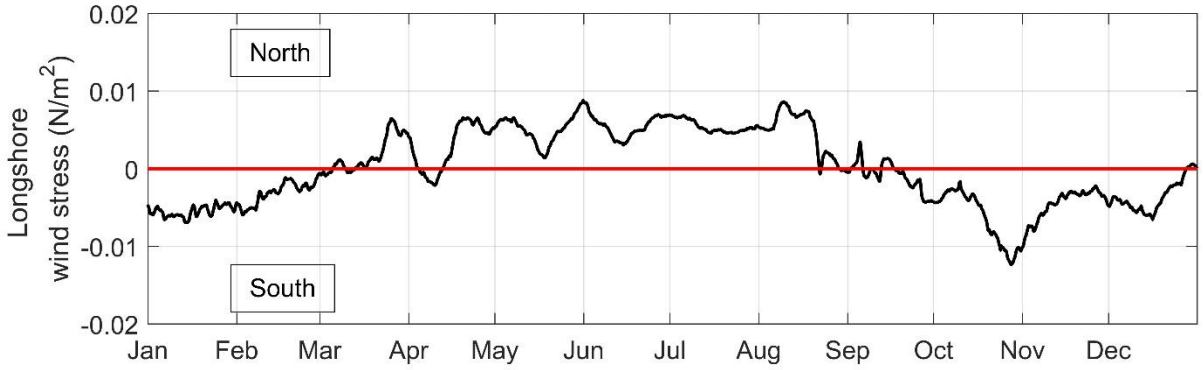

Figure 6.7. Composite year of the weekly running-average of longshore wind stress.

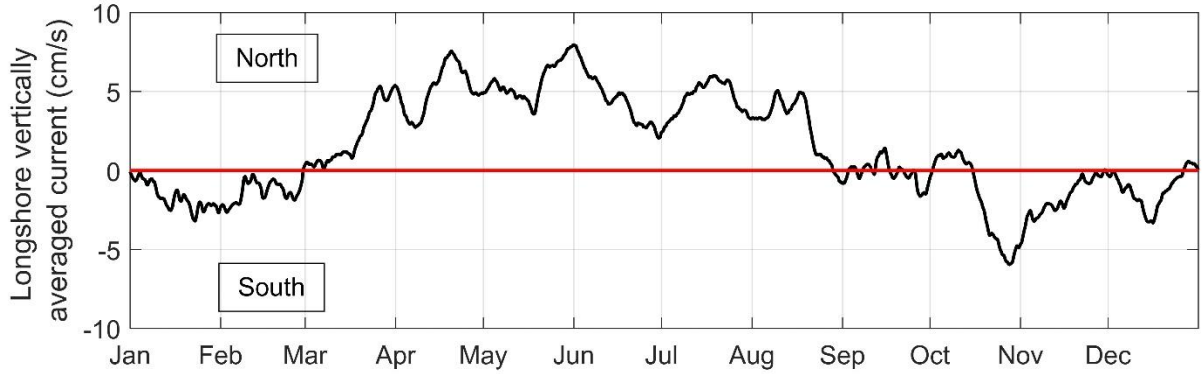

Figure 6.8. Composite year of the weekly running-average of longshore current.

CHAPTER 7: CORRELATION OF CURRENTS AND WAVES

7.1 Correlation of currents and wave energy dissipation.

Based on a) the findings of Montoya and Dally (2016) for the near-balance in wave-induced Radiation Stress, b) the averaging of the longshore currents measured by the ADCP, and c) the wind analysis conducted thus far, the reason for the distinct long-term net N-S transport along the central Brevard County shoreline has not convincingly revealed itself. However, if we examine the correlation between the currents and wave energy, the solution to the enigma becomes apparent. Before doing so, it is noted that the years 2006 and 2009 display excessive noise in their wave measurements, and the year 2011 does not have waves measurements beyond October 29th; therefore, these years are omitted from the subsequent analysis. For the remaining seven years, we will see that on average wave height (H_{mo}) is larger when the longshore current is heading to the south (0.95 m) than when the current is going to the north (0.73 m) as is shown in Table 7.1.

Table 7.1 Yearly averages of energy-based significant wave height (H_{mo}) when Longshore current is toward the north and when it is toward the South from Spessard for 2002, 2003, 2004, 2005, 2007, 2008 and 2010.

Year	Average H_{mo}(m) when Longshore current is toward the north	Average H_{mo}(m) when Longshore current is toward the south
2002	0.71	0.86
2003	0.67	0.90
2004	0.73	1.00
2005	0.73	1.06
2007	0.83	0.97
2008	0.76	0.95
2010	0.70	0.90
Average	**0.73**	**0.95**

Because wave energy density is proportional to H_{mo}^2 and group velocity in shallow water is roughly proportional to $H_{mo}^{1/2}$ the energy flux into the surf zone is proportional to $H_{mo}^{5/2}$. Neglecting wave reflection, the rate of energy dissipation due to wave breaking in the surf zone is equal to this energy flux. Arguing that the rate of wave energy dissipation governs the mobilization and suspension of sediment in the surf zone, the longshore transport should be indicated by the product of the longshore current and $H_{mo}^{5/2}$. Referring to Table 7.2 we find a much stronger correlation between southerly directed currents and $H_{mo}^{5/2}$ as compared to the correlation between northerly directed longshore currents and $H_{mo}^{5/2}$. In fact, on average the southerly directed conditions are more than twice as correlated as the northerly directed conditions. This would appear to be the most plausible explanation for the net long-term north-to-south transport known to characterize the region.

Table 7.2 Yearly correlations between northerly longshore current and $(H_{mo})^{5/2}$ and between southerly longshore current and $(H_{mo})^{5/2}$ from Spessard for 2002, 2003, 2004, 2005, 2007, 2008 and 2010.

Year	Correlations between Northerly Longshore current and $H_{mo}^{5/2}$	Correlations between Southerly Longshore current and $H_{mo}^{5/2}$
2002	0.29	0.48
2003	0.18	0.42
2004	0.53	0.59
2005	0.08	0.55
2007	0.18	0.63
2008	0.23	0.54
2010	0.12	0.44
Average	**0.23**	**0.52**

7.2 Storm Analysis

Frequently, most of the longshore transport in the nearshore is driven by the combination of wave obliqueness and swash zone processes. Analysis of the wind-driven current outside the surf zone would be relevant to modeling the shape and intensity of the longshore current inside the surf zone because the two should match at the breaker line. Hypothesizing that storms dominate the net longshore transport climate, following Montoya and Dally (2016) a storm is herein defined as whenever H_{mo} exceeds 1.75 m, which in this case, represents 4% of the data. Figure 7.1 presents the histogram of H_{mo} for 2002, 2003, 2004, 2005, 2007, 2008 and 2010. The dataset for the seven years has an average H_{mo} of 0.82 m, a standard deviation of 0.42 m, and skewness of 1.26. The maximum significant wave height observed in the record is 4.02 m, occurring during Hurricane Jeanne.

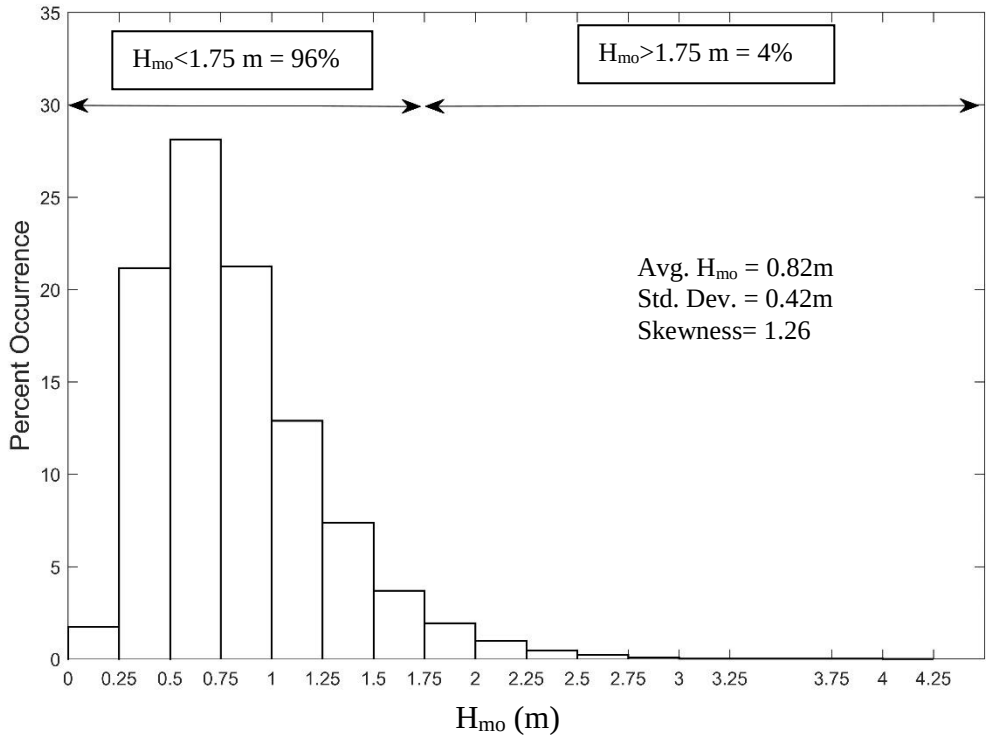

Figure 7.1. Histogram of energy-based significant wave height (H_{mo}) from Spessard for 2002, 2003, 2004, 2005, 2007, 2008 and 2010.

First, the number of storms were computed for each one of the seven years, where the significant wave height exceeded the threshold of 1.75 m. These results show that 2004, 2005 and 2008 were very active years, with a total of 11 storms each year. In contrast, 2002, 2003, 2007 and 2010 were less active, with 4, 7, 8 and 6 storms respectively. Second, the percent of waves approaching from shore-normal ($69^o < \theta_{mean} < 77^o$), northeast ($\theta_{mean} < 69^o$), and southeast ($\theta_{mean} > 77^o$) directions were computed for each one of the seven years. For all the years the percent of waves approaching shore-normal ($69^o < \theta_{mean} < 77^o$) was similar ranging between 22% and 31%. For 2003, the percent of waves approaching from the northeast ($\theta_{mean} < 69^o$) was slightly lesser (31%) than the percent of waves approaching from the southeast ($\theta_{mean} > 77^o$) (41%). For the rest of the years,

the percent of waves approaching from the northeast ($\theta_{mean}<69^o$) was significantly greater (39% to 61%) than the percent of waves approaching from the southeast ($\theta_{mean}>77^o$) (11% to 34%). Thus, for the analyzed seven years, it would be expected a dominant north to south transport, as a result of waves approaching more frequently from the northeast (average for the seven years is 43%).

Table 7.3 Percent of occurrence of energy-based significant wave height (H_{mo})>1.75m from Spessard for 2002, 2003, 2004, 2005, 2007, 2008 and 2010.

Year	Number of storms H_{mo}>1.75m	Percent of occurrence		
		Northeast θmean <69°	Shore-normal 69°<θmean<77°	Southeast θmean >77°
2002	4	39	27	34
2003	7	31	28	41
2004	11	44	22	34
2005	11	39	27	34
2007	8	41	31	28
2008	11	61	28	11
2010	6	47	29	24
Average		**43**	**27**	**29**

A storm analysis for each one of the seven years allows the correlations between the northerly directed longshore current and the radiation stress in the longshore direction (S_{xy}), and between the southerly directed longshore current and the radiation stress in the longshore direction (S_{xy}) to be determined, as is presented in Table 7.4. The computed correlations between the southerly longshore current speed ($-V_{long}$) and the integrated-based Radiation stress (S_{xy}) was higher than the correlations between the northerly longshore current speed ($+V_{long}$) and the integrated-based Radiation stress (S_{xy}) for 2002, 2003, 2005, 2008 and 2010. Thus, for the combined seven years, the average correlation between the southerly longshore current speed ($-V_{long}$) and the integrated-based Radiation stress (S_{xy}) is 0.51, which is higher than the average

correlation between the northerly longshore current speed ($+V_{long}$) and the integrated-based Radiation stress (S_{xy}) (0.40). Additionally, from Table 7.4 can be noted that for storms with H_{mo} above 1.75 m the percent of occurrences for the southerly directed longshore current ($-V_{long}$) are greater than the percent of occurrences for the northerly directed longshore current ($+V_{long}$) for each one of the seven years. As a result, for the combined seven years, the average percent of occurrence for the southerly longshore current ($-V_{long}$) is 73%, which is significantly higher than the average percent of occurrence for the northerly longshore current ($-V_{long}$) (27%). As was expected, the above correlations and percent of occurrences for storms with H_{mo} above 1.75 m clearly support the assumption that higher waves come more often from the northeast, promoting a net long-term north-to-south transport as has been observed at this location.

Table 7.4 Correlations between the northerly directed longshore current and the radiation stress in the longshore direction (S_{xy}), and between the southerly directed longshore current and the radiation stress in the longshore direction (S_{xy}). Percent of occurrence of northerly directed longshore current and southerly directed longshore current for the energy-based significant wave height (H_{mo})>1.75m from Spessard for 2002, 2003, 2004, 2005, 2007, 2008 and 2010.

Storms with H_{mo} > 1.75 m				
Year	Correlation between North Longshore current and S_{xy}	Correlation between South Longshore current and S_{xy}	% occurrence North Longshore current	% occurrence South Longshore current
2002	0.53	0.79	29	71
2003	0.16	0.49	14	86
2004	0.90	0.01	23	77
2005	0.44	0.72	21	79
2007	0.52	0.37	28	72
2008	0.32	0.44	45	55
2010	-0.07	0.75	27	73
Average	**0.40**	**0.51**	**27**	**73**

CHAPTER 8: CONCLUSIONS

The methodology for extracting the tidal signal from the water surface by utilizing the data from the Trident Pier station worked effectively, enabling the water column to be normalized and measurements contaminated by surface echo to be eliminated. Decomposing each current into longshore and cross-shore components produced time series that meaningfully represent the behavior of the vertical structure of the currents for each one of the ten years of available data.

It is clearly concluded that yearly averages of the mean vertical profile do not substantially represent the vertical structure of the currents. This is mainly due to the large variability in both the wind and wave climate, which often forces the nearshore current to change rapidly. Consequently, the resulting mean current profile for a year has a small mean structure but with large standard deviation at every level of the normalized water column. Computing basic statistics is useful in understanding the seasonal behavior of the vertical structure of the currents, with monthly averaged mean profiles revealing the tendency of the longshore current to flow toward the north during summer months, and to flow toward the south during winter months. For most of the years, the mean profile of the longshore current is northerly directed in the upper layers of the water column, and slightly southerly directed at the bottom layer. For all the analyzed years, the mean profile of the cross-shore current shows significant larger magnitudes in the upper layers of the water column than at the bottom, with one zero-crossing point, around 0.90 normalized elevation, which is a result of the mass balance and the resulting return flow.

Computing the net volume flux for the longshore and cross-shore component from the mean vertical profile revealed that 2003 is the only year with a total net longshore volume flux toward the south. Also, the mean cross-shore volume flux is on the order of magnitude smaller than the longshore volume flux, indicative of the fact that ideally the depth-integrated cross-shore flux should be zero due to the presence of the shoreline. Ideally, there would be zero net cross-shore discharge, but it could not be attained due to the inability to measure the wave-induced mass flux Stokes Drift at the very surface (Stokes, 1847), as well as the discharge below the blanking distance of the ADCP.

Subjecting the data to Empirical Orthogonal Function Analysis proved to be quite useful in representing the vertical structure of the nearshore currents. It has been discovered that two preferential modes of variability in the longshore and cross-shore currents account for more than 99% of the total variance each year for all ten years. For the longshore current, mode-1 contains most of the variability at the upper layers of the water column, with a significant reduction in variability at the bottom. Similarly, mode-1 of the cross-shore current exhibits most of the variability at the upper layers of the water column, and a notable reduction in variability at the bottom, but with phase opposition of the surface and bottom layers, which is physically consistent with the idealized solution of wind blowing over a bounded domain. For each one of the ten years, there is a rotation of the current to the right (clockwise) at the very surface. The rotation angle increases and the variance decreases with depth below the surface. The spiral structure of the water column follows a surface Ekman veering, but for which the ratio between the depth of the sea (h) and the depth of wind current (D) is very small. Consequently, the upper layer of the current is almost aligned with the direction of the wind. As was expected, there is a high correlation between

the wind direction and the current direction in the upper layer of the water column, confirming that in the nearshore area Coriolis acceleration affects the currents in a lesser degree than in deep water. Instead, the spiral structure appears to be driven by the requirement for offshore-directed flow in the lower water column to balance the onshore flow in the upper water column driven by the predominantly onshore mean wind stress and the wave-induced mass transport in the wave crest (Stokes Drift). The spiral structure of the water column obtained from the Empirical Orthogonal Function Analysis is consistent with the theoretical analysis by Ekman (1905), confirming the importance of long-term records that allow the testing and improvement of theory.

Monthly correlations between 2-hour block-averaged time series of longshore current and wind speed revealed some of the seasonal patterns of the wind and longshore current, in which the upper layer of the water column is highly correlated with the longshore component of the wind speed for most of the winter months, and less correlated for most of the summer months. The lower layer of the water column is less correlated with the wind, but with similar patterns during winter and summer months. In a similar way, the cross-shore current at the upper layer of the water column is highly correlated with the cross-shore component of the wind speed for most of the winter months, and less correlated during the summer months. The negative correlation between the cross-shore current in the lower layer of the water column and the wind is due to the return flow required because of the nearby shoreline.

It appears that the enigma encountered by Montoya and Dally (2016) in that the radiation stress (S_{xy}) was only weakly north-to-south, whereas the shoreline offsets at nearby inlets would indicate a much stronger N-S bias, is herein explained by the higher correlation between southerly directed currents and wave energy flux than northerly directed currents and wave energy flux. This

indicates that there exist essential facets that need to be addressed in the development and refinement of longshore transport models and formulas. It is suggested that future research might attempt to incorporate this important correlation of wind and wave forcing with the resulting currents and sand entrainment, either deterministically or stochastically. With more reliable longshore transport formulas, shoreline evolution modeling, the development of inlet sediment budgets, and coastal science and engineering as a whole will benefit.

REFERENCES

Absalonsen, L. & Dean, R.G. (2010). "Characteristics of shoreline change along the sandy Beaches of the State of Florida: an Atlas" Retrieved from http://nsgl.gso.uri.edu/flsgp/flsgpm10001.pdf.

Bacopoulos, P., Dally, W.R., Hagen, S. & Cox A. (2011). Observations and simulation of winds, surge, and currents on Florida's east coast during Hurricane Jeanne (2004).

Book, J. W., Perkins, H., Signell, R. P., and Wimbush, M. (2007). The Adriatic circulation experiment winter 2002/2003 mooring data report: a case study in ADCP data processing. Naval Research Laboratory, Oceanography Division. 6-8.

Cosoli, S., Gacic, M., Mazzoldi, A. (2008). Variability of currents in front of the Venice Lagoon, Northern Adriatic Sea.

Dally, W.R. (2011). Analysis and utilization of long-term data from a nearshore ADCP IEEE/OES/CWTM 10th Working Conference on Current, Waves and Turbulence Measurement, CWTM 2011.

Ekman, V. W. (1905). On the Influence of the Earth's Rotation on Ocean-Currents.

Garrett, J.R., (1977). Review of drag coefficients over oceans and continents. Monthly Weather Review, 105(7), 915–929.

Hubertz, J.M., (1986). Observations of local wind effects on longshore currents. Coastal Engineering, 10, 275–288.

Kennedy, A., and Dean, R.G., (2005). "Wave Gauge Orientation at Melbourne Beach, FL," contract report to the Florida Beaches and Shore Resources Center, 11pp.

Leadon, M., Dally, W.R., Osiecki, D. (2002). Florida Coastal Forcing Project (FCFP).

Longuet-Higgins, M. S. and Stewart, R. W., (1964). "Radiation stresses in water waves; a physical discussion, with applications," Deep-Sea Research, 11 (4): 529–562

Montoya, L.H. and Dally, W.R. (2016). Journal of Coastal Research, in press.

Montoya, L.H. (2014). Analysis of a 10-year Nearshore Wave Database and its Implications to Littoral Processes. UNF theses and dissertations. Paper 494.

Munchow, A. and Chant, R. J.: Kinematics of inner shelf motion during the summer stratified season off New Jersey, J. Phys. Oceanogr., 30, 247–268, 2000.

Starr, V.P., “A momentum Integral for Surface Waves in Deep Water”, J. Mar. Res., Cambridge, Vol. 6, No. 2,1947.

Stokes, G.G., 1847. On the theory of oscillatory waves. Trans. Camb. Philos. Soc. 8, 441-455. Reprinted in: Stokes, G.G. (1880). Mathematical and Physical Papers, Volume I, Cambridge University Press. 197-229.

Venegas, S. A.: Statistical methods for signal detection in climate. Danish Center for Earth System Science, University of Copenhagen, DCESS Report 2, 2001.

Whitney, M. M. and Garvine, R. W.: Wind influence on a coastal buoyant outflow, J. Geophys. Res., 110, C030104, doi:10.1029/2003JC002261, 2005.

APPENDIX A: 2-h Average Wind Vectors (m/s) and 2-h Average Surface Current Vectors (cm/s) for 2002

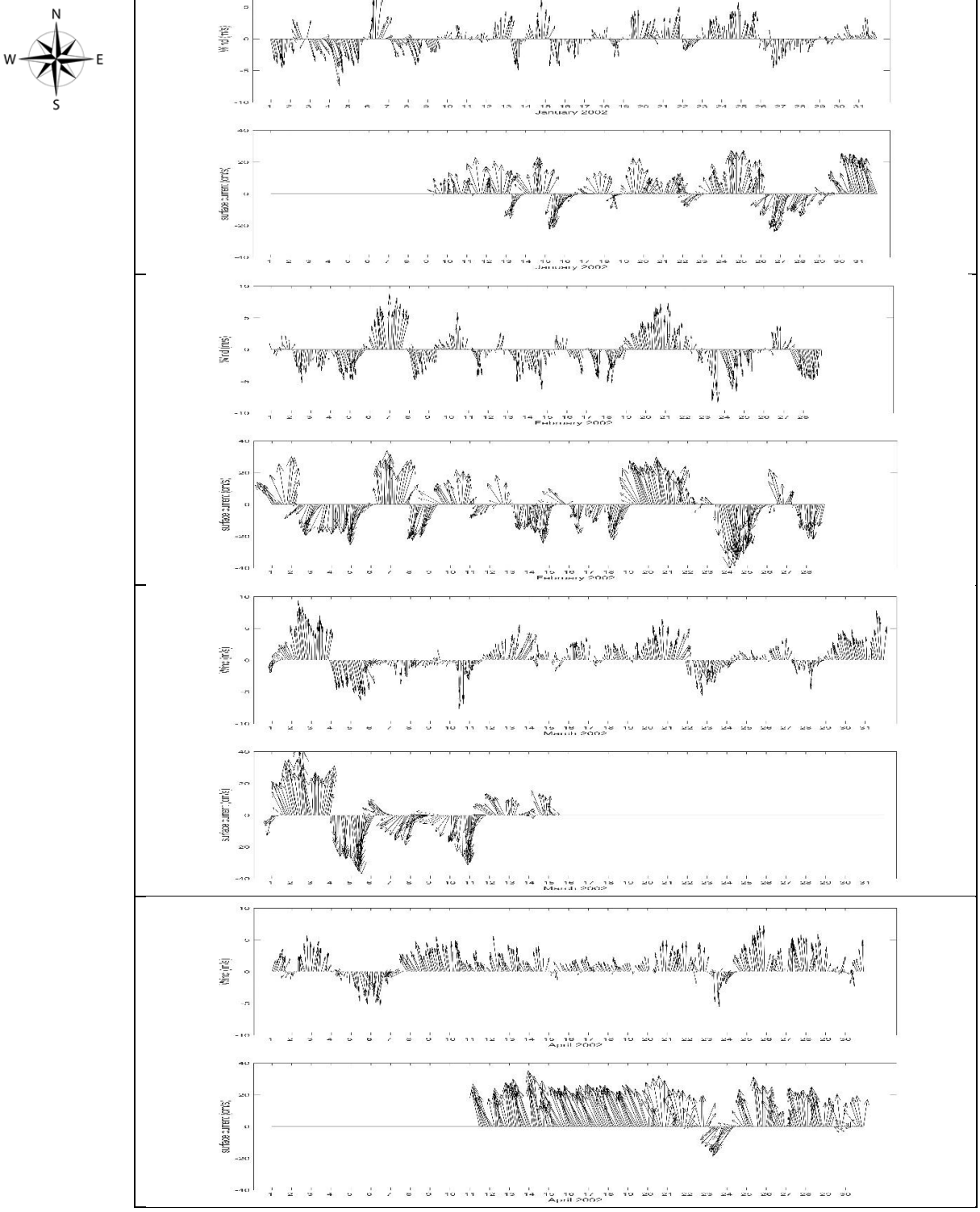

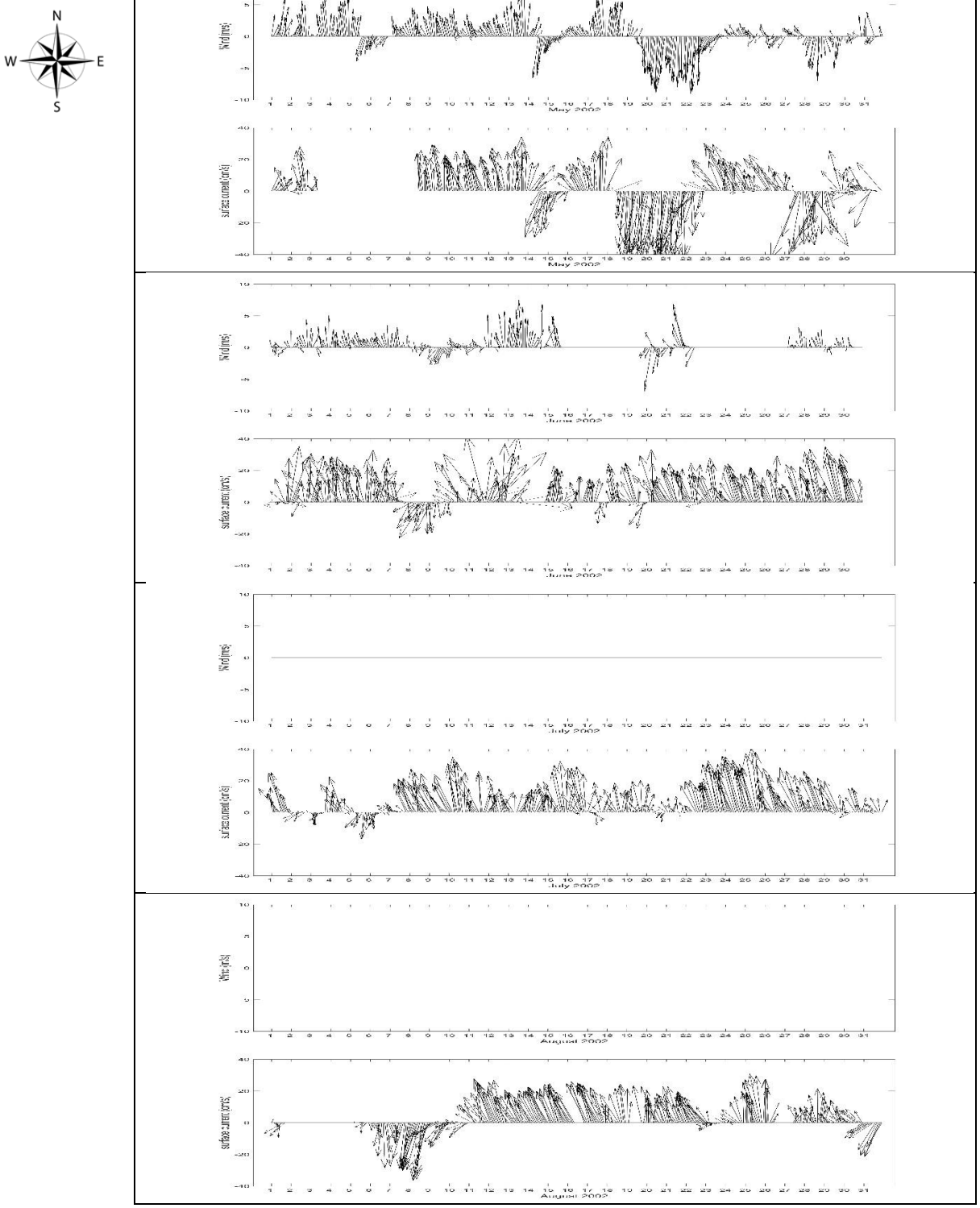
N
W
E
S
May 2002
June 2002
July 2002
August 2002

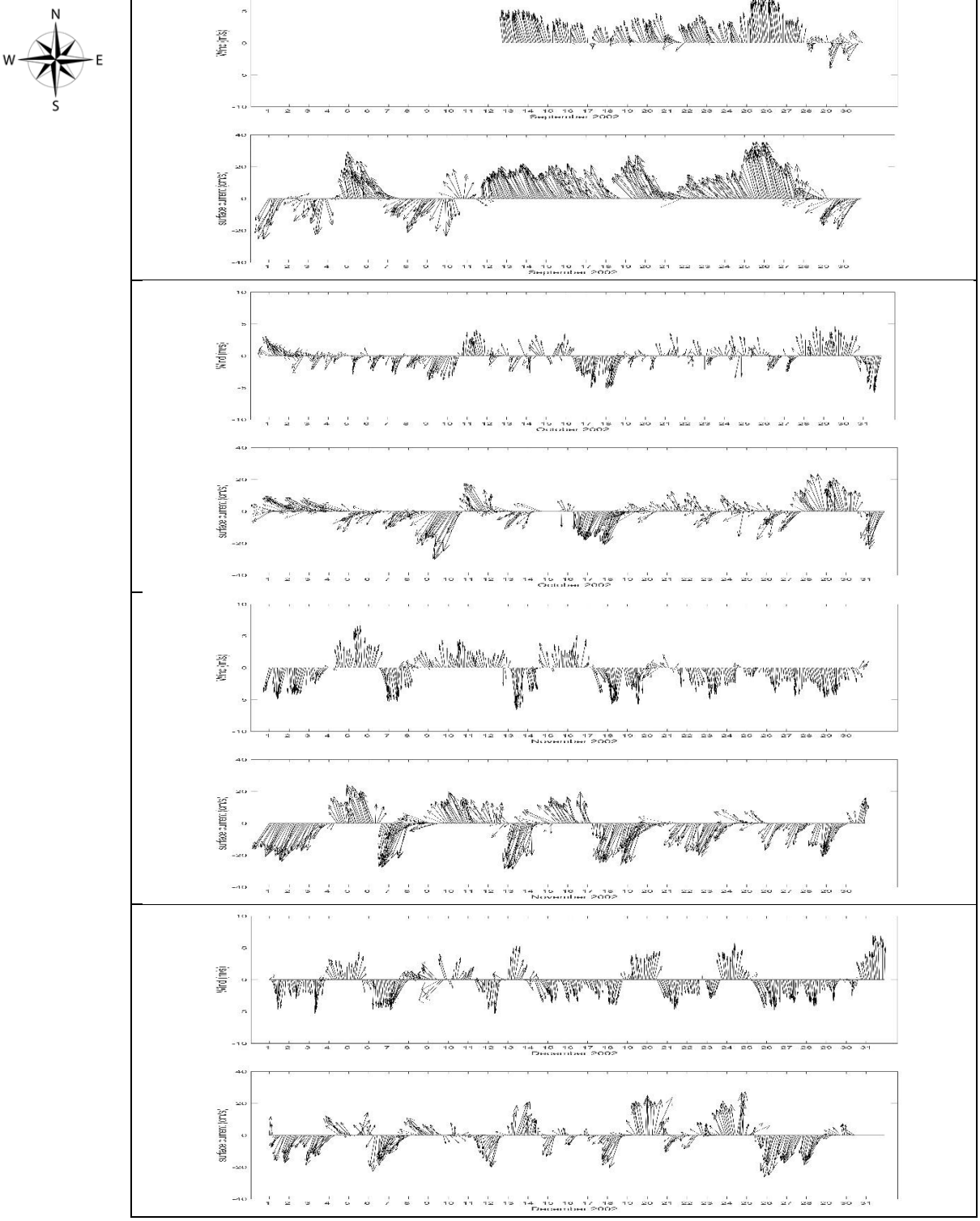
N
W
E
S
Wind (m/s)
September 2002
surface current (cm/s)
September 2002
Wind (m/s)
October 2002
surface current (cm/s)
October 2002
Wind (m/s)
November 2002
surface current (cm/s)
November 2002
Wind (m/s)
December 2002
surface current (cm/s)
December 2002

APPENDIX B: 2-h Average Wind Vectors (m/s) and 2-h Average Surface Current Vectors (cm/s) for 2003

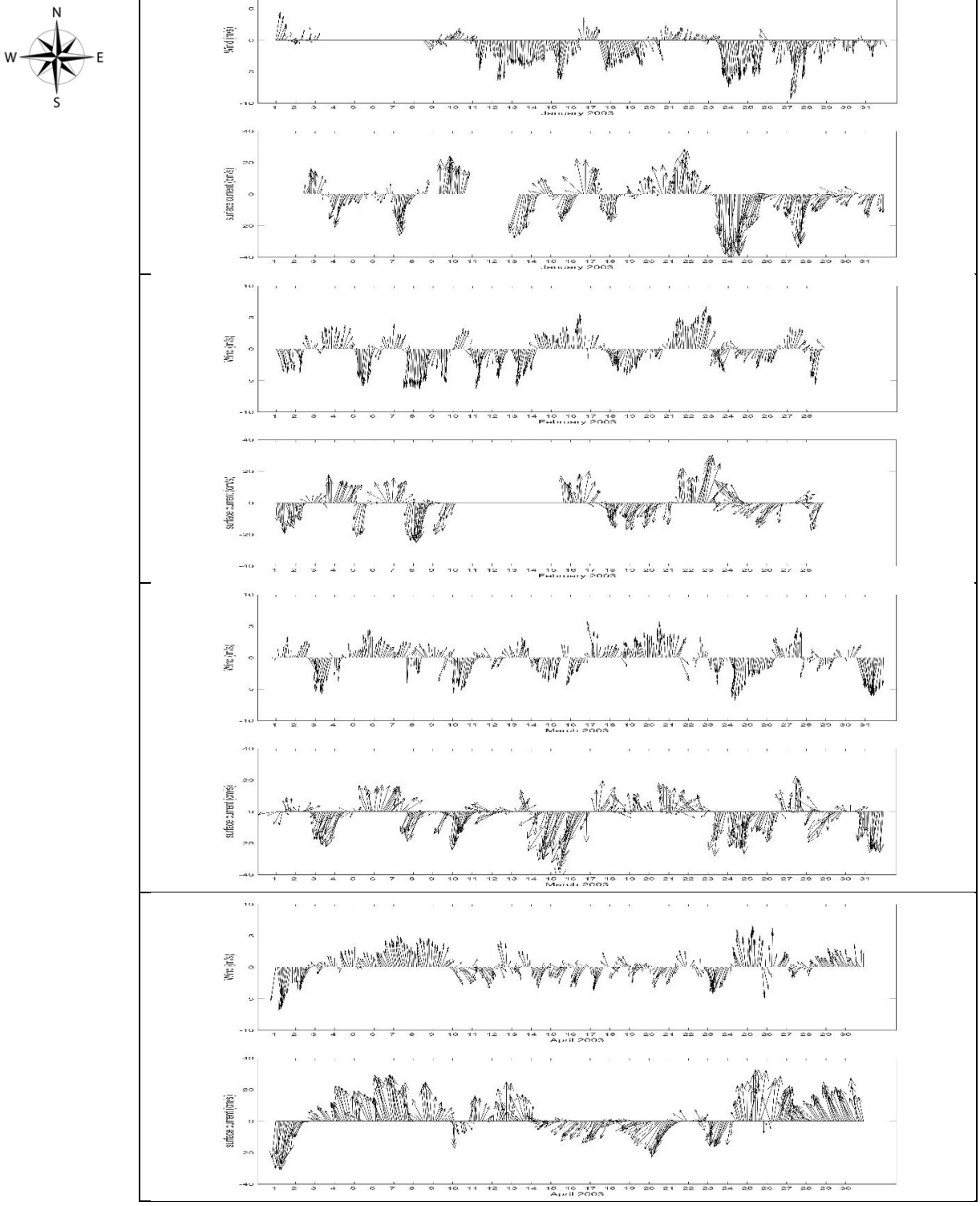

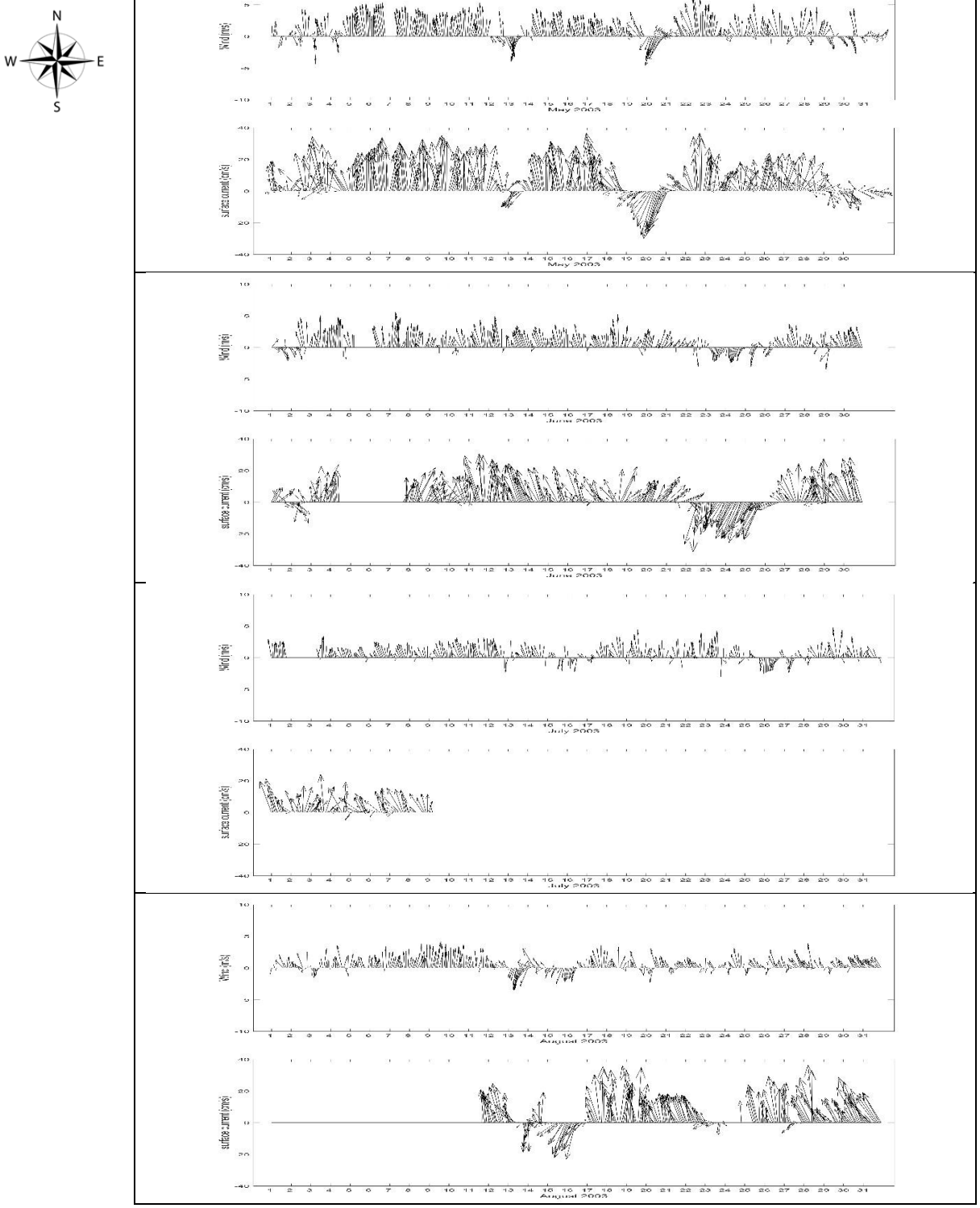
N
W
E
S
May 2003
June 2003
July 2003
August 2003


N
W
E
S

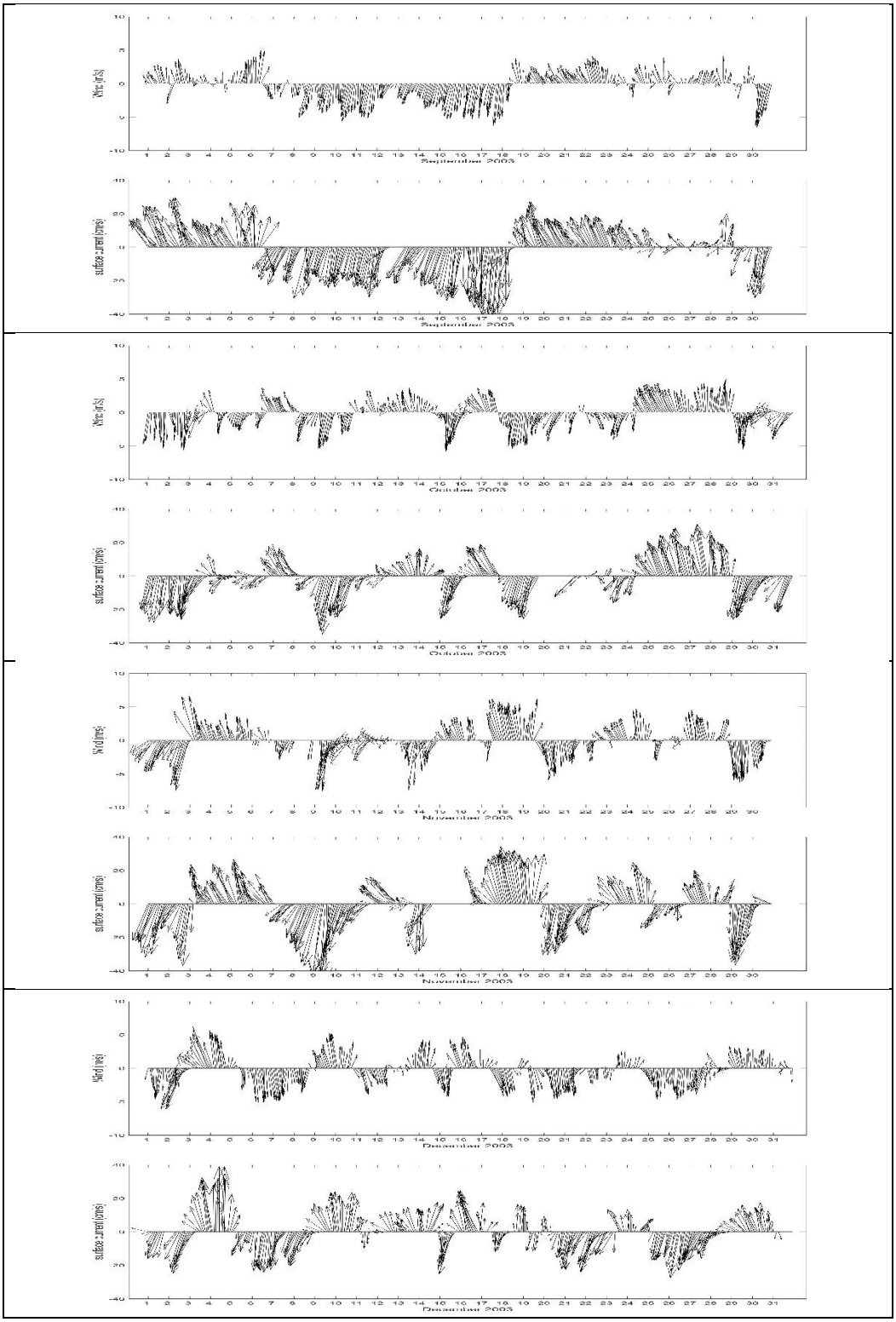
Wind (m/s)
September 2003
surface current (cm/s)
September 2003
Wind (m/s)
October 2003
surface current (cm/s)
October 2003
Wind (m/s)
November 2003
surface current (cm/s)
November 2003
Wind (m/s)
December 2003
surface current (cm/s)
December 2003

APPENDIX C: 2-h Average Wind Vectors (m/s) and 2-h Average Surface Current Vectors (cm/s) for 2004

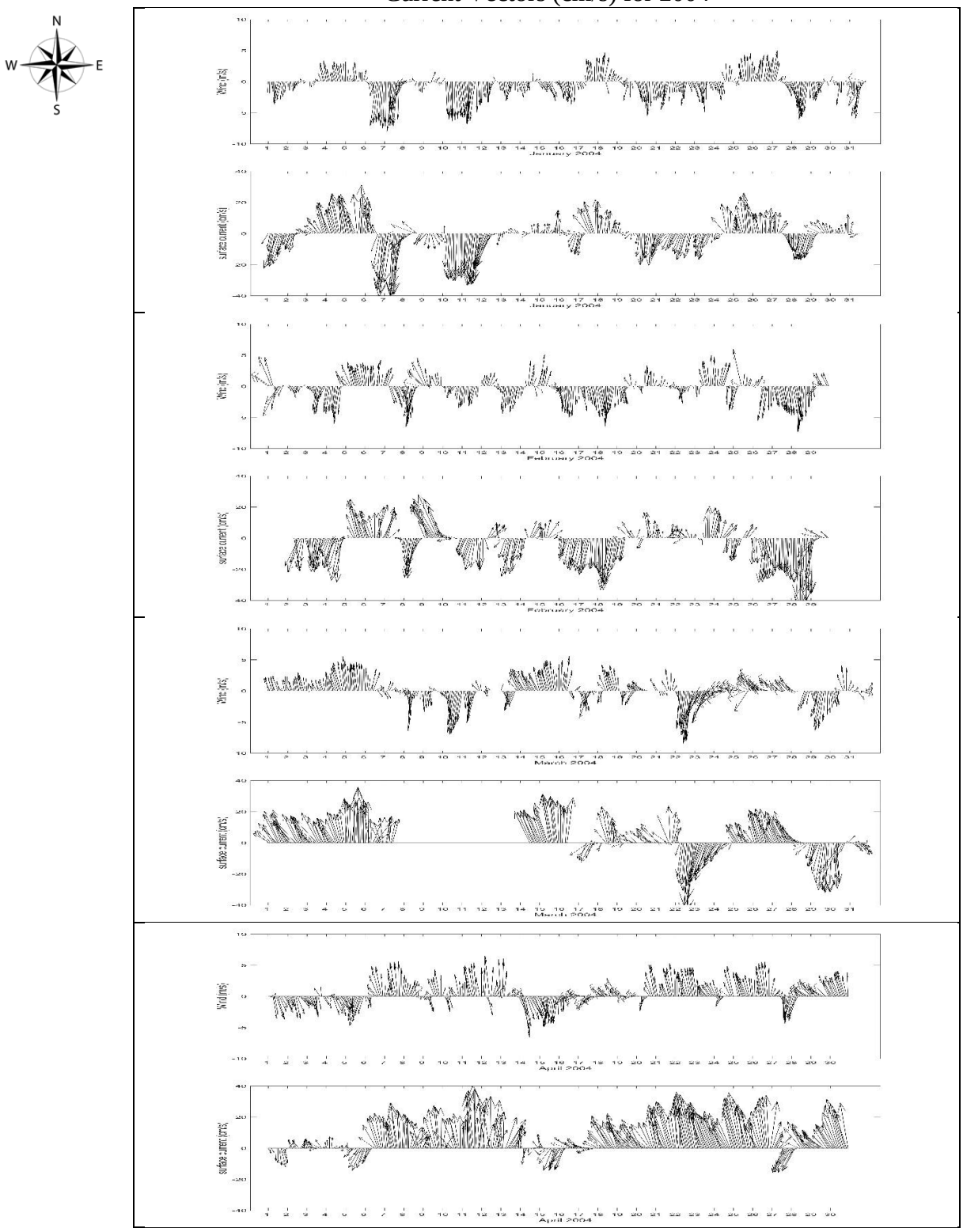

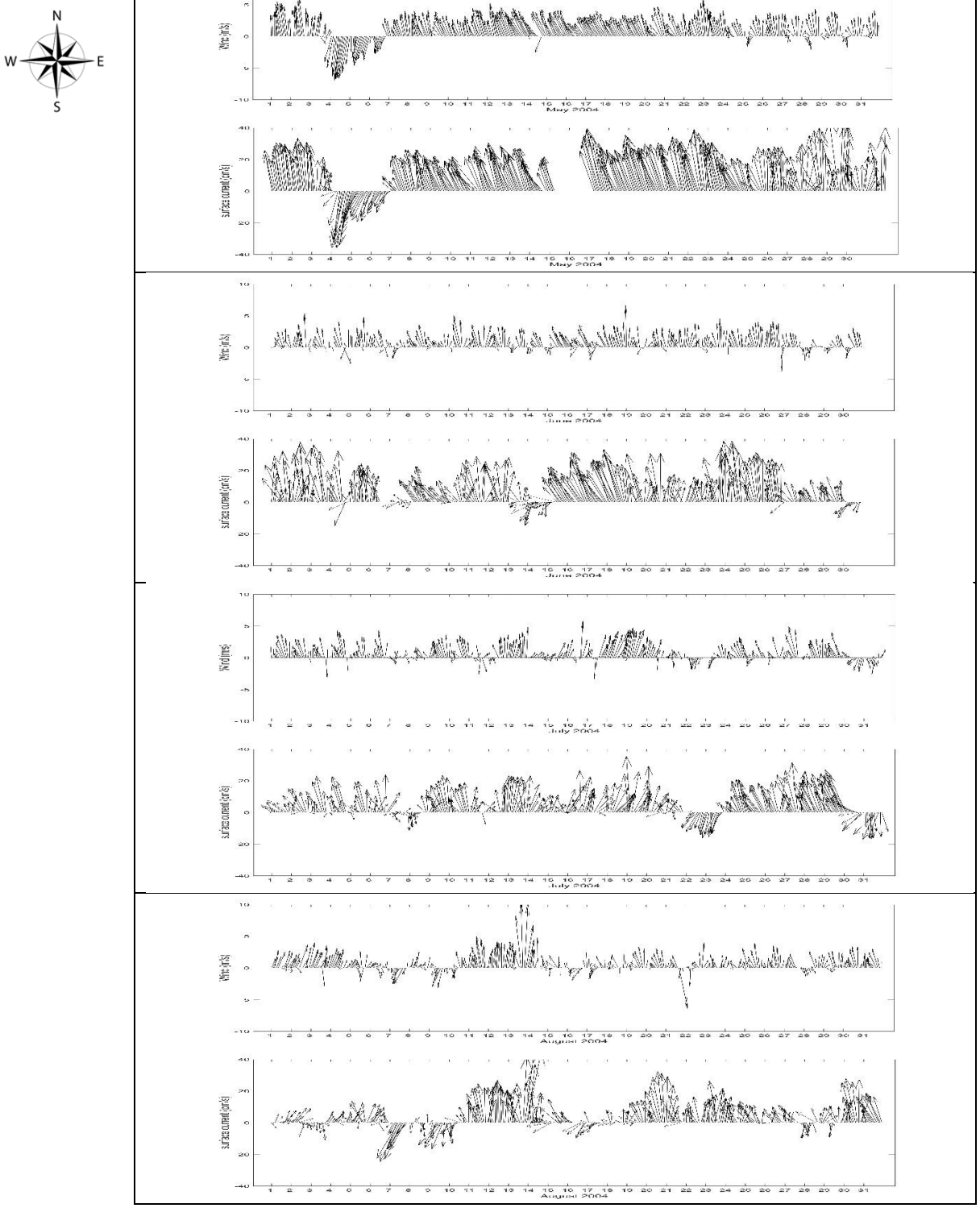
N
W
E
S
May 2004
June 2004
July 2004
August 2004


N
W
E
S

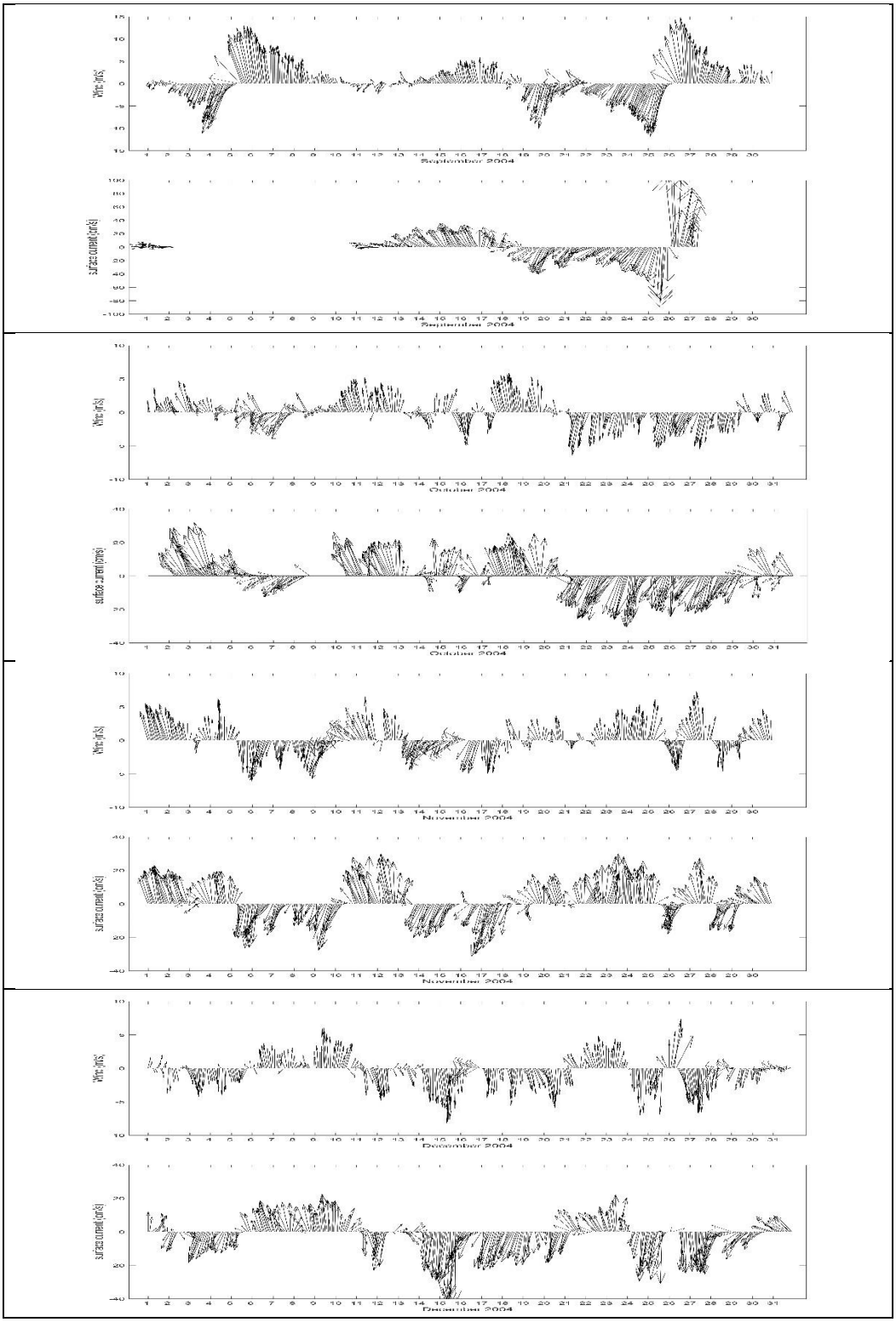
Wind (m/s)
September 2004
surface current (cm/s)
September 2004
Wind (m/s)
October 2004
surface current (cm/s)
October 2004
Wind (m/s)
November 2004
surface current (cm/s)
November 2004
Wind (m/s)
December 2004
surface current (cm/s)
December 2004

APPENDIX D: 2-h Average Wind Vectors (m/s) and 2-h Average Surface Current Vectors (cm/s) for 2005

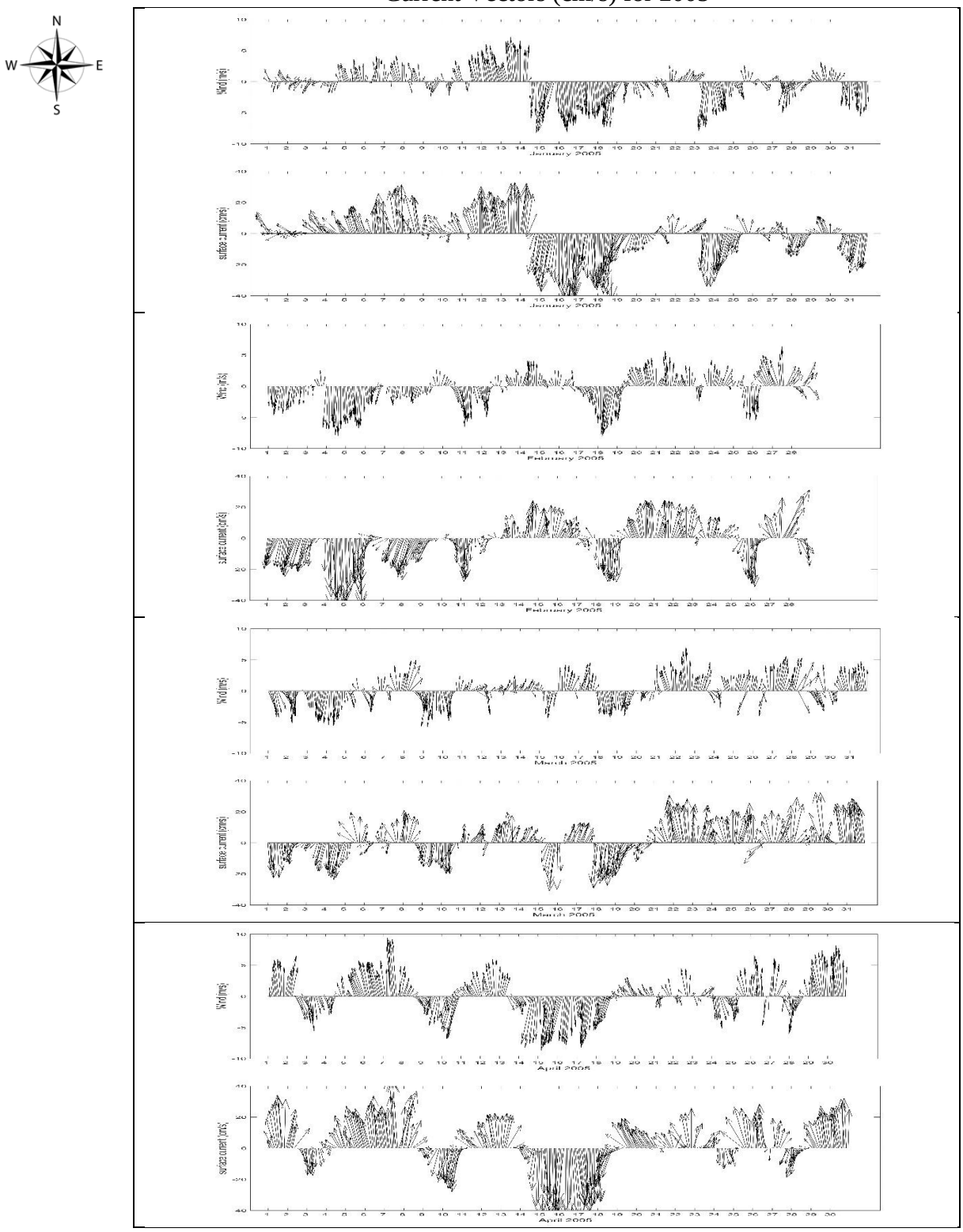

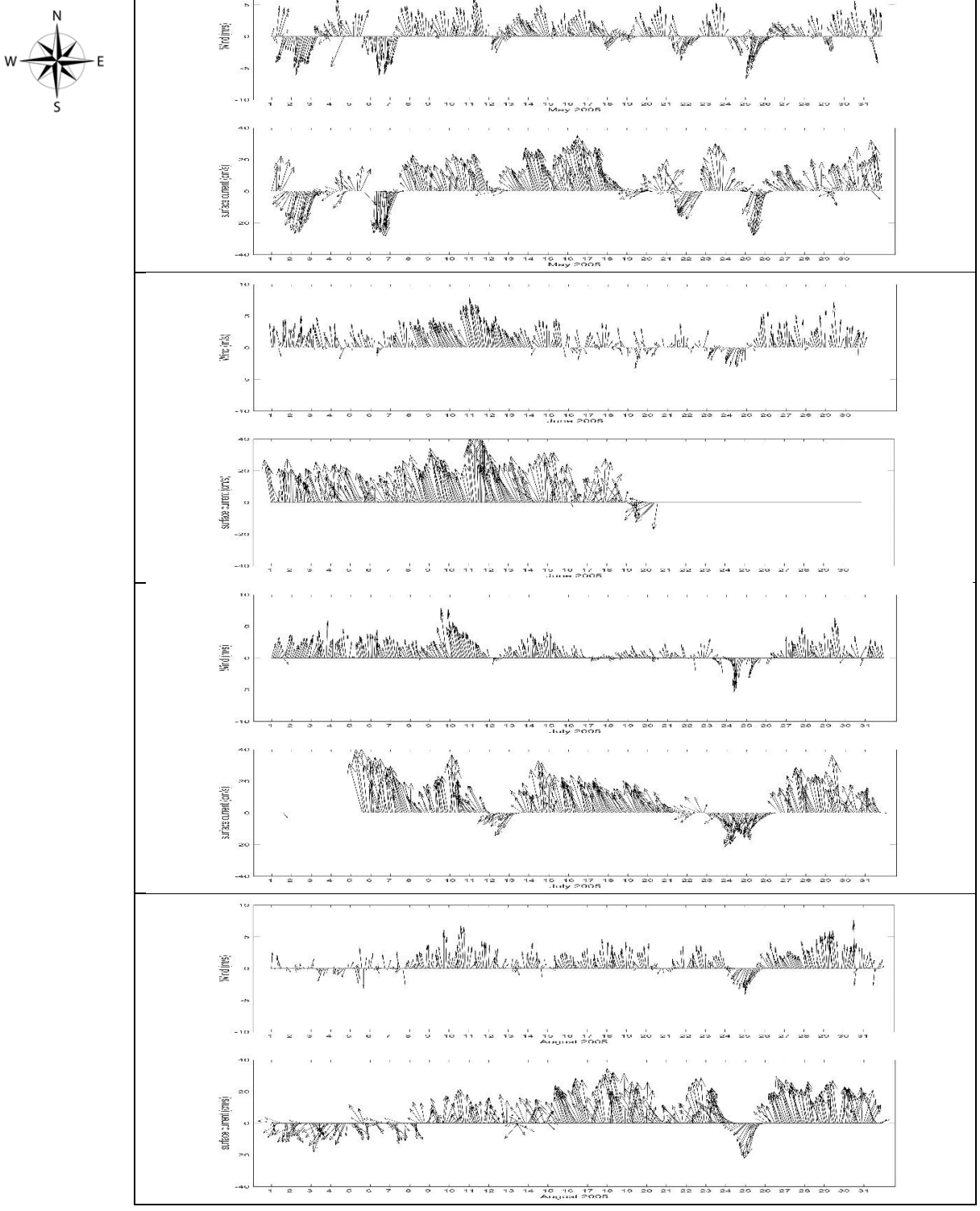
N
W
E
S
May 2005
June 2005
July 2005
August 2005


N
W
E
S

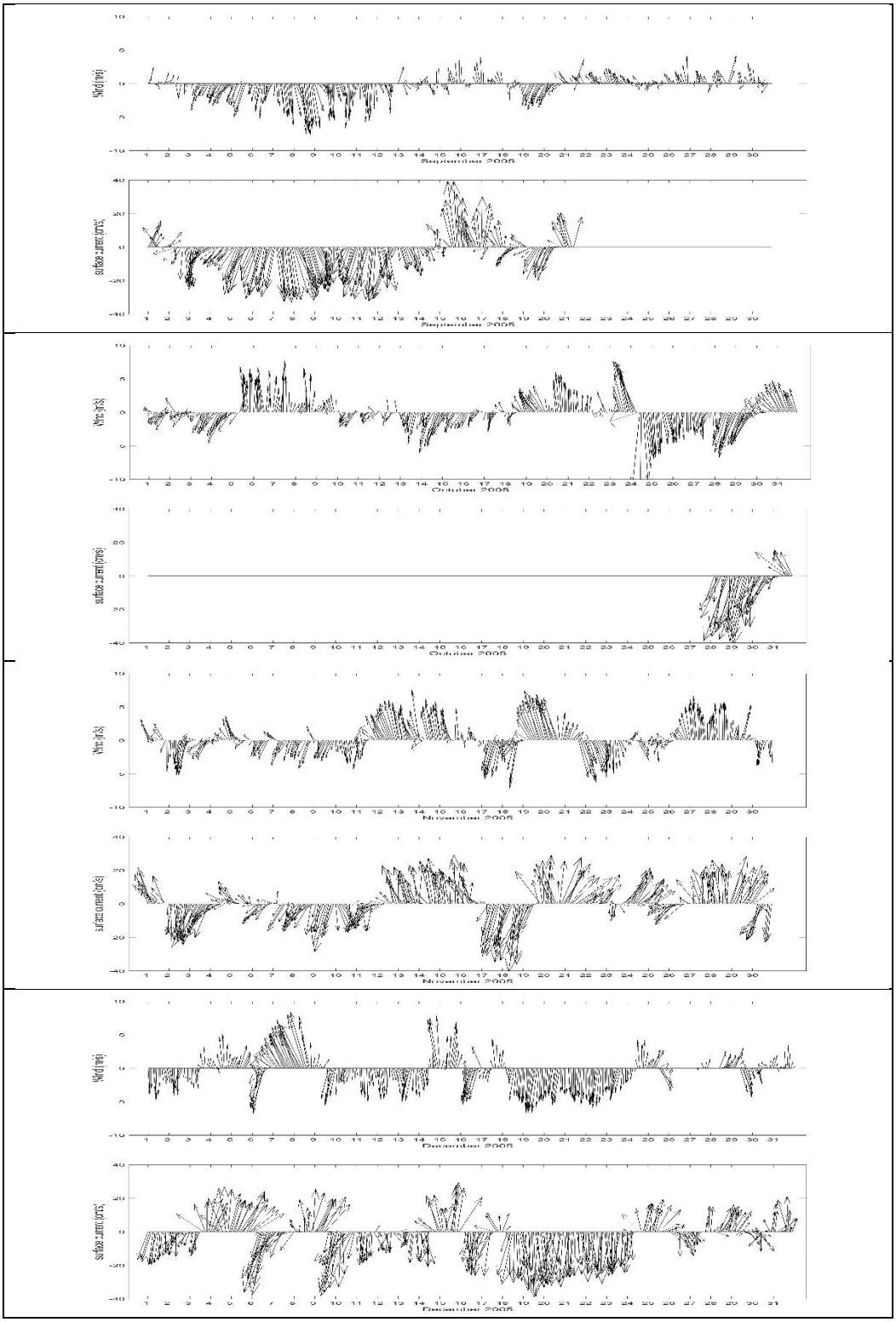
Wind (m/s)
September 2005
surface current (cm/s)
September 2005
Wind (m/s)
October 2005
surface current (cm/s)
October 2005
Wind (m/s)
November 2005
surface current (cm/s)
November 2005
Wind (m/s)
December 2005
surface current (cm/s)
December 2005

VITA

Carolina Burnette was born and raised in Colombia; she graduated with a Civil Engineering degree in 1998 from the Industrial University of Santander. She had the opportunity to work for the Department of Transportation and the Sewer and Environmental Company in Colombia for almost seven years. She moved to the United States in 2005 and decided to start a family and be a stay at home mom to raise her two beautiful daughters who are now six and two years old. Carolina enrolled in the master in Coastal Engineering at the University of North Florida in the fall of 2014, where she had the opportunity to work on several research projects with Dr. Dally. In June 2016, Carolina was hired by the US Army Corps of Engineers to join the Coastal Planning Section.